RHEINISCHE FRIEDRICH-WILHELMS-UNIVERSITY OF BONN

Infrared sense in snakes – behavioural and anatomical examinations (*Crotalus atrox*, *Python regius*, *Corallus hortulanus*)

Dissertation

to obtain the graduation of
Doctor rerum naturalium (Dr. rer. nat.)

presented to the biological department of the
faculty of mathematics and sciences

by
Jill Ebert

Bonn, September 2007

Angefertigt mit der Genehmigung der Mathematisch-Naturwissenschaftlichen Fakultät der Rheinischen Friedrich-Wilhelms-Universität Bonn

1. Gutachter: Prof. Dr. Horst Bleckmann
2. Gutachter: PD. Dr. Helmut Schmitz

Tag der mündlichen Prüfung: 18. Dezember 2007

Erscheinungsjahr: 2008

Index

1 Introduction

The overall scope of this study was to examine behavioural and morphological aspects of the infrared (IR) sense in three different snake species. For this purpose a pitviper and a python were behaviourally tested on their IR detection threshold. Furthermore, the structure of the IR sensitive labial areas of a pit-bearing boa was morphologically investigated. The following introduction provides the necessary background knowledge.

1.1 Infrared radiation

Electromagnetic radiation of wavelengths longer than that of visible light, but shorter than that of radio waves, is defined as infrared radiation. The spectrum spans three orders of magnitude with a wavelength between approximately 750 nm and 1 mm (e.g. Bergmann and Schaefer, 1987; Meschede, 2002).

The IR spectrum is often subdivided into smaller sections, e.g. near infrared, which is the region closest in wavelength to the radiation detectable by the human eye (0.78-3 µm), followed by mid (3-50 µm) and far infrared (50-1000 µm) (Bergmann and Schaefer, 1987). However, international standards for the subdivision of the spectrum are not available.

The source of IR radiation is heat or thermal radiation, produced by the motion of atoms and molecules in an object. Some animals have expanded their sensory information input by developing IR radiation detection mechanisms, in addition to other senses, e.g. the visible electromagnetic radiation detection mechanisms (vision). This enables them to additionally 'see' emitted thermal radiation.

1.2 IR perception in the animal kingdom

Temperature is one important variable of the environment. Within the animal kingdom some species are known to perceive and utilize the presence of and the changes in thermal energy in their environment (Barrett et al., 1970). IR receptors enable them to detect the changes in thermal energy. The IR sense is employed in various ways, e.g. in prey detection, thermoregulation or protection from heat damage. Among mammals, the common vampire bat (*Desmodus rotundus*) is discussed in the context of IR reception (Kishida et al., 1984; Kuerten and Schmidt, 1982). In the world of insects, some blood-sucking bugs (e.g. *Rhodnius prolixus*) are discussed to be IR sensitive (Schmitz et al., 2000). Additionally, pyrophile beetles (e.g. *Melanophila acuminata, Merimna atrata, Acanthocnemus nigricans*) are known to possess an IR sense (e.g. Evans, 1964, 1966; Evans and Kuster, 1980; Kreiss et al., 2005;

Mainz et al., 2004; Schmitz and Bleckmann, 1998, Schmitz et al., 2002). Furthermore, two families of the snake taxa also include IR sensitive representatives (e.g. Barrett et al., 1970). Depending on the species, the IR receptors are of diverse structure and position, e.g. in the snout region of snakes, in the case of beetles on the ventral side of the thorax (*M. acuminata*, *A. nigricans*) or of the abdomen (*M. atrata*).

1.3 IR sense in snakes

The IR sense evolved independently within two distantly related families of snakes: in the primitive Boidae (boas and pythons) and in the subfamily Crotalinae (pitvipers including rattlesnakes, copperheads and bamboo vipers) of the advanced Viperidae (e.g. Barrett et al., 1970; Bullock and Diecke, 1956; Kluge, 1991; Molenaar, 1992; Nobel and Schmidt, 1937).

The integration of both IR and visual information enables IR sensitive snakes to achieve a unique portrayal of their surrounding by 'seeing' different regions of the electromagnetic spectrum. They image visual light with their eyes and also perceive images of their thermal environment by detecting IR radiation at wavelengths centred around 10 µm, which matches the IR emission peak of homoeothermic animals, i.e. potential prey (e.g. Gamow and Harris, 1973; Grace et al., 1999).

Despite their structural differences, the IR sensitive organs of crotaline and boid snakes are analogous and serve similar biological functions (de Cock Buning, 1984), i.e. primarily the detection of mainly homoeothermic prey and accurate predatory targeting, even in the absence of visual cues (e.g. Barrett et al., 1970; Bullock and Barrett, 1968; Bullock and Diecke, 1956; de Cock Buning et al., 1981; Goris and Nomoto, 1967; Grace et al., 2001; Hartline, 1974; Kardong and Mackessy, 1991; Kardong, 1993, 1996). Furthermore, it is known that pitvipers also use their IR sense for spatial orientation, e.g. finding basking places for thermoregulation (Krochmal and Bakken, 2000, 2003; Krochmal et al., 2004). In addition, their IR sense is discussed in the context of selecting a den site (Sexton et al., 1992) or avoiding predators (Greene, 1992).

1.4 Differences in pit morphology

Pitvipers possess a forward-facing loreal pit situated between the nostril and the eye on each side of the head (see 2.1.1 Fig. 1 for a representative). These (1-5 mm deep) cavities (Barrett et al., 1970; de Cock Buning, 1985) expand into a depression of the maxillary bone (Dullemeijer, 1959). The pit opening is narrower than the base. A 10-15 µm thick IR receptor

bearing membrane suspended near the cavity back divides the latter into an inner and outer chamber (e.g. Barrett et al., 1970; Molenaar, 1992). This membrane consists of three layers: the richly innervated nervous layer sandwiched between two cornified (0.5-1.5 μm thick) epidermal layers (Bullock and Fox, 1957; Lynn, 1931; Nobel and Schmidt, 1937). The nervous layer is associated with a high concentration of vascular beds (Barrett et al., 1970).

The loreal pits function similarly to a pinhole camera. The radiation of an IR source impinges on a certain part of the TNM bearing membrane, which allows a determination of the angle (therefore position) of the IR source (Bakken and Krochmal, 2007; Gamow and Harris, 1973; Newman and Hartline, 1982). Due to the frontal position of the loreal pits the IR visual fields of each pit overlap strongly and cover the frontal region.

In contrast to the pitvipers, the pit-bearing boid snakes show a wide variety in shape, size and positioning of more simply constructed pits (Lynn, 1931; see 2.1.2 Fig. 2 for a python and 2.1.3 Fig. 3 for a boa representative). Unlike pitvipers, boids usually possess their IR receptors within simple, shallow depressions in (pythons) or between (boas) specialised labial scales (Noble and Schmidt, 1937; Ros, 1935; Warren and Proske, 1968). The position, number, size and shape of these supra- and/or infralabial depressions differ from species to species (Maderson, 1970; Molenaar, 1992). Some IR sensitive snakes (e.g. *Boa constrictor*) even lack labial depressions altogether (Barrett et al., 1970; von Duering, 1974; von Duering and Miller, 1979). In this case the IR receptors are located in the labial scales (von Duering, 1974). In all boids the receptors are located in the outer epithelium of the labial scales and are supported by epithelial cells (Amemiya et al., 1996b; Molenaar, 1992).

In pit-bearing boids each pit functions similarly to a pinhole camera. However, the information of several pinhole cameras is computed in a specific brain area (tectum opticum, see below) (Newman and Hartline, 1982). Due to the arrangement of the pits not only the frontal but the lateral regions are covered in the IR visual field. It is assumed that the variation of forms of the pits or labial depressions and the distribution of the IR receptive areas influence image formation. However, this has not yet been examined for any pit-bearing boa so far.

1.5 Scale surface structure above IR receptors

Not only does the scale morphology have an influence on the IR perception, but also the surface structure of the scale above the IR receptors might influence the perception mechanism. The surfaces show an array of microscopic pores, which seems to be unique in IR sensitive snakes (Amemiya et al. 1995). According to Amemiya et al. (1995) and Campbell et

al. (1999) they appear to function as a sort of optical grating to reflect the visible light while facilitating the passage of IR rays. These microscopic pores are always associated with the IR receptor-bearing scales (Amemiya et al., 1995).

1.6 Morphology of IR receptors and the neural pathway of IR reception

The IR receptors of all IR sensitive snakes are similar (Molenaar, 1992). The IR receptors are unmyelinated free nerve endings, so-called terminal nerve masses (TNMs), which contain dense concentrations of mitochondria and oxidative enzymes, e.g. succinate dehydrogenase and ATPase (Bleichmar and de Robertis, 1962; Meszler, 1970; Meszler and Webster, 1968). The function of the TNMs as IR receptors has already been proven in previous investigations (e.g. de Cock Buning et al., 1981 a, b; Warren and Proske, 1968). The transduction process is unknown so far. The TNMs are closely associated with a capillary bed, which is discussed in the context of energy and oxygen supply and cooling (Amemiya et al., 1996a; Molenaar, 1992). The TNMs arise from palmate preterminal swellings and extend between the epithelial cells (Bleichmar and de Robertis, 1962; Bullock and Fox, 1957; von Duering, 1974). The dendrites of the TNMs converge to nerves whose bundles lead to the V^{th} cranial nerve (Nervus trigeminus). The pit organs of pitvipers are innervated by branches of the ophthalmic and maxillary nerve; thereby each branch supplies a different area of the membrane (Barrett et al., 1970; Bullock and Fox, 1957). The innervation of the boids IR receptors also involves the mandibular branch of the trigeminal nerve (Molenaar, 1992). In comparison to pitvipers in boids the innervation pattern is more complex and even varies among species. According to de Cock Buning (1985), in pythons the first rostral pits of the supralabial scale are innervated by the ophthalmic branch whereas the other supralabial pits are innervated by the maxillary branch. Molenaar et al. (1979) found distinct groups of IR receptors in *Python reticulatus*, which are innervated by distinct nerve bundles. Moreover, individual pits seem to be innervated by the same branches that diverge from bundles to neighbouring pits of the same group (Molenaar, 1992).

The trigeminal system of IR sensitive snakes consists of the common trigeminal system (equivalent to the one found in other vertebrates) and the lateral descending trigeminal system, which is placed lateral to the first mentioned in the medulla oblongata (Kishida et al., 1984; Molenaar, 1992; Newman and Hartline, 1982). The primary afferent fibres of those sensory branches of the trigeminal nerve that lead to the TNMs build the Lateral trigeminal tract descendens (lttd) and terminate ipsilateral in the Nucleus of the lateral trigeminal tract descendens (LTTD) in the medulla oblongata. There, the projections from the different

branches of the Nervus trigeminus are still topographically distinguishable (Molenaar, 1978). This LTTD is unique to all IR sensitive snakes (Molenaar, 1974; Schroeder and Loop, 1976). From there on the neural processing pathways of IR information differ in the crotaline and boid snakes. In boids, the efferent projections from the LTTD reach the nuclear complex of the nuclei N. rotundus and N. pararotundus, located in the dorsal thalamus and pretectum (Molenaar, 1992), and then directly ascend to the tectum opticum in the mesencephalon (Molenaar, 1992; Molenaar and Fizaan-Ostveen, 1980; Welker et al., 1983). In pitvipers, there is an intermediate nucleus (RC: Nucleus reticularis caloris) between the LTTD and the Tectum opticum (Kishida et al., 1980; Newman et al., 1980; Stanford et al., 1981).

The Tectum opticum of IR sensitive snakes is not only the target of the ascending IR pathways, but also of the visual information processes by revealing IR, visual and visual-IR neurons terminating in a similar region (Kass et al., 1978; Terashima and Goris, 1975, 1976). Cross-modality interactions take place in IR and visual neurons (Molenaar, 1992). Similar to in boids, the efferent fibres in crotalines run from the Tectum opticum to the Nucleus rotundus in the diencephalon and from there to the ADVR (anterior dorsal ventricular ridge), a processing area in the telencephalon (Berson and Hartline, 1988).

1.7 Background of the objectives and working hypothesis

Several behavioural studies have addressed IR perception in snakes (e.g. Grace et al., 2001; Grace and Woodward, 2001; Theodoratus et al., 1997). Early studies revealed the pit organs to be heat sensitive organs (e.g. Ros 1935; Noble and Schmidt 1937). Other behavioural investigations focused on prey detection (Chiszar et al., 1986; de Cock Buning et al., 1981a; Grace et al., 2001; Grace and Woodward, 2001; Haverly and Kardong, 1996; Kardong, 1996; Kardong and Mackessy, 1991) and the functional usage of the IR sense in the context of thermoregulation (Krochmal and Bakken, 2000, 2003; Krochmal et al., 2004).

Young and Aguiar (2002) used behavioural changes during stimulus presentation as evidence for sensory perception in rattlesnakes in order to investigate the auditory system. In this study a similar methodical approach was used to investigate the IR sense. Unlike an electrophysiological approach (which can only record a part of the neural processing mechanisms, depending on the methods, e.g. evoked potentials, single cell recordings or multi-unit recordings), the behavioural approach does not only take the entire neural processing of stimulus perception into account, but also adds information on the relevance of the perceived. Up to now, no study has used this advantage of a behavioural approach to explore the IR detection range, i.e. the IR sensitivity of snakes. In one part of this dissertation

a behavioural approach was used to examine the IR sensitivity of two different ground-dwelling snake species, i.e. one representative of a pitviper (*Crotalus atrox*) and one representative of a python (*Python regius*).

The sensitivity of their IR senses, i.e. their detection ranges, should give further insight into the different possible functions of the pit organs. The IR detection threshold is defined as the minimum IR irradiance contrast of an object against the background at a critical distance. The IR irradiance of an object is defined as the amount of radiant flux impinging on a unit surface area-unit (W/cm^2). The threshold level is the minimal irradiance contrast i.e. the thermal differential between target and ambiance (Theodoratus et al., 1997) which leads to a neural and/or behavioural response.

Several electrophysiological investigations were performed on the IR sensitivity and detection thresholds of pitvipers. A temperature rise of 0.003 °C applied via flowing water on the pit membrane of *Crotalus* was the threshold determined by recordings at the trigeminal nerve (Bullock and Cowles 1952; Bullock and Diecke 1956). Stimulation of the pit organ with IR-lasers revealed a threshold of 0.1 mW/cm^2 at the membrane (e.g. Goris and Nomoto 1967; Moiseenkova et al. 2003; Terashima et al. 1968). Recordings of the stimulation in the midbrain tectum of *Calloselasma* with a heating element revealed a threshold of 10.76×10^{-3} mW/cm^2 (de Cock Buning et al. 1981a, de Cock Buning 1983a, b). Calculated detection ranges span from 66.6 cm for a mouse whose body temperature was 10 °C above ambient temperature (de Cock Buning 1983b) to less than 5 cm for a mouse-like stimulus at 37 °C (Jones et al. 2001). In contrast to the extensive electrophysiological research on pitvipers, only one IR irradiance threshold level for boids was investigated in *Python reticulatus* by means of electrophysiological recordings in the Tectum opticum (de Cock Buning, 1983b). Applying a modified Stefan Boltzmann formula for his results, de Cock Buning calculated an energy value of 59.8×10^{-6} W/cm^2 and a detection distance of 28.3 cm for an IR stimulus of the size (25 cm^2) and temperature (30 °C) of a mouse (10 °C higher than the ambient temperature). The Stefan Boltzmann formula describes the total energy radiated per unit surface area of an object which is proportional to the fourth power of the thermodynamic temperature.

All these estimates on IR detection thresholds are based on electrophysiological recordings of IR sensitive neurons. So far, a behavioural set-up has never been used to examine detection thresholds. One aim of this study was to compare detection thresholds of separately evolved IR sensory systems, i.e. pitviper perception versus python perception in a behavioural context. Based on the above mentioned advantages of the behavioural approach, it is assumed that the

detection threshold to a similar stimulus is lower than revealed in previous electrophysiological studies.

Most IR sensitive snakes possess pit organs, which accommodate IR-sensitive thermoreceptors. However, some morphological (e.g. shape) and functional (e.g. structure, processing) properties of the pit organs in the crotaline and boid snakes differ. The general morphology of the pits of pitvipers and pythons, as well as pitless boas are reasonably well investigated (e.g. Amemiya et al., 1996a, b; Bleichmar and de Robertis, 1962; Gopalakrishnakone, 1984; Hisajima et al., 2002; Ros, 1935; von Duering, 1974, von Duering and Miller, 1979).

However, up to now boas with labial pits have not been paid much attention to. This lack of knowledge probably results from the fact that most snakes of the subfamily Boinae do not possess labial pits; the only exceptions are species of *Epicrates*, *Corallus* and *Sanzinia* (Lynn, 1931). In contrast, most snakes of the subfamily Pythoninae have labial pits. Therefore, python species have usually been employed in investigations of pit-bearing boids (e.g. Grace et al., 1999; Lynn, 1931; Noble and Schmidt, 1937; Ros, 1935; Warren and Proske, 1968). In general, only limited work has been done on boas, and then it was primarily associated with the pitless *Boa constrictor* (e.g. Bullock and Barrett, 1968; von Duering, 1974; von Duering and Miller, 1979). Lynn (1931) briefly described the histological structure of the labial pits of the boa *Corallus caninus* (formerly *Boa canina*). His examination focused on the description of the nerve distribution. Ros (1935) provided a description of the labial scales of *Sanzinia madagascariensis* (formerly *Corallus madagascariensis*) in her examinations of different boid (mainly pythons) species and emphasised the difference of the pit positioning of this boa species (between scales) and various python species (in the scales). However, she described the histological pit structure for *Python sebae* in greater detail. Nobel and Schmidt (1937) carried out histological examinations after demonstrating *Corallus hortulanus* to be IR-sensitive in behavioural experiments. They showed unmyelinated nerve fibres for the first time, which end in 'knoblike enlargements' in the epidermis and described rich capillary supply in the underlying dermal region associated with the nerve fibres.

In this study *C. hortulanus* was chosen, because of its extraordinary zigzag-shaped labial scales, forming directionally arranged depressions rather than mere pits (e.g. *C. caninus*). The unique morphology of these labial depressions is assumed to be significant for *C. hortulanus´* mechanism of IR perception, but nothing is known about the enhancement mechanism for image formation or sensitivity.

Prerequisite for an elucidation of the significant functional morphology is the knowledge of the location and the structure of the IR receptive TNMs in the labial scales. This was investigated at the light- and electron microscopic level, revealing TNM areas which pick up IR radiation from different directions. This led to the assumption of a possible topological representation of the labial scales´ TNM areas in the LTTD, in order to facilitate directional IR perception. The projection from the forward-oriented TNM area is hypothesized to lead to a different part of the LTTD than the projection of the backward-oriented TNM areas of the same pit.

In addition, the surface structure of the TNM bearing labial scales is observed to be different to the surface structure of other body scales. This difference presumably aids IR reception.

The extraordinary labial scale form, correlated with the knowledge of the location and size of the TNM areas led to a three dimensional (3-D) reconstruction of a precise directional IR perception model for *C. hortulanus*. The resulting IR reception field allowed the decoding of the underlying directional reception mechanism. This model helps to understand how labial scale morphology can enhance spatial resolution by a mechanism completely different from any other IR system that we know.

2 Material and methods

2.1 Natural history of the study species

Three different snake species were involved in the investigations. Each study species is a representative of the three known IR sensitive subfamilies (e.g. Barrett et al., 1970; Bullock and Diecke, 1956). Western diamondback rattlesnakes (*Crotalus atrox*) belong to the Crotalinae, whereas ballpythons (*Python regius*) belong to the Pythoninae and Amazon tree boas (*Corallus hortulanus*) belong to the Boinae.

2.1.1 Western diamondback rattlesnake (*Crotalus atrox*)

Fig. 1: *Crotalus atrox* photographed from the front and side. Rattlesnakes possess a pair of loreal pits, which are located just below the nostrils on each side of the head (yellow arrows).

Western diamondback rattlesnakes occur almost from coast to coast in the southern United States and northern Mexico, their distribution ranging in a broad band from central southern California and Sonora to the Gulf of Mexico in Texas and extending into the north-east of Mexico (Mattison, 1996). Animals of this species usually exceed 100 cm in length, but rarely grow larger than 200 cm (Mattison, 1996). They have a heavy-bodied habitus. The name rattlesnake is derived from the rattle (consisting of loose interlocking segments, which are remnants of shedded skin) on the end of the short black and white annulated tail. Rattlesnakes possess a wide and spade-shaped head with a round snout region (Rubio, 1998). The IR sensitive receptors are embedded in the two loreal pits (see Fig. 1). The rattlesnakes´ retractable fangs are long, curved and hollow, to enable the injection of the potent venom into the prey.

C. atrox is a terrestrial species and usually inhabits arid lowlands with scrubby vegetation and rocky outcrops, e.g. low desert regions and prairies, but it can also be found in rocky hills as well as in low mountainous areas (Mattison, 1996; Rubio, 1998). The activity pattern of the rattlesnakes is closely linked to seasonal and daily temperature cycles. During periods of excessive heat they are primarily nocturnal, but also active during daytime at more moderate temperatures. During winter they go into hibernation (Klauber, 1982; Mattison, 1995, 1996). Rattlesnakes are ambush hunters; however, they actively choose their hunting spot (Greene, 1992). They largely prey on mammals (e.g. different mice and rat species, chipmunks, squirrels, prairie dogs and rabbits) as well as on birds, but rarely on amphibians, lizards and other snakes (Mattison, 1996).

Western diamondback rattlesnakes are easily excitable and quick to react (Klauber, 1982; Mattison, 1996). When threatened they display their typical defensive behaviour of rattling and coiling up into a striking position (i.e. forming a S-shaped loop with the body and raising the head well off the ground), which is sometimes accompanied by hissing and lunging (Mattison, 1995).

2.1.2 Ballpython (*Python regius*)

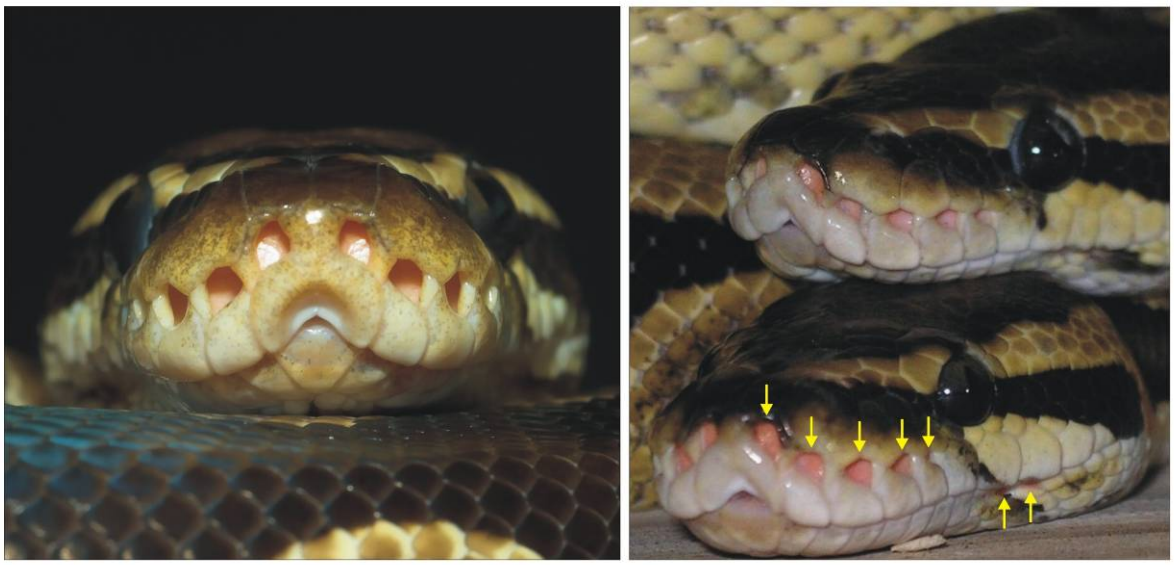

Fig. 2: *Python regius* photographed from the front and side. This species possesses five pits on the supralabial scale row and two to three small infralabial pits (yellow arrows).

Ballpythons, also known as Royal pythons, are native to western Africa. According to Walls (1998) they occur in Senegal and Gambia, their range extending southwards to Ghana and the Nigeria area and eastwards over the savannas to Sudan and northern Uganda. *P. regius* is

considered to be the smallest member of the python species. It has a strong body with a short tail, rarely exceeding a length of more than 150 cm in total (Kirschner and Seufer, 2003). The head is clearly set off from the neck with a narrowing but round snout region (see Fig. 2). There are five pits on the supralabial scales on each side and usually two to three smaller pits situated caudally on each infralabial scale row (see Fig. 2). The IR receptive areas are embedded in these pits.

P. regius is a primarily ground-dwelling species, although capable of climbing, and a typical inhabitant of savanna regions (e.g. Mehrtens, 1987; Stafford, 2000). Although occasionally discovered in rainforests (e.g. Butler and Reid, 1986; Luiselli et al., 1998), ballpythons are usually found in bushland as well as in cultivated land with numerous rodent burrows and termite mounds to withdraw to during the day (Greer, 1994). The burrows provide shelter with a constant temperature and humid conditions and therefore are used as hiding places, especially during the breeding season (from October to February; Trutnau, 2002).

Pythons primarily hunt during the time between dusk and dawn. They are ambush hunters, thereby employing the typical sit-and-wait strategy (Merthens, 1987). They prey on various small mammals, e.g. mice, rats, shrews, squirrels, and occasionally on bats and birds as well (Luiselli and Angelici, 1998; Luiselli et al., 1998), which they constrict.

Ballpythons are docile snakes. Eponymous is their typical defensive posture, i.e. they coil their body into a ball with the head on the inside for protection when threatened.

2.1.3 Amazon tree boa (*Corallus hortulanus*)

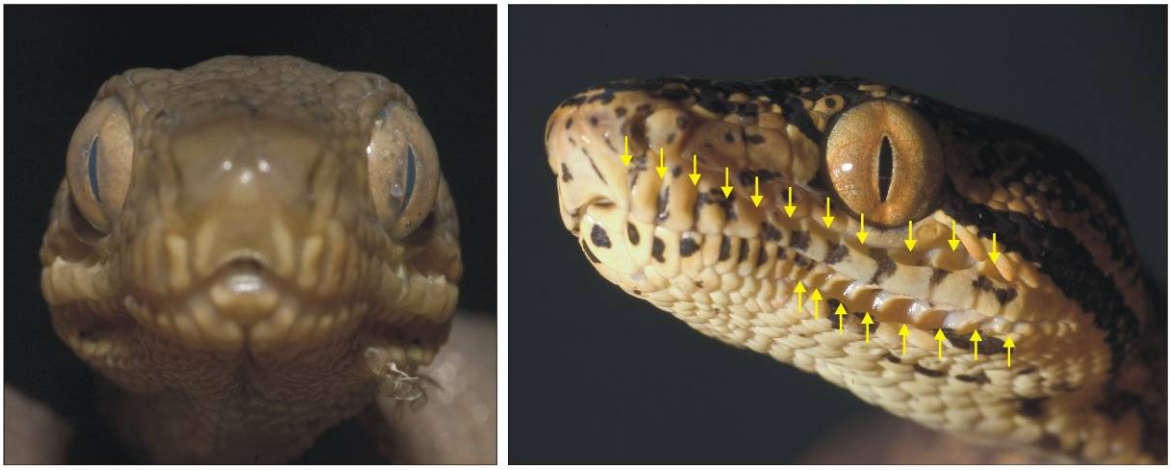

Fig. 3: *Corallus hortulanus* photographed from the front and side. Note the extraordinary and variably shaped eleven supra- and eight infralabial scale depressions of this boa (yellow arrows).

The Amazon tree boa is a geographically wide-ranging neotropical snake species. It occurs in northern South America, its range extending throughout the entire Amazon rain forest basin to drier regions in Brazil and Peru, as well as on several West Indian Islands (Henderson, 1993; Mattison, 1995; Merthens, 1993). As the name tree boa implies *C. hortulanus* is an arboreal species. The body shape is slender and higher than wide with a long tail, which is well adapted to holding onto branches. Usually, adult Amazon tree boas attain a length of about 150 cm to 200 cm (Mattison, 1995). The head is of triangular shape, relatively large and clearly set off from the thin neck region. The IR sensitive receptors are situated in the depressions between the scales of the upper and lower lip (see yellow arrows, Fig. 3).

C. hortulanus occurs in a variety of habitats, encompassing dense rainforest vegetation as well as a wide array of shrub and tree species of cooler forests and drier areas or even banana plantations (Merthens, 1993; Seigel and Collins, 1993; Henderson and Winstel, 1995). The Amazon tree boa is an active forager but will also ambush prey, hunting largely at twilight hours and during the night (Merthens, 1993). Its diet mainly consists of mammals (e.g. rodents), birds and bats, as well as lizards (Henderson, 1993; Merthens, 1993). Similar to other snake species, the boas exhibit ontogenetic variation in diet (i.e. they feed on lizards as juveniles and on birds and mammals as adults). Like pythons, they kill their prey by constriction.

The Amazon tree boa exhibits a natural defensive aggression. When provoked it readily adopts a typical S-shaped striking position, lunges and strikes.

2.1.4 Animal husbandry of the study species

All snakes were captive bred, either born in the Institute or obtained from commercial dealers. The snake housing rooms (one of them was also the experimental room) were kept at a constant temperature of 22 °C ± 2 °C during the time of experiments. The terrestrial snakes (*C. atrox* and *P. regius*) were housed individually or in pairs in heated terrariums with a hide box as a shelter. *C. atrox* was kept at an ambient temperature of 28 °C ± 1 °C (humidity: 35 % ± 5 %) and a 12 h light/12 h dark cycle. *P. regius* had an ambient temperature gradient of 25 °C up to 30 °C ± 1 °C (humidity: 65 % ± 5 %) with a natural light/dark cycle. The arboreal *C. hortulanus* was communally housed in a heated terrarium provided with tree branches as climbing and resting possibilities. The ambient temperature was 28 °C ± 1 °C with a high humidity (80 % ± 10 %) and the light/dark cycle was 12 h/12 h.

All snakes were provided with water ad libitum and were maintained on a diet of one mouse every 10 to 14 days (juvenile rattlesnakes, juvenile pythons and all Amazon tree boas)

or one to two juvenile rats once a month (adult pythons). If a snake showed signs of shedding (indicated by a milky blur over the eyes), it was not fed until shedding had occurred. Depending on the individual feeding frequency and housing temperatures, shedding on average took place every 6 to 12 weeks, in rare cases almost up to 6 months.

Animal husbandry and all experiments were conducted in accordance with the 'Principles of Animal Care' Publication No. 86-23, revised 1985 by the National Institutes of Health.

2.2 Behavioural experiments

The behavioural investigations of the IR thresholds were conducted with 12 juvenile western diamondback rattlesnakes (*Crotalus atrox*) and 22 ball pythons (*Python regius*) (14 juveniles and eight adults) of both sexes. The rattlesnakes' ages varied from four to 12 months with snout-vent lengths of 45 cm to 80 cm. The ages of the pythons varied from one-and-a-half up to eight years with snout-vent lengths of 69 cm to 85 cm for the juvenile and 108 cm to 141 cm for the adult pythons.

The behavioural investigation of the pythons was conducted in cooperation with Sarah Mueller in the course of her diploma thesis (Mueller, 2005) under my supervision. Both, the rattlesnake and the python experiments are published (Ebert and Westhoff, 2006; Ebert et al., 2007). They are presented in the following.

2.2.1 Snake preparation

To exclude visual information all snakes were blindfolded with a strip of black duct tape (Fig.4, insets) prior to experimenting. To apply the strip of duct tape to the head and eyes, the pythons merely had to be held gently behind the head. The rattlesnakes were pinned down with a snake hook behind the neck, then gripped behind the neck and made to bite into a piece of plastic foam to avoid bite injuries. The whole procedure usually did not take longer than 2 to 3 minutes and had to be repeated after each shedding, as the duct tape was also cast off. The pythons additionally were marked with white lines (1 cm in length), starting between the eyes and continuing along the spine in 5 cm steps. This was necessary for the video recordings, with which the behavioural responses were later evaluated. The snakes were allowed to adapt to the blindfolding (and marking in the case of pythons) for at least one day before testing. If the snakes managed to rub off part of the tape, they were excluded from the experiments until their next shedding. Only snakes that were not in moulting and had had their last meal at least two days previous to testing were involved in the experiments.

2.2.2 Experimental set-up

The snakes were tested in a circular arena with a diameter of 220 cm (Fig. 4). Surrounding the arena, a 150 cm high barrier made out of 1 cm thick white Styrofoam shielded the snake from unwanted IR stimuli.

A square Peltier element (PKE 128 A 0021, Peltron GmbH, Germany) of 16 cm^2 was used as an IR stimulus. The Peltier element (PE) was mounted at the lower end of a motor driven pendulum, which could be presented to the snake at any (horizontal) position within the circular arena (see Fig.4). The pendulum with the IR source was attached to a sliding rail of a beam (c.f. Fig.4). The distance between the snake's head and the IR source was measured to a precision of 0.5 cm. As previous recordings with a thermoscanner and IR camera (2.2.6) revealed that the emitted body temperature of a mouse (N=5) lies between 34 °C and 35 °C, the temperature of the PE was adjusted to 34.4 °C ± 0.5 °C (rattlesnakes) or to 34.5 °C ± 0.5 °C (pythons). The temperature of the PE was constantly monitored with a sensor (PT 100, Peltron GmbH, Germany; height: 10 mm, width: 2 mm), which was attached to the surface of the PE and connected to a thermal feedback control unit (PRG H75, Peltron GmbH, Germany) to keep the temperature constant. The IR radiation was controlled by a shutter (shielded with insulating Styrofoam), which was positioned in front of the PE. When the shutter was closed the temperature in front of the shutter was 23.5 °C ± 0.5 °C, which hardly differed from the ambient room temperature of 23 °C ± 1 °C. The rattlesnakes had an average body temperature of 24 °C ± 1 °C and the pythons of 28 °C ± 1 °C as measured with an IR-thermometer (minitemp TM, Raytech, USA).

At the beginning of each session the rattlesnakes and juvenile pythons were placed in a lockable hide box on a platform elevated 30 cm from the floor to prevent them from escaping. The platform was placed in the centre of the arena for testing distances from 10 cm to 100 cm. For experiments with adult pythons the platform was elevated to 80 cm above the floor. For rattlesnake sessions with distances above 100 cm the platform was moved towards one side of the barrier utilising a minimum testing distance of 70 cm and a maximum testing distance of up to 160 cm. Overlapping distances (70-100 cm) were tested for reasons of comparability.

Video recordings of all experimental sessions of *Python regius*

A (black and white) CCD module camera (Conrad, Germany) with a 2.5 mm focal distance objective was mounted above the platform (c.f. Fig. 4) and connected to a computer (IBM, USA). The software used for recording was the Vidcap32.exe program (Microsoft, USA) with a frame rate of 3 frames per second. A video analysis program developed by M. Hofmann (Version 1.01) was employed for frame by frame analysis of the behavioural responses (compare 2.2.4, *P. regius*).

Fig. 4: Schematic sketch of the experimental set-up. 1: IR source (PE), 2: scale (100 cm), 3: video camera (not shown). Arrows indicate the moving directions of the IR source. Insets show representatives of the two snake species *C. atrox* and *P. regius*, both blindfolded.

2.2.3 Snake exposure protocol

The behavioural experiments were performed according to the following protocol:

Enclosed in a hide box the snake was placed on the platform in the arena set-up. After an adaption phase (10 min for the rattlesnakes; 2 min for the pythons) the lid of the hide box was lifted. The pythons received a further adaption phase of at least 2 min. Thereafter, as soon as

the snake faced the PE, the pendulum was set into oscillation (0.5 Hz, oscillation amplitude: 30 cm, speed: 0.3 m/s) while the shutter was simultaneously opened to expose the PE for 10 s before it was shut and the oscillation was stopped again. Then the behavioural response of the snake was documented: the behaviour of the rattlesnakes was evaluated directly and written down. The behaviour of the pythons was also evaluated directly, but it was also additionally video recorded and independently re-evaluated again later. These video recordings were started 2 s before the stimulus presentation and ended after 20 s. During the further experimental session the distance between the PE and the snake's head was arbitrarily varied within predetermined 10 cm intervals (e.g. 10-20 cm, 20-30 cm, etc.). The stimuli presentation distances for the rattlesnakes ranged from 10 cm to 100 cm (maximum testing distance: 100 cm) and 70 cm to 160 cm respectively, whereas juvenile pythons were tested from 10 cm to 60 cm and adult pythons were tested from 10 cm to 100 cm. The arbitrary stimuli distance dispersal had been determined beforehand. At most one IR stimulus was applied to the rattlesnakes per minute and maximally one IR stimulus per 90 s to the pythons. The experimental sessions lasted 60 min for the rattlesnakes and adult pythons and 45 min for the juvenile pythons. Despite shorter sessions for juveniles, it was possible to apply a similar number of IR stimulus presentations to both the adult pythons and juvenile pythons per session (because they were more attentive). If a snake escaped from the platform the session was terminated. In the case of the rattlesnakes, experimenting was also terminated if the animal showed no behavioural responses to five consecutive stimuli, one of which had to be at a distance of less than 40 cm (test range: 10-100 cm) and one less than 85 cm (test range: 70-160 cm). After each session the hide box was cleaned with liquid soap and water and dried thoroughly to eliminate possible olfactory influences of the predecessor.

To test habituation, IR stimuli were presented to both the rattlesnakes and pythons from constant distances in 60 min sessions with one stimulus per 90 s at most. The rattlesnakes were tested at the distances of 30 cm, 60 cm, 90 cm and 120 cm, whereas the pythons were tested at the distances of 15 cm and 30 cm. Moreover, habituation was tested over the course of sessions.

Several precaution steps were undertaken to minimise habituation: the length of a session was restricted; rattlesnakes were not tested more often than every second day; pythons were not tested more often than every third day and did not undergo more than four experimental sessions altogether.

2.2.4 Evaluation criteria of behavioural responses

The behaviour of the snakes was scored as a response if a distinct change was observed while presenting the stimulus. The following behaviours were observed and evaluated:

***Crotalus atrox*:**

'Head jerks': The rattlesnake showed rapid lateral head movements towards the PE independently of directed movements of the body during the 10 s of IR stimulus presentation.

'Tongue-flicking': The rattlesnake showed directed tongue-flicking towards the PE. Tongue-flicking could occur once or several times. In rare cases the tongue followed the movement of the pendulum.

'Freezing': The rattlesnake paused abruptly for 2 s to 10 s during body movement.

'Fixing': The rattlesnake was coiled up, but its head was in motion. It directed its head frontally to the IR source, stopped moving and fixed it (for at least 3 s), when given an IR stimulus.

'Rattling': The rattlesnakes rattled at least once during the presentation of an IR stimulus, while their head was directed towards the PE.

***Python regius*:**

'S-Form': The upper third of the python's body tensed further in comparison to the previous video frame, so that the S-shaped posture tightened. The tense S-shaped body posture is the typical striking posture (defence or attack) for *P. regius* (own observations). To measure the posture tightening, a straight line was drawn between the marking on the head and on the second spine marking. The lengths of the line in the last frame before the S-form started and in the frame in which the snake showed the most distinctive body tension were compared to measure whether there was a minimal length reduction of at least 1 cm (see Fig. 5a). The head had to be directed frontally (± 25°) towards the PE.

'Freeze and fix': The python paused abruptly during body movement, directed its head frontally (± 25°) towards the PE and 'fixed' it for at least 3 s. In the analysis a line was drawn from the tip of the snout to the marking on the head (see Fig. 5b). This line was copied to the corresponding video frames. The position of the head had to be unaltered for at least nine frames which is equivalent to 3 s.

'Follow and fix': The python followed the movement of the pendulum with its head or in addition with its whole neck region. The reciprocation of this head/neck movement had to occur synchronously to the oscillating pendulum. A line between the tip of the snout and the

marking on the head was drawn for analysis (see Fig. 5c). This line was copied to the following frames, in which minimally half of the head had to cross the line at least three times. The head had to stay within a 25° angle.

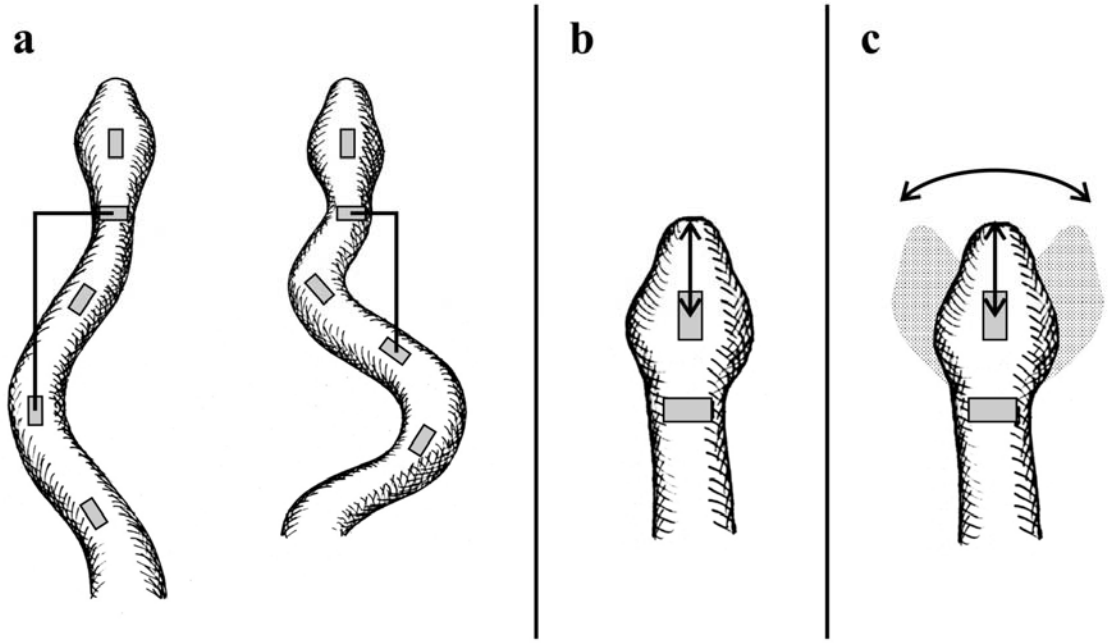

Fig. 5: Depiction of the video analysis of the python's behavioural responses. (a) 'S-form': reduction of the length of the markings of at least 1 cm; (b) 'freeze and fix': the position of the head had to be unaltered for at least 3 s; (c) 'follow and fix': minimally half of the python's head had to cross the line at least three times.

2.2.5 Control experiments for both species

The above named responses are also part of the normal, i.e. non-stimulus-evoked behavioural repertoire. To differentiate between the above defined behavioural responses and the coincidence of these behaviours, control trials were conducted. These trials were performed with 1) an oscillating pendulum but inactive PE, 2) an inactive PE and fixed pendulum (sham), or 3) using an active PE and oscillating pendulum but obscuring the pit organs with Styrofoam balls and tape. For the latter, Styrofoam was cut into small pieces ($Ø \leq 0.5$ mm) and inserted in layers into the pits. Then the whole labial pit region was covered with black duct tape.

As a further control of the evaluation of the behavioural criteria of *C. atrox*, a number of the video recordings (N=5, n=39) were scored twice, once by the experimenter and again by naïve volunteers.

2.2.6 IR images of mice

Most information dealing with body temperatures of mice and rats presents temperature values between 37 °C and 38 °C (e.g. Beynon and Cooper, 1997). Thereby, the emitted temperature of the body is not considered. However, for the behavioural experiments described above it was a prerequisite to know the emitted body temperature of the typical snake prey, i.e. mice.

Recordings with a thermoscanner (AGEMA-Thermovision THV 450 D, resolution: 0.1 °C) revealed that the emitted body temperature of laboratory mice (N=3) lies between 34 °C and 35 °C at an ambient room temperature of about 23 °C ± 1 °C. This result was confirmed by a subsequent measurement of mice (N=2) with an IR camera (IR-Flex Cam, Goratec) under similar conditions. An exemplary IR image of the temperature radiation of a mouse is depicted in Fig. 6. The image revealed a heterogeneous thermal profile of the mouse, which underlay changes when the mouse moved. The warmest radiating areas were the face region, especially the eyes and ears, and the upper neck and back region as well as the tail.

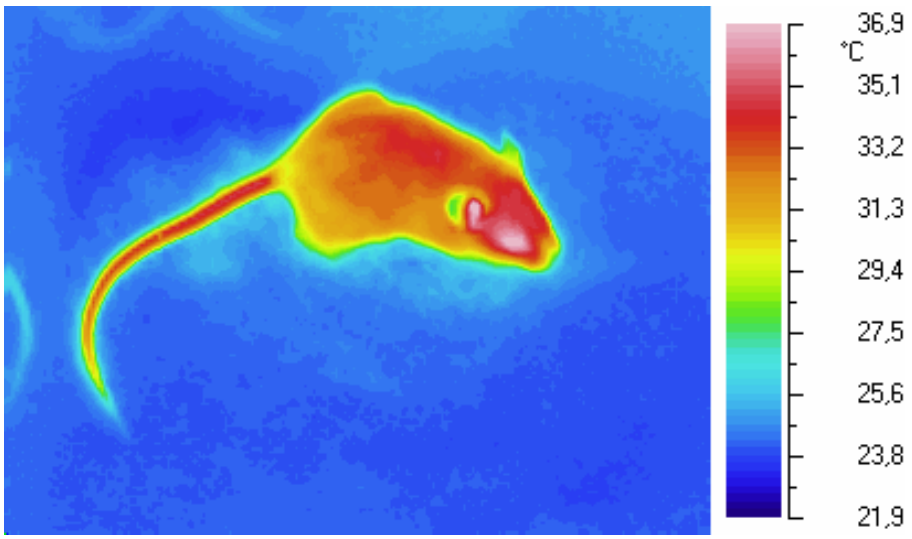

Fig. 6: The image shows the thermal profile of a laboratory mouse measured with an IR camera at an ambient temperature of about 23 °C.

2.2.7 Statistics

The applied statistical standard methods were gathered from common literature (Zoefel, 1992; Sternstein, 1996; Kesel at al., 1999). The data was statistically analysed with the aid of the calculation programmes Microsoft Office Excel (2003) and SPSS (Version 10.1) as well as OriginPro 7.0.

Chi^2 –Tests were used to determine whether a result (e.g. behavioural response rate) differed significantly from control level or equipartition. A Mann-Whitney-U-Test was used when comparing data obtained from different groups of individuals. A Friedman-Test was used to determine whether the snakes habituated over all experimental sessions.

2.2.8 Calculation of the irradiance contrast

For both rattlesnakes and pythons, the irradiance contrast of the presented IR stimulus was calculated for the respective distance range using a modified Stefan Bolzmann formula (compare de Cock Buning, 1983b). The irradiance contrast is the temperature contrast between stimulus and background.

$$\text{Irradiance contrast (W/cm}^2) = \frac{\sigma \times A \times (T_2^4 - T_1^4)}{\pi \times D^2} \text{ , where}$$

σ: constant of Stefan Bolzmann (5.6522 x 10^{-12} W/($cm^2 \cdot K^4$))
A: radiating area (cm^2)
T_2: temperature (°K) of heat exchanger
T_1: temperature (°K) of the shutter
D: distance (cm)

2.3 Anatomical investigations

In total 12 Amazon tree boas (9 juvenile and 3 adult *Corallus hortulanus*) of both sexes and one horned viper (*Vipera ammodytes*) were involved in the anatomical investigations. The snakes' ages varied from 1 month to several years with snout-vent lengths of 58 cm to 175 cm. Most boas were employed in different methodical approaches, i.e. light microscopy as well as transmission and scanning electron-microscopy, succinate dehydrogenase (SDH) staining and tracer experiments. The boas involved in the investigations of the receptor areas (SDH staining and for light and transmission electron-microscopy) were 'freshly' shedded (2 to 10 days after shedding their skin). This is important, because in boids, the intraepidermal terminal nerve masses (TNMs) are shedded and renewed periodically with each shedding cycle (Amemiya et al., 1996 a).

2.3.1 Succinate dehydrogenase staining

Six boas were anesthetised with 3-4 ml isoflurane (1-chloro-2,2,2-trifluoromethyl difluoromethyl ether, Curamed, Delta Select GmbH, Germany) in an air tight plastic box and were then decapitated with a sharp pair of scissors. For the SDH staining the (freshly)

dissected labial scales were immediately frozen and stored at -20 °C until further treatment. The labial scale rows were serially cross- or horizontally-sectioned (20 µm thick sections, see Fig. 7) with a cryostat (2700-Frigocut, Reichert-Jung, Austria) and mounted on microscopic slides (Super Frost Plus, Menzel GmbH, Germany). Thereafter, the sections were air dried for 2-3 hours at room temperature, before they were incubated in a nitro blue tetrazolium (NBT)-succinate-solution (N6876 - 500 MG, Sigma-aldrich, Germany, see appendix 8.1.1) for 3-4 hours.

SDH was successfully used by Goris et al. (1989) to stain and therewith locate the mitochondria-rich TNM areas. Therefore, as a control every other cross-section of the entire upper scale row was incubated in NBT solution without succinate, whereas the other sections were incubated with succinate. As it is succinate which evokes the enzyme reaction in the mitochondria and stains the mitochondria in the TNMs, solutions without succinate should fail to stain the cross-sections.

After phosphate buffer washing, the sections were dehydrated with a graded ethanol series, transferred into isopropanol and xylene, and covered with glass slides. The sections were investigated with a light microscope (Leitz DM RBE, Germany) and used for the examination of size and placement of the IR-receptive areas. The dimensions of the SDH-stained individual TNM areas were measured with the aid of a micrometer mounted on a microscope, the respective distances of sections and losses in between (in total 6 %) considered, and plotted onto the photograph of the labial scale of the investigated boa.

Pictures were taken with a digital camera (Nikon Coolpix 950, Japan) of the head and of all sections with the aid of a microscope.

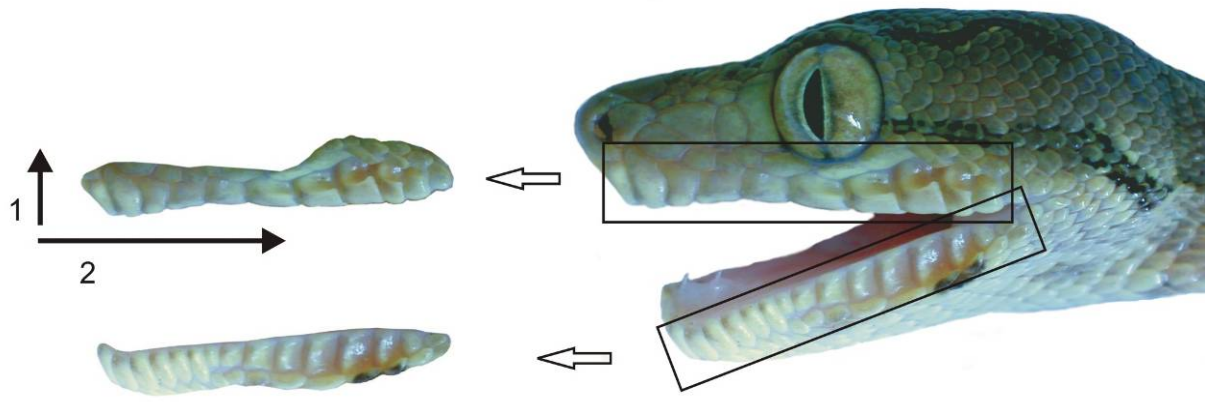

Fig. 7: The dissected supra- and infralabial scale rows are depicted, as well as the two cutting planes for the 1: cross-sections and 2: horizontal-sections.

One horned viper (*V. ammodytes*) was used as a control. Since representatives of vipers are not IR sensitive, no TNMs are expected in the labial scales, hence no SDH staining should occur. The dissected labial scale row of one side (see Fig. 8) was serially cross-sectioned (20 µm). The SDH staining procedure was identical to that of the boas and conducted simultaneously.

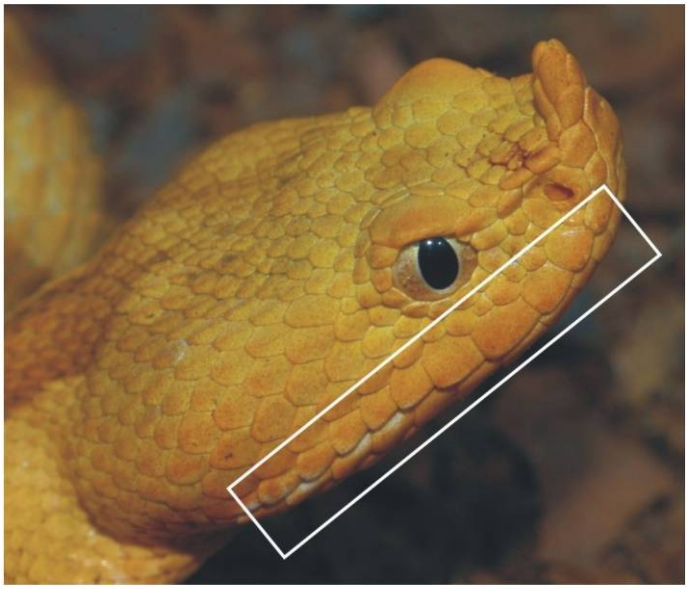

Fig. 8: As a control investigation the dissected supralabial scale row (see white frame) of the viper *V. ammodytes* was stained with SDH.

2.3.2 Light microscopy and transmission electron-microscopy

For the investigation of the ultra-structure of the IR-receptive areas a juvenile and an adult boa were used. The juvenile boa (age: 1 month, snout-vent length: 53 cm) was anaesthetised with 3-4 ml isoflurane and dispatched, before the labial scale rows and control areas (scales of the head and neck area) were dissected. The adult boa (age: at least 3 years, snout-vent length: 175 cm) underwent a perfusion procedure before decapitation. It was anaesthetised with (3-4 ml) isoflurane and in addition treated with an injection of ketamin (60 mg/kg body mass, Curamed, Delta Select GmbH, Germany) to relax the muscles and to immobilize the boa. Then, the snake was perfused on ice by rinsing with 0.1 M and 325 mOsm phosphate buffer at pH 7.2 using a catheter inserted in the left aortic arch, followed for at least 20 minutes by a 2.5 % glutardialdehyde fixation in 0.1 M phosphate buffer. After decapitation, the labial scale rows and control areas were dissected.

The dissected labial scale rows and control scales of the boas were prepared for electron microscopy. Fixation was carried out by incubation in a 2.5 % glutardialdehyde in 0.1 M

phosphate buffer solution (325 mOsm, pH=7.2) overnight. The samples were washed with phosphate and cacodylate buffer and fixed in 1.5 % osmium tetroxide for 2 hours in 0.1 M cacodylate buffer (400 mOsm, pH=7.1). After dehydrating with a graded ethanol series, the samples were embedded in Epon 812 (see appendix 8.1.2 for detailed procedure description). Semi-thin cross sections (0.5 µm) were cut with glass knives (Plano GmbH, Germany) as well as with a diamond knife (Diatom, Switzerland) on a microtome (OMU 3, Reichert, Austria). The semi-thin sections were stained with a 0.05 % toluidine blue-borax-solution (for about 1 min) and examined with a light microscope (Leitz DM RBE, Germany). Occasionally, when TNM areas were visible in the semi-thin sections, ultra-thin (60-80 nm) sections were prepared for transmission electron-microscopy (TEM) with a diamond knife (DDK, Delaware Inc., USA) on an ultracut microtome (Reichert-Jung, Austria). The ultra-thin sections were stained with uranyl acetate and lead citrate according to the standard procedure (see appendix 8.1.2.3). Examination was conducted with a transmission electron microscope (Zeiss EM 109, Germany).

TEM picture slides (Ilford Pan F 50 Plus) were taken with the installed camera of the TEM. The picture negatives were scanned (Epson F3200) and edited with the programmes Adobe Photoshop® (Version 7.0, Adobe® Systems Incorporated 2007) and Corel Draw (Version 12, Corel Corporation 2007).

3-D reconstruction of an exemplary IR sensitive labial scale area

A series of 230 semi-thin sections covering a region of 3740 µm in length (i.e. rostral caudal extent along the supralabial scale) were used for the reconstruction of the exact position and dimension of the TNM areas of the three last caudal supralabial scale depressions (8^{th}, 9^{th} and 10^{th}) of the left side of the head. For this purpose the semi-thin sections were photographed with a Nikon Coolpix 950 (Japan). The digital images were fed into the graphic programme The GIMP (Version 2.2.10, http://docs.gimp.org/) to trace the outline of the epidermal layer of the sections and to mark the position of the TNM areas (see Fig. 9). The data was then transferred to the software Amira (Version 3.0, TGS Inc., San Diego, USA), which was used for the 3-D reconstruction. The respective distances between the sections were calculated, the losses of semi-thin sections in between (in total 5 %) were also considered.

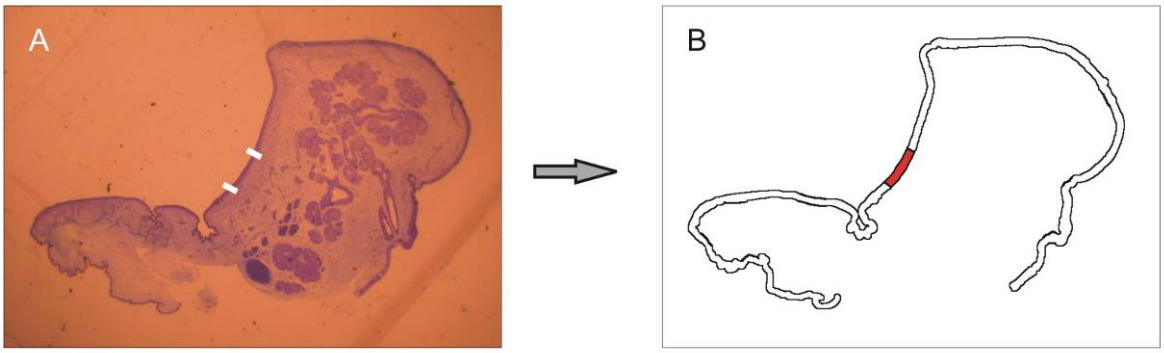

Fig. 9: (A) The location of the TNMs in the semi-thin sections was marked and the outline of the semi-thin sections was traced. (B) Both pieces of information were combined and functioned as the basis for the 3-D reconstruction.

2.3.3 Scanning electron microscopy

For the investigation of the scale surfaces by means of scanning electron microscopy (SEM), three boas were anaesthetised with 3-4 ml isoflurane and decapitated. The supra- and infralabial scale rows and scales from control areas (e.g. upper head and neck region as well as dorsal and ventral body scales, see Fig. 10) were dissected. The scale tissue was kept in 70 % ethanol until further processing. Prior to the dehydration procedure, the samples were cleaned in an ultrasonic water basin for 30-40 s. The labial scale tissue was dehydrated by a graded ethanol series (80 % (for 1h), 90 %, 96 %, 100 %, isopropanol (I-II), 15 min in each), immersed in a hexamethyldisilazane (HMDS; Art. 3840.2, Roth, Germany) and isopropanol solution in a ratio 1:1 and then in pure HMDS for 5 min. Thereafter, the material was allowed to air dry for at least 24 hours at room temperature.

HMDS has been used with success on a variety of insect tissues (Nation, 1983). Therefore HMDS was chosen, because, according to Nation (1983), it avoids shrinking or distortion of the tissue and thus preserves good surface detail.

After drying, the sample was mounted on standard stainless steel stubs with carbon glue (Leit-C, Neubauer, Germany) and allowed to dry before it was sputter-coated with a (palladium) gold layer (thickness: 30 nm) and inspected with a scanning electron microscope (SEM) (Leo 440i, Leica, Nensheim; Cambridge Stereoscan 200) at a magnification factor of about 21000.

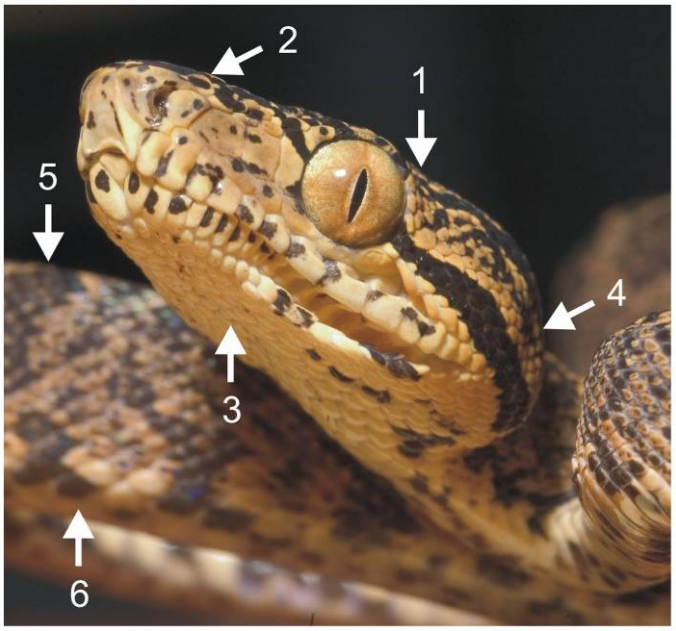

Fig. 10: Aside from the scale surfaces of the supra- and infralabial scale row several other control areas were investigated by SEM: 1, 2: upper head region; 3: lower head region; 4: neck region; 5: dorsal body scales; 6: ventral body scales.

Scanning electron microscope picture analysis

In order to investigate surface pores of the labial scales, the magnification of the SEM pictures had to be standardized: in each picture 9 μm^2 of the upper right corner was taken (see Fig. 11 (step 1)). Then, the SEM pictures were imported into a graphic programme (The GIMP, Version 2.2.10, http://docs.gimp.org/). There, in the first step, the black and white values were emphasized (via filter function). Then, the colour threshold value was shifted towards black, i.e. dark grey values turned black and the light ones white (see Fig. 11 (step 2)). A self-programmed Matlab file (Version 6.5, The Mathworks Inc., USA) enabled a qualitative analysis of the pore areas (in percent) by comparing the black and white parts of the SEM pictures.

The ratio of the pore (black) to the non-pore (white) areas as well as the total number of pores of the respective excerpt was calculated. The truncated pore areas in the margin region of the analysed excerpts were only valued if they were of the same size or larger than the smallest complete pore area of the respective excerpt.

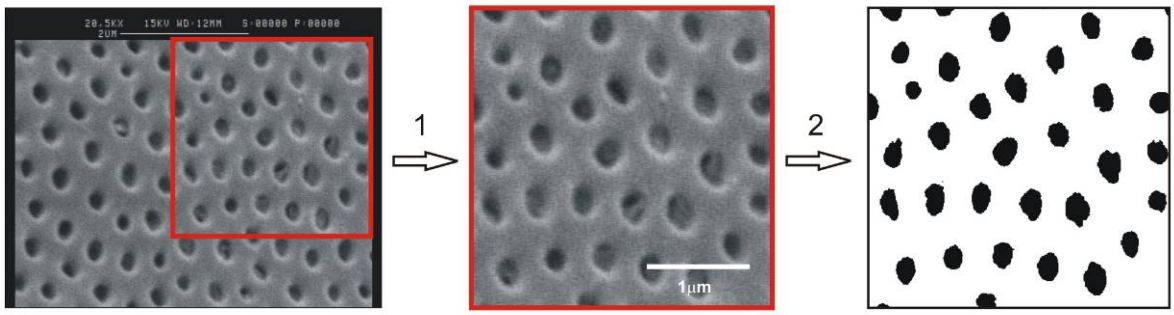

Fig. 11: The SEM pictures were standardized (step 1) and converted into black and white (step 2), before the ratios of the pore areas (black) and non-pore areas (white) were calculated.

2.3.4 Tracing experiments

In total 7 boas (4 juveniles and 3 adults) were involved in the tracing experiments. In all experiments the boas were anaesthetised with 3-5 ml isoflurane (Curamed, Delta Select GmbH, Germany). Then, the skin of the respective labial scales was scraped off with a sharp scalpel and/or a needle. The tracer, usually biotinylated dextran amine (BDA) and in one case biocytin (see boa 7, appendix 8.2, Tab. 9), was applied with a needle and rubbed into the injury with a drop of distilled water. Thereafter, the boas lived for varying periods of time (2-10 days, see appendix 8.2, Tab. 9) before they were again anaesthetised and finally dispatched. After decapitation, the brain was immediately dissected and fixed in a 4 %-paraformaldehyde solution with 0.1 M phosphate buffer for two days in a fridge (6 °C). Before the brain was embedded in agar (4 %) the remaining parts of the meninges of the brain were removed. The relevant brain area (grey square, Fig. 12) was cut cross-sectionally (cutting plane: grey arrow, Fig. 12) into 100 µm slices with a razor-blade using a vibratom (752M Vibroslice, Campden Instrumentals Ltd., UK). The slices were treated with ABC-Kit (Elite PK-6100 standard, Vector Laboratories, USA) before they were stained with triton-diaminobenzidin(DAB)-solution. For a precise description of the AB-Complex treatment and staining procedure see appendix 8.1.3.1. The brain slices were examined with a light microscope (Leitz DM RBE).

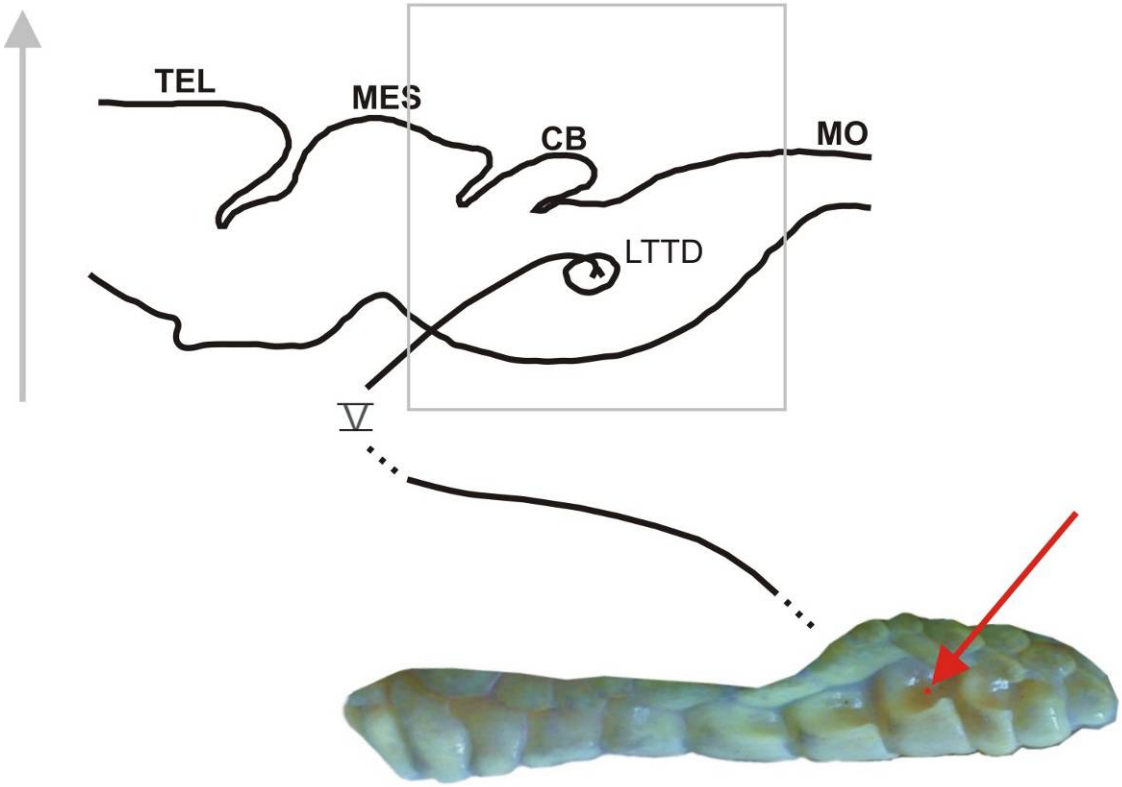

Fig. 12: The tracer was applied to the TNMs of the selected labial scale area (here: the red arrow depicts the location of the BDA tracer application on the backward-pointing scale area in the second last caudal depression of the left supralabial scale row). The tracer was allowed a certain amount of 'running time' (e.g. seven days) via the dendrites of the trigeminal nerve leading to the Nervus trigeminus (V) to reach the LTTD in the Medulla oblongata (MO).

The experimental procedure for each boa differed slightly to test for possible influences on the result, since only the very first experiment was successful and could not be clearly repeated thereafter (compare results, 3.2.4). In the successful case, the BDA tracer (MW 3000, Lot: 65A11, Molecular Probes, Eugene, USA) was applied onto the backward-pointing scale area on the left second caudal supralabial depression (see Fig. 12), as well as on the backward-pointing scale area on the right second rostral infralabial depression. The tracer was allowed a running time of seven days. The respective differences in the following experiments (e.g. location of the tracer application, tracer and the time of survival) are shown in the appendix (appendix 8.2, Tab. 9).

After successful staining the relevant brain slices were dyed with neutral red (Sigma-Aldrich, Germany) by following the typical standard procedure (see appendix 8.1.3.2). The digital picture of the brain section shown in the results (3.2.4, Fig. 35) was only edited in brightness, contrast and colour intensity.

2.3.5 Cast of a boa head as a functional model

A cast of a *C. hortulanus* head made out of plaster was built as a functional model for the receptive areas of IR radiation. A decapitated head of an adult boa was kept in fixative (see appendix 8.1.4). The head was entirely covered with one component silicone (734, Dow Corning Corp., Germany) in multiple layers and was allowed to dry thoroughly. The silicone was stiff enough to maintain the exact proportions of the head. The silicone layer was cut longitudinally and carefully pulled off the head. The cut was pasted with silicone and the cast was filled with plaster, which was allowed to dry overnight (Ceramofix casting powder, Eberhard Faber GmbH, Germany). The silicone was removed and the TNM areas were marked in colour onto the cast, using the measurements of the size and placement of the SDH stained areas of the cross-sections. For this purpose acrylic matt paint (Marabuwerke GmbH, Germany) in four different colours was painted onto the cast with a fine hair brush under a dissecting microscope (Zeiss, Germany). The upper labial TNM areas pointing forwards were coloured in blue and the areas pointing backward in red. In contrast the TNM areas at the lower labial scales pointing forward were coloured in yellow and the areas pointing backward in green (see Fig. 13).

The boa cast was mounted on a tripod with its reference point positioned in the centre of a perimeter. The reference point on the cast was the centre between the eyes at the height of the lower edge of the supralabial scale row. A position fixed camera (Nikon D200, Japan) with a macro lens (Nikon AF-S Micro Nikkor 105mm 1:2,8 G ED VR, Japan) was directed towards the reference point in the same horizontal and vertical plane, at a distance of 20 cm.

Pictures of (the left side of) the cast in the horizontal and vertical plane were taken in different angles by adjusting the orientation of the boa cast in the perimeter: different angles in the horizontal plane (starting from – 40° in 10° steps to the front of the head (0°) and then up to 150°, see Fig. 13), under three conditions in the vertical plane: 1. horizontal head position (0°), 2. head pointing upwards in a 45° angle (+45°), 3. head pointing downwards in a 45° angle (-45°). To consider the complete receptive field of view the angle range of 0° to 40° had to be included because frontal IR radiation impinges on both sides of the head.

Each of the different coloured areas of the labial depressions were measured for the respective angle and their total area size was calculated with the image processing and analysis programme ImageJ (Version 1.3; Rasband, 1997-2006) and calculated with Excel (Version 2003, Microsoft). The values of the TNM areas from the left side of the head of a single individual served as the basis for the reconstruction of the infrared-receptive field of view.

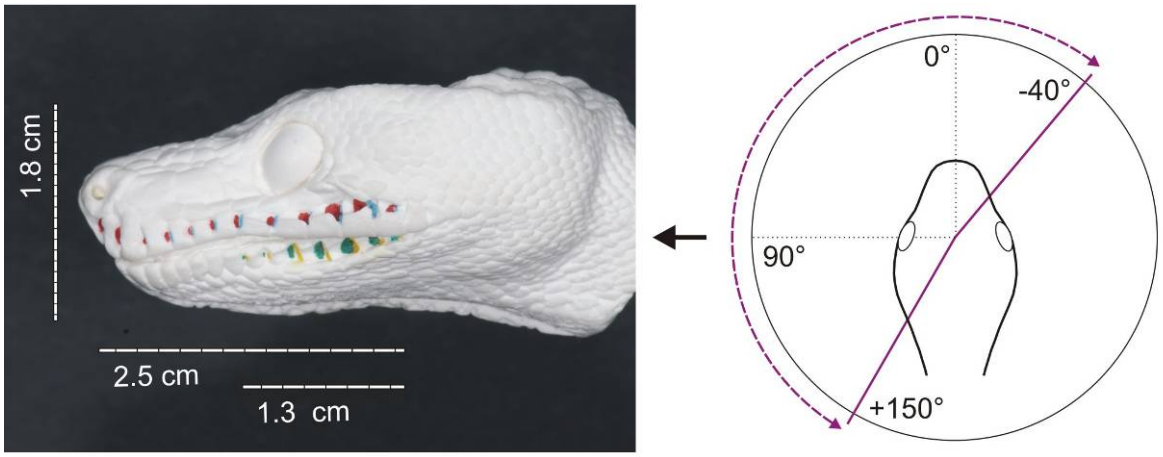

Fig. 13: Exemplary picture of the boas head cast photographed in a 90° angle in the horizontal plane and head position. The differently coloured TNM areas in the depressions of the supra- and infralabial scale rows and their length are shown as well as the height of the head cast. The purple dotted circle line depicts the complete rotational angle of the photographed cast ranging from -40° over the frontal head position (0°) to 150°.

3 Results

3.1 Behavioural experiments

3.1.1 Behavioural responses of *Crotalus atrox*

During 130 experimental sessions the rattlesnakes (N=12) were exposed to 1705 IR stimuli, offered at distances between 10 cm and 160 cm. In 1655 cases the snakes' responses could be scored unequivocally; the remaining 50 trials produced equivocal results and were not included in the data analysis. Of the 1655 unequivocal trails, 760 trails produced a positive response. At distances of up to 100 cm ($10 \leq N \leq 12$) 80 sessions with 1304 stimuli were conducted, and within the distance range of 70 cm to 160 cm ($7 \leq N \leq 12$) 50 sessions with 396 stimuli (see also Tab. 1) were conducted. Data from these two separate acquisition sets was pooled for the overlapping distances (70–100 cm).

Tab. 1: Overview of the databases for the analysis of *C. atrox´* responses and control experiments.

Experiment	**Number of Animals**	**Number of Sessions**	**Number of IR Stimuli Settings**	**Remarks**
IR detection range	12	130	1655	80 sessions with 1304 stimuli presentations (up to 100 cm) 50 sessions with 396 stimuli presentations (from 70-160 cm)
control experiment for hidden cues	9	9	108	cold PE
control experiment to assess spontaneous response-like behaviour	8	8	158	sham experiment: fictive IR stimuli, i.e. inactive PE
control experiment with blocked pit organs	4	8	201	IR stimuli at close distances (≤32 cm)
habituation	6	24	292	Four constant distances (30, 60, 90, 120 cm)
control of response assessment	5	5	39	

The rattlesnakes responded to the IR stimulus with a variety of combinations of the five classified behavioural reactions (see 2.2.4), of which only 'tongue flicking' (29.2 %), 'head jerks' (4 %) and 'fixing' (1.8 %) occurred solitarily. 'Freezing' and 'rattling' only occurred in combination with 'tongue flicking' and/or 'head jerks' and/or 'fixing'. Four main responses

were observed, which amount to 82 % of all positively-scored responses. These responses were stimulus-directed 'tongue-flicking' (29.2 %), 'head jerks' and 'tongue-flicking' (21.8 %), 'tongue-flicking' and 'fixing' (15.6 %), and 'head jerks' in combination with 'tongue-flicking' and 'fixing' (15.2 %). Other combinations of behavioural responses including 'rattling' and 'freezing' did not exceed 3 % occurrence in any combination. The proportions of the (total number of) behavioural responses (solitarily or in combination) exceeding 2 % are depicted in the respective 15 distance intervals in Fig. 14.

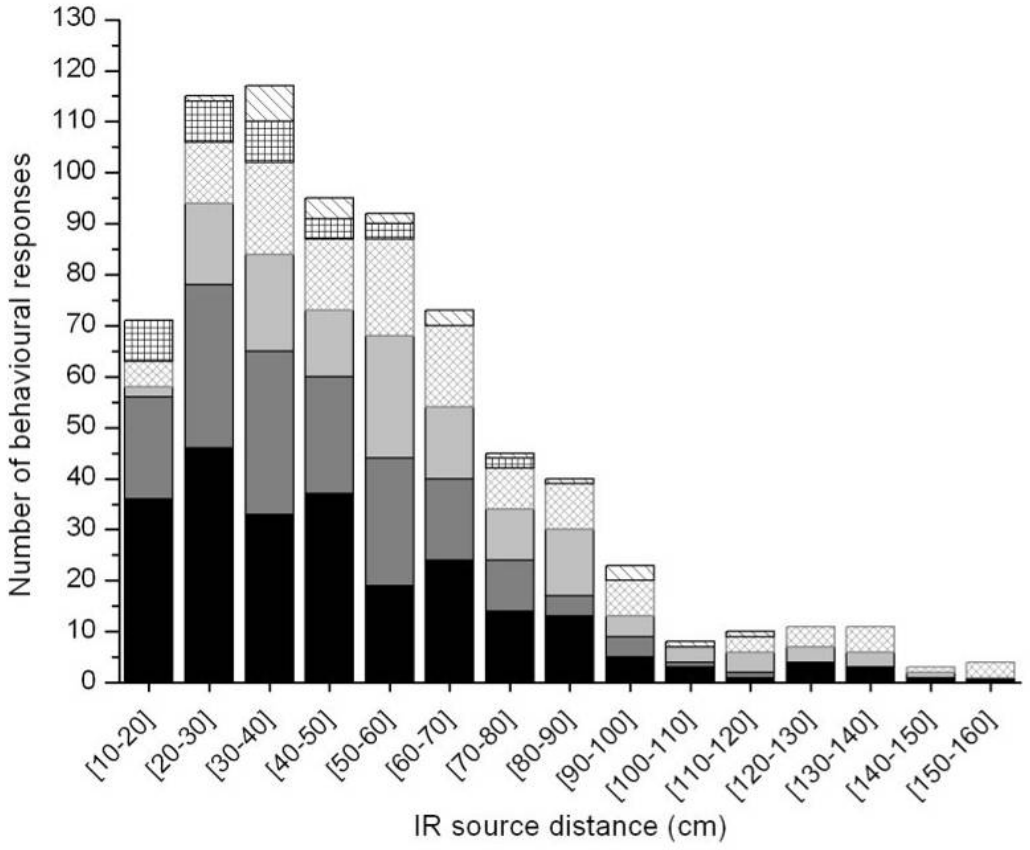

Fig. 14: Total number of positive behavioural responses shown over the IR stimulus distance intervals (class width: 10 cm). Behaviours are broken down into 'tongue flicking' (black), 'tongue flicking and head jerk' (dark grey), 'tongue flicking and fixing' (light grey), 'head jerk, tongue flicking and fixing' (rhombic grey pattern), 'head jerk' (chequered pattern), and 'head jerk and fixing' (striped).

Positive responses (pooled in 10 cm distance classes) ranged from 67 % (shortest source distance: 10 cm) to 13 % (farthest source distance: 160 cm) (see Fig. 15). The relationship between source distance and response rate was not constant; the response rate roughly remained constant between 50 cm and 80 cm source distance, and decreased sharply beyond the 100 cm source distance (Fig. 15). At 100 cm the response rate was significantly above

(Chi^2 = 12.202, df = 1, p = 0.0001) the control level of 29 % (see below 3.1.1.1), but beyond 100 cm values the snakes' responses to the stimulus cannot be distinguished from the control level (Chi^2 = 0.301, df = 1, p = 0.787).

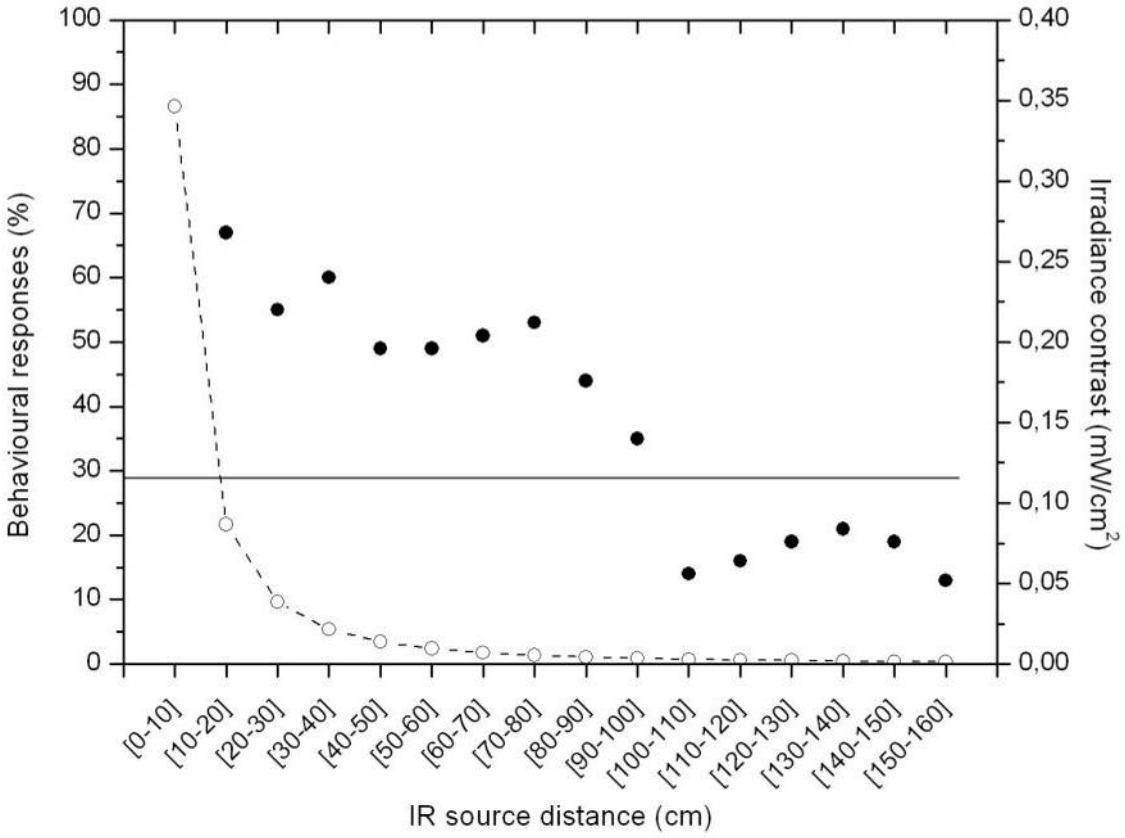

Fig. 15: Percentages of behavioural responses as a function of IR source distance (black dots). Class width was 10 cm. Dotted line: Irradiance contrast of the IR stimulus calculated in mW/cm^2 and plotted as a function of the distance. Solid line: Baseline of spontaneously occurring behaviour (i.e. non-stimulus-bound behaviour) resulting from control trial data.

3.1.1.1 Control experiments

As expected, individual rattlesnakes responded at different rates during the control trials. Overall, the following ranges of positive responses were observed: trials with oscillating pendulum but inactive PE (0 % - 29 %), inactive pendulum and inactive PE (0 % - 22 %), and blocked pit organs (0 % - 13 %). The highest positive response rate observed (29 %) is taken as the control level or baseline.

3.1.1.2 Control of response assessment

In addition to the experimenter two further control persons independently assessed the behaviour of the rattlesnakes. Five snakes were exposed to 39 IR stimuli in five sessions. One person judged three cases (8 %) differently from the experimenter and the second person two cases (5 %). In all but one case the behavioural responses were judged more critically (i.e. 'no response') by the experimenter.

3.1.1.3 Habituation

IR stimuli were presented at a distance of 30 cm (N=6, $10 \leq n \leq 37$), 60 cm (N=6, $7 \leq n \leq 29$), 90 cm (N=6, $4 \leq n \leq 18$) and 120 cm (N=6, $5 \leq n \leq 9$) (see Fig. 16). All rattlesnakes (N=8) habituated to the IR stimuli. The percentage of positive responses decreased with increasing stimulus number and with increasing IR source distance. However, the habituation curves of individual rattlesnakes differed. For instance, at a distance of 30 cm one snake responded to the first six stimuli in 67 % of the cases, thereafter no responses occurred. At the distance of 30 cm another individual responded to the IR stimuli with the same percentage even after 30 stimulus presentations.

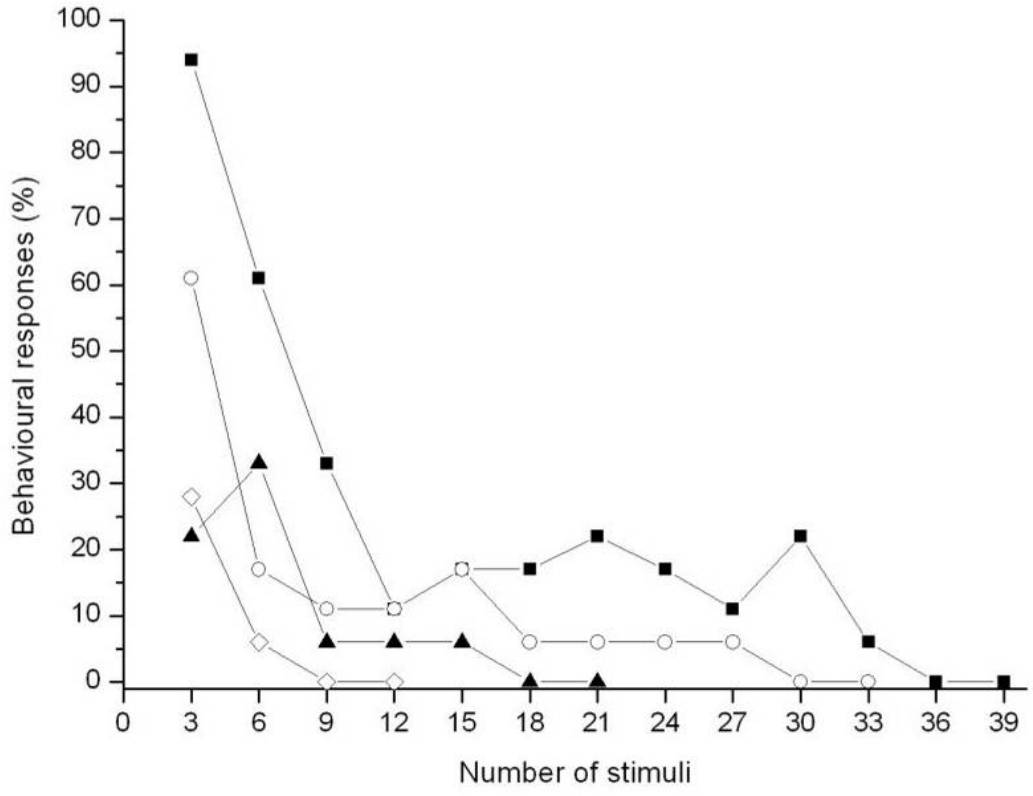

Fig. 16: Behavioural responses plotted as a function of repeated stimulation for four different distances. Note the response decrement to IR stimuli (N=6, in each case three consecutive responses were pooled) at the distances 30 cm (squares), 60 cm (dots), 90 cm (triangles) and 120 cm (diamonds).

3.1.2 Behavioural responses of *Python regius*

In total 1552 IR stimuli were presented to *Python regius* (N=22) in 79 experimental sessions with 20 stimulus presentations per session on average (see below). Thereof, 140 IR-stimulus presentations produced ambiguous results and were excluded from data analysis. In these cases the snakes had left the experimental platform or technical difficulties had led to an abortion of the recording. In the remaining 1412 IR stimulus presentations the pythons responses could be scored unequivocally. Of these, 221 stimulus presentations evoked positive responses (see also Tab. 2). The IR stimulus presentations and the responses were pooled in distance classes of 10 cm. Video analysis allowed a precise evaluation of the behavioural responses and furthermore a verification of the experimenter's unbiased assessment by control persons.

Tab. 2: Overview of the database for the analysis of *P. regius´* responses and control experiments.

Experiment	Number of animals	Number of sessions	Number of IR stimuli presentations	Remarks
IR stimulus detection distance	18	79	1412	juvenile & adult pythons
control experiment for hidden cues	6	6	116	cold but moving PE
control experiment to assess spontaneous response-like behaviour	6	6	355	sham experiment: fictive IR stimulus, i.e. inactive PE
control experiment with blocked pit organs	6	6	93	IR stimulus presentations at close distances (≤ 30 cm)
habituation	12	12	245	two constant distances (15, 30 cm)

Three main behavioural reactions were observed during IR stimulus presentations and evaluated. These responses were the 'S-form' (36.2 %), 'freezing and fixing' (31.9 %) and 'following and fixing' (2.8 %). These responses also occurred in combination: 'S-form' with 'freezing and fixing' (17.4 %), 'S-form' with 'following and fixing' (9.4 %), 'following and fixing' with 'freezing and fixing' (1.9 %) and all three combined (0.5 %). The proportions of the (total number of) behavioural responses exceeding 2 % are depicted in Fig. 17 in the respective distance intervals.

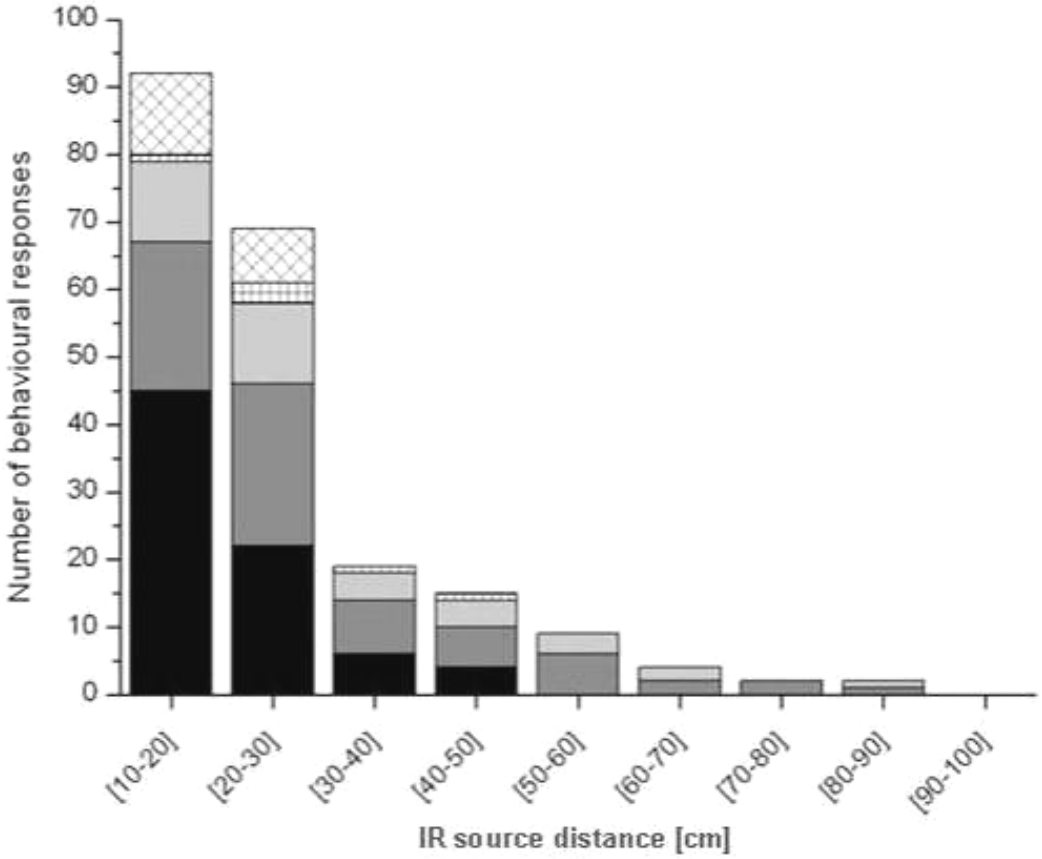

Fig. 17: Total number of positive behavioural responses shown over the IR-stimulus distance intervals (class width: 10 cm). Behaviours are broken down into 'S-form' (black), 'freeze and fix' (dark grey), 'S-form' with 'freeze and fix' (light grey), 'follow and fix' (chequered pattern) and 'S-form' with 'follow and fix' (rhombic pattern).

Assuming that the body length might influence the behavioural reaction to the IR stimulus at farther distances (within the snakes´ direct reach), adult pythons (N=8) were tested up to distances of 100 cm, whereas juvenile pythons (N=10) were tested up to 60 cm. All other experimental conditions were identical. The Mann-Whitney-U-Test showed no significant difference in the response behaviour of juvenile and adult pythons (10-20 cm interval: N_1=10, N_2=8, U=38.5, p=0.897; 20-30 cm interval: N_1=10, N_2=8, U=29, p=0.36; 30-40 cm interval: N_1=10, N_2=8, U=28.5, p=0.315) (Fig. 18). Therefore, data from all individuals were pooled. In any case, the adult pythons did not consistently respond to stimuli greater than 60 cm.

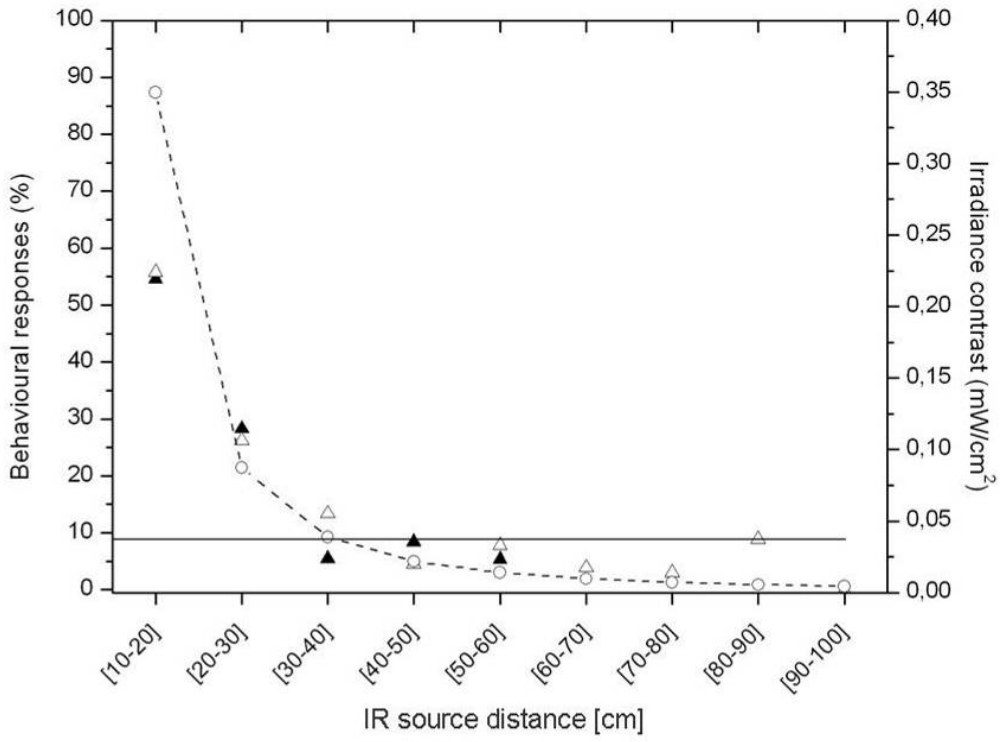

Fig. 18: Relative behavioural responses of juvenile (black triangles) and adult (white triangles) pythons as a function of IR source distance. Class width was 10 cm. Dotted line with white dots: Irradiance contrast of the IR stimulus calculated in mW/cm^2 and plotted as a function of distance. Solid line: Baseline of spontaneously occurring behaviour resulting from control data.

The decline of the irradiance contrast of the IR source over the increasing distance is shown in Fig. 18. The behavioural response rate followed the decline. It dropped below the control level of 8.6 % (see below 3.1.2.1) in the 30-40 cm interval. Single behavioural responses of single individuals occurred up to 90 cm. One individual responded quite continuously over all distance intervals to the IR stimulus. As there were very few IR stimulus presentations for the interval 80-90 cm this resulted in a high response rate value for this interval. However, as this response rate value does not differ from the baseline, it is considered to be not significant.

The pythons only significantly responded up to a distance of 30 cm. The response rate in the distance intervals up to 30 cm is significantly above (Chi^2=54.731, df=1, p=0.0001) the control level of 8.6 %, but beyond 30 cm distances the python's responses to the IR stimulus cannot be distinguished from the control responses (Chi^2=1.596, df=1, p=0.138).

3.1.2.1 Control experiments

The pythons responded individually at different rates during the control trials. The following positive responses were observed: trials with an oscillating but inactive PE (8.6 %), trials with

a non-moving and inactive PE (2.5 %), and trials with an oscillating and active PE, whilst the pit organs were blocked (3.3 %). The highest average positive response rate (8.6 %) was taken as the control level.

3.1.2.2 Habituation

To test habituation, IR stimuli were presented at two constant distances (see Fig. 19). At a distance of 15 cm (N=6, $15 \leq n \leq 25$) the percentage of positive responses decreased with increasing stimulus number. At most 21 stimulus presentations were responded to consecutively. The results of the samples were significantly different from equipartition (Chi^2=18.168, df=8, p=0.019), which shows that the pythons habituated at this distance.

Stimuli presentations at 30 cm distance (N=6, $15 \leq n \leq 30$) hardly evoked any responses (in 7.3 % of the cases), and therefore did not allow any conclusions about habituation.

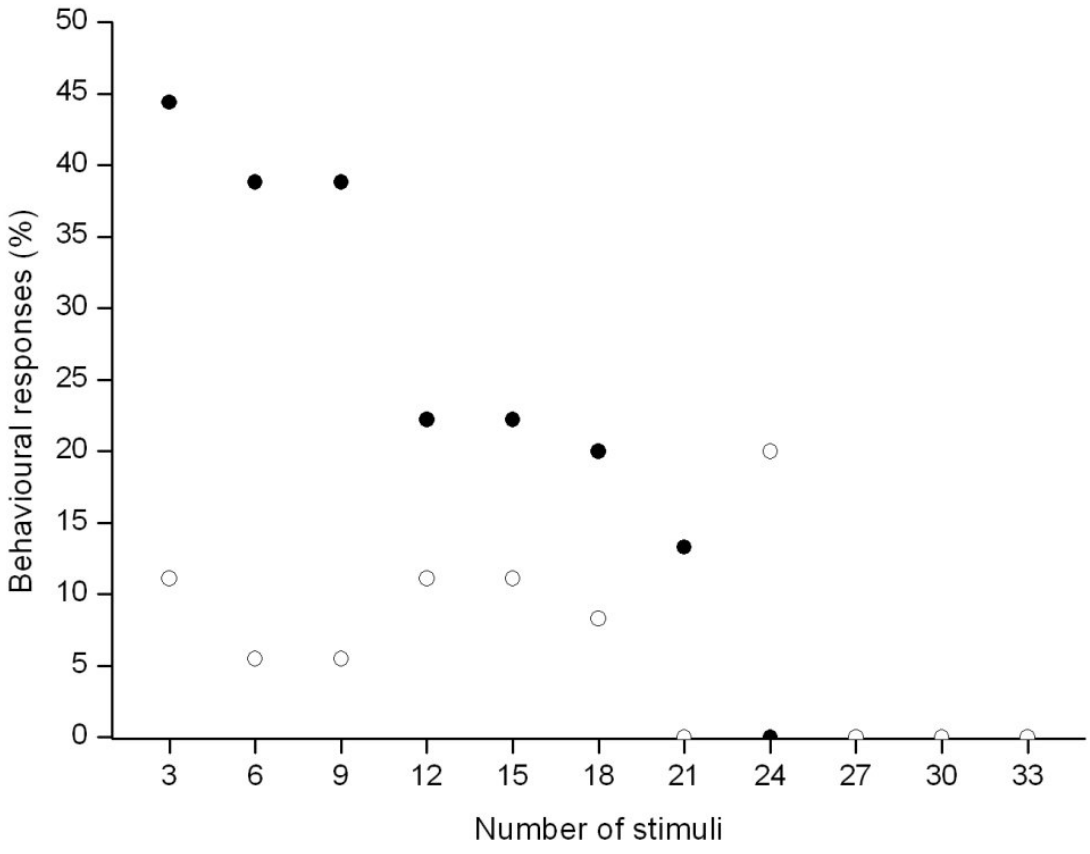

Fig. 19: Relative behavioural responses plotted as a function of repeated stimulation for the distances of 15 cm (black dots) and 30 cm (circle).

In addition, the habituation effect over the course of sessions (only main sessions) was investigated. The Friedman-Test (Chi^2=2.719, df=3, p=0.437) revealed that the pythons (N=18) did not habituate over the course of all main experimental sessions.

3.1.2.3 Video analysis versus direct response assessment

In contrast to the real time evaluation of the rattlesnake experiments, all of the experimental sessions with pythons were evaluated from videotape, as well as in real time during the experiments. Ninety-eight percent of the real-time evaluated behavioural responses were identical to the results of the independently re-evaluated video recordings. The remaining 2 % of the responses were assessed more critically during direct evaluation.

3.2 Anatomical investigations

C. hortulanus´ labial scale morphology is especially conspicuous in the frontal region of the supralabial scale row, showing zigzag-shaped depressions between the front scale and the two following rostral scales on each side of the head, as well as from the 6th scale on, where they form zigzag-shaped deep folds with ridges in between. Moreover, the 8th to the 10th supralabial caudal scales possess an outgrowth on the bottom edge, which partly shields the scale emarginations and depressions, just as the bulge of the scale row above the supralabials does. The infralabial scales however, only possess deep depressions in approximately the caudal half of the labial scale rows.

3.2.1 Succinate dehydrogenase staining experiments

The cross- and horizontal cryostat sections of the entire supra- and infralabial scale rows revealed TNMs that are especially rich in mitochondrial enzyme succinate dehydrogenase (SDH) (Fig. 20 and Fig. 21). The control sections, which were incubated in NBT solution without succinate, did not show any stained structures. This clearly confirmed that SDH is an excellent marker for the presence of TNMs in the labial scales. In contrast to those of the boa, sections of labial scales of the IR non-sensitive horned viper (*V. ammodytes*) were not stained by SDH, again confirming that the SDH staining is specific for IR receptors.

The size of the stained areas varied depending on the investigated section of the scale (see encircled purple areas in Fig. 20). The stained areas occurred in a repetitive pattern (Fig. 21), namely in the fundus of the depressions, with unstained areas in between.

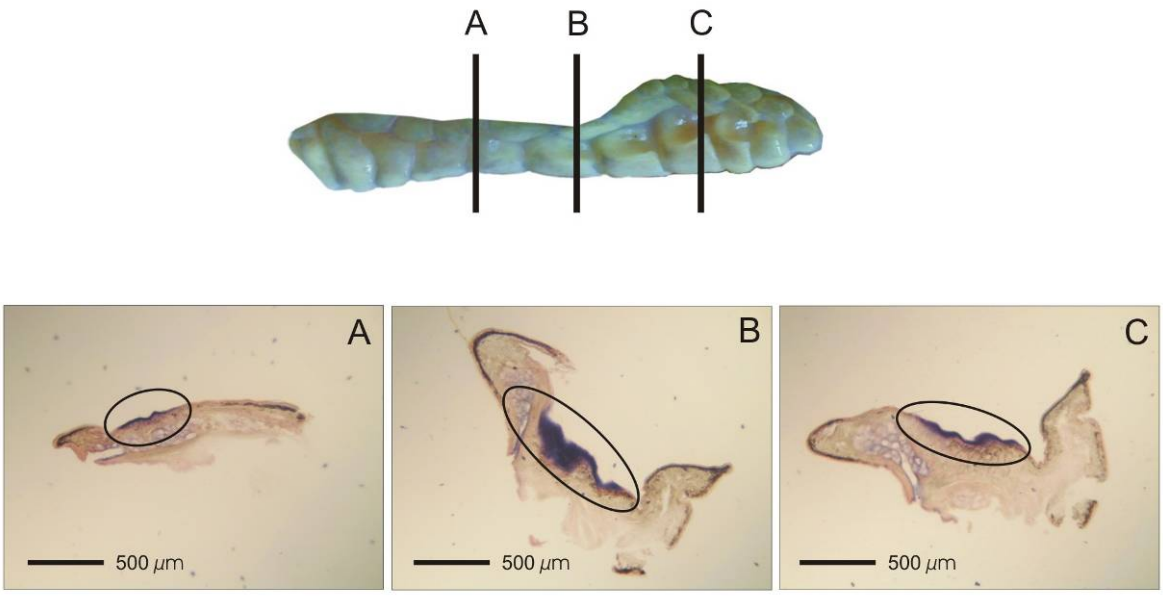

Fig. 20: Three exemplary cross-sections (20 µm) with SDH-stained TNM areas (encircled in black) along the supralabial scale row (for location see black bars above). Section orientation guide: left part of the section is the edge of the upper lip; right is the upper part of the supralabial scale; top is the surface of the supralabial scale; bottom is the inner tissue of the supralabial scale. Only the encircled areas are SDH stained, all other darker areas result from pigmentation.

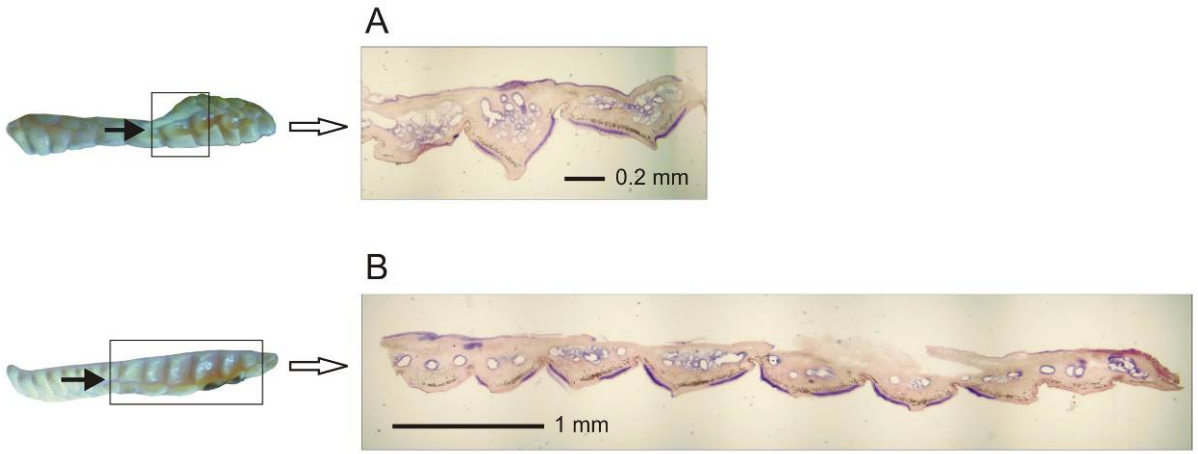

Fig. 21: Horizontal-sections of A) two depressions of the supralabial scale and B) the entire caudal infralabial scale area (see black box on the respective labial scale, black arrow on the left depicts the cutting plane). Overlapping areas of the digital pictures were put together in one picture. Section orientation: top is the interior tissue of the scales, bottom is the outer edges of the scales. TNM areas are stained in blue along the scale surface (compare also Fig. 20).

Both, the supra- and the infralabial scale rows were stained. The horizontal-sections of the supralabial scale row and their staining are similar to the infralabial scale row (see Fig. 21).

However, in contrast to the supralabial scale row only the caudal half of the infralabial scale row was stained, since the TNMs are only present there.

The horizontal-sections show that all labial scale depressions contain TNM areas. The length sizes of the SDH-stained TNM areas in the cross-sections of the supralabial scale row ranged from 3 µm up to 82 µm. The cross-sections of the infralabial scale row revealed TNM area length sizes of 1 µm up to 62 µm. The cryostat sections are only partially dimensionally stable due to straining. However, the results allow an approximation of the dimensions of the TNM areas along the supra- and infralabial scale row (see Fig. 22).

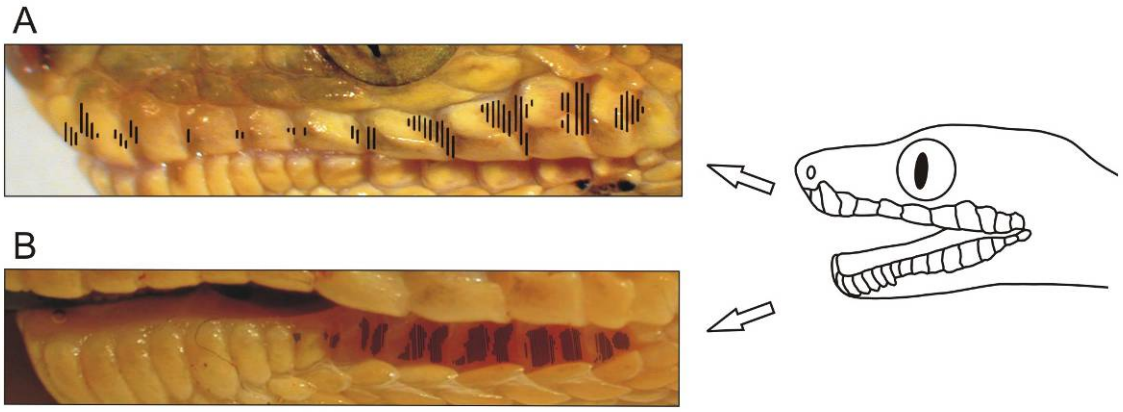

Fig. 22: Reconstruction of the size and location of the TNM areas (hatched in black) for the A) supra- and B) infralabial scale row drawn onto a photograph of the snakes´ labial scales.

The reconstruction reveals that the TNM areas are only situated within the labial depressions. The size of the depressions varies (see Fig. 22 A, B) as well as the size of the TNM areas. The 3rd to the 5th supralabial depressions are much shallower and narrower than the others and have much smaller TNM areas (Fig. 22 A). The dimensions of the TNM areas in the infralabial depressions are similar except the first two, which are distinctly smaller (Fig. 22 B). The TNM areas in the infralabial depressions lie underneath the deep depressions of the caudal supralabial scale row.

3.2.2 Light microscopic and transmission electron microscopic investigations of the labial scales

The presence, distribution and approximate dimensions of the TNM areas were revealed by the SDH staining. However, the frozen sections were 20 µm thick which only allowed an approximation of the size. For a more precise resolution (especially of the epidermal and dermal structures) thinner sections were necessary. The supralabial scale row (8th to the 10th scales) with its TNM areas was three-dimensionally (3-D) reconstructed. For this purpose, a

series of semi-thin sections of the 5th to the 12th supralabial scales (total length: 9 mm) interspersed with ultra-thin sections of a juvenile boa were prepared. Moreover, the scales of an adult boa were prepared; unfortunately, they turned out to be too large to be cleanly transferred onto the microscopic slides.

As the scale morphology varies greatly, the size and shape of the semi-thin sections differed within the series. A picture of a semi-thin section within a TNM area is shown in Fig. 23 and an excerpt of higher magnification in Fig. 24. The layer at the top of the sections is the epidermal layer, which contains a monolayered array of TNMs and other epidermal receptors such as bubble receptors. The TNMs consist of accumulations of free nerve endings. Usually the epidermal area, which contains TNMs, is (slightly) thicker than the regular epithelial layer. Beneath the epidermal layer, nerve fibres and capillaries are visible (see Fig. 24). The dendrites of these nerve fibres derive from the TNMs and congregate in the Nervus trigeminus. The capillaries are periodically arranged in a regular capillary bed and are always associated with the TNM areas. Furthermore, glands (presumably saliva glands) lie within the scale structures.

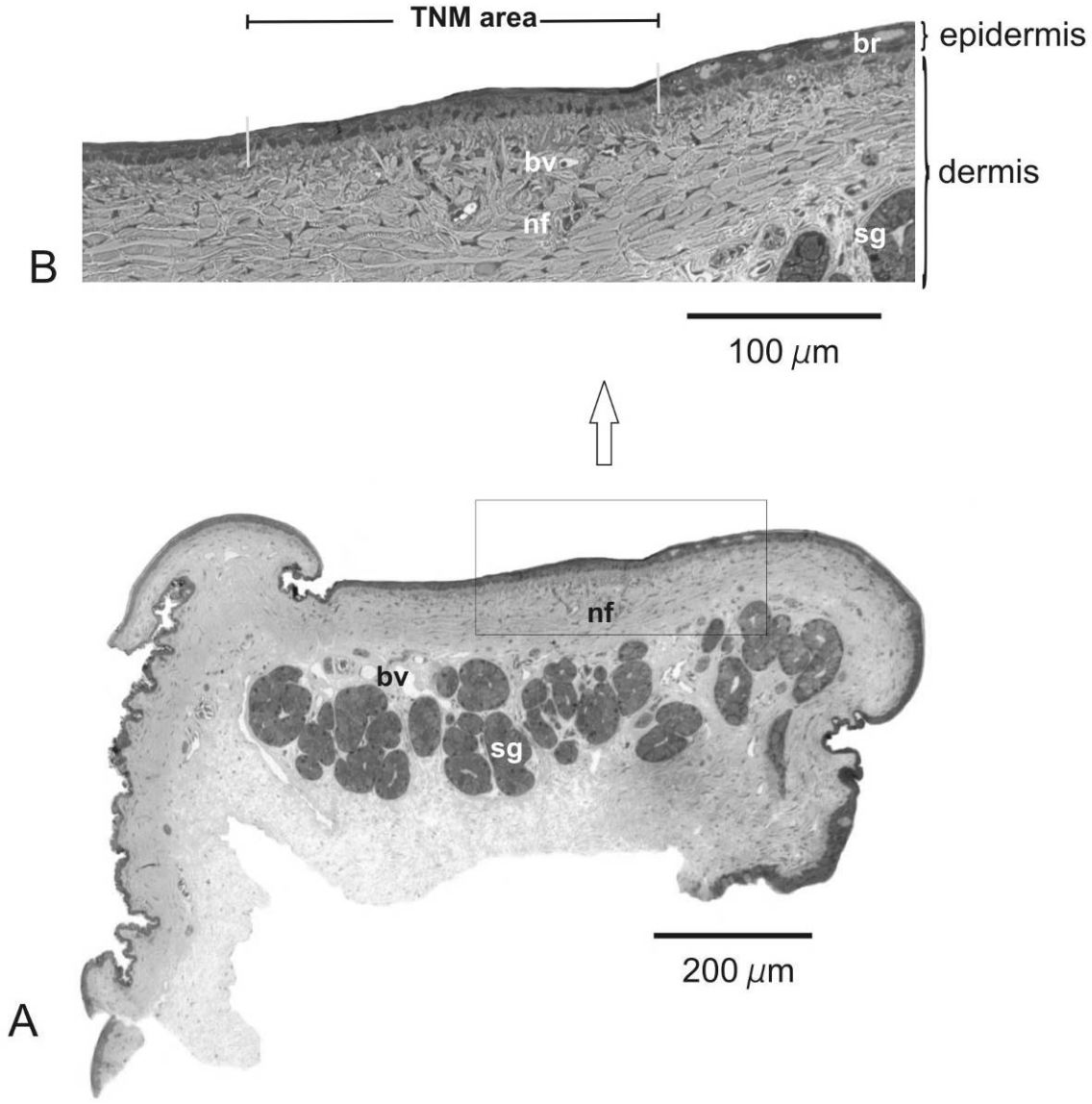

Fig. 23: A) Semi-thin section and B) an enlargement of the TNM area of the rostral part of the 7th supralabial scale containing blood vessels (bv), bubble receptors (br), nerve fibres (nf), presumable salivary glands (sg), terminal nerve masses (TNM). Section orientation guide: top of the section is the scale surface (dark grey layer); left is the upper edge of the supralabial scales; right is the edge of the upper lip; bottom of the section is the interior tissue of the scales.

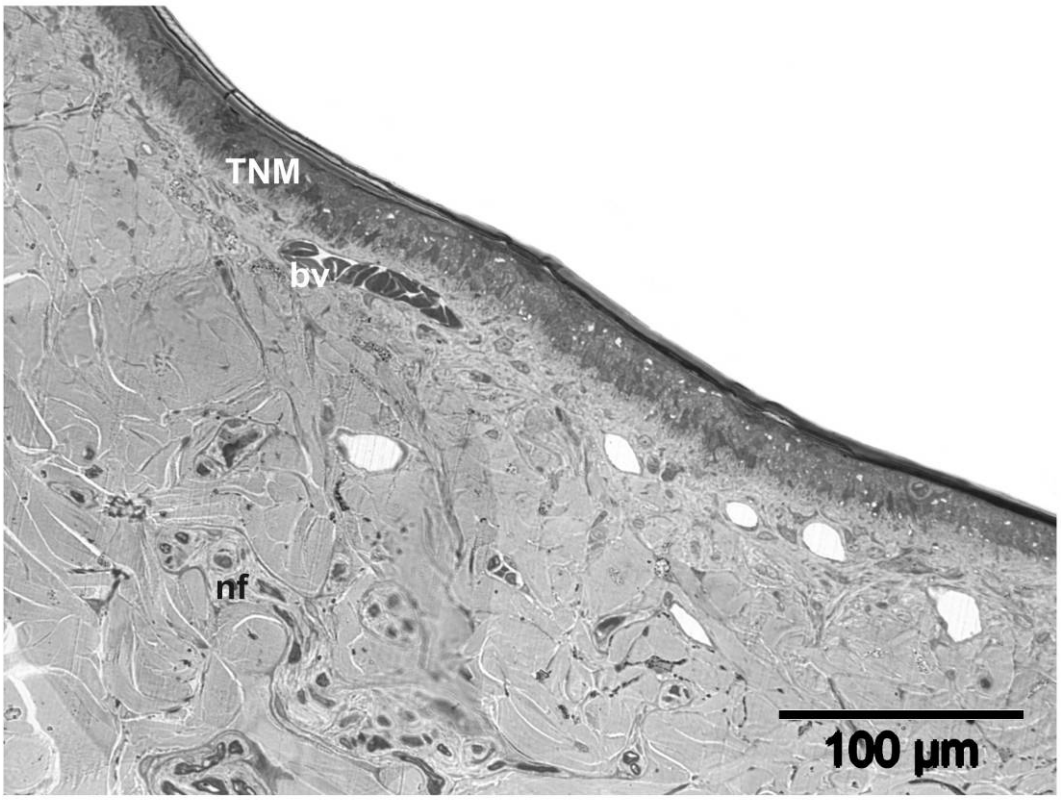

Fig. 24: Semi-thin section excerpt of a representative TNM area. Beneath the TNMs in the epidermal layer the associated off-branching nerve fibres (nf) towards the IR receptive TNMs and a capillary bed (bv: blood vessel) are present in the dermal layer.

TEM investigations were conducted for a more detailed insight into the epidermal layer and a closer look at the TNMs (Fig. 25). The TNMs are embedded between epithelial cells and are densely packed with mitochondria (see Fig. 25 B). These TNMs are located 2 µm to 6 µm (on average about 4 µm, n=7 TEM pictures) below the surface of the scales, i.e. beneath the three strata (see below). The TNM layer spanned the entire epithelium. The height of the boas' epithelium containing TNMs ranged from 11 µm up to 30 µm (median: 18 µm; n=20 investigated areas measured within the reconstructed region). The width of the TNM areas ranged from 10 µm up to 324 µm (n=20 semi-thin sections, measured in the regions of the largest supralabial depressions with the longest TNM areas according to the SDH staining, see 3.2.1, Fig. 22 A). The total TNM area sizes vary greatly in accordance to the variance between the supralabial scales.

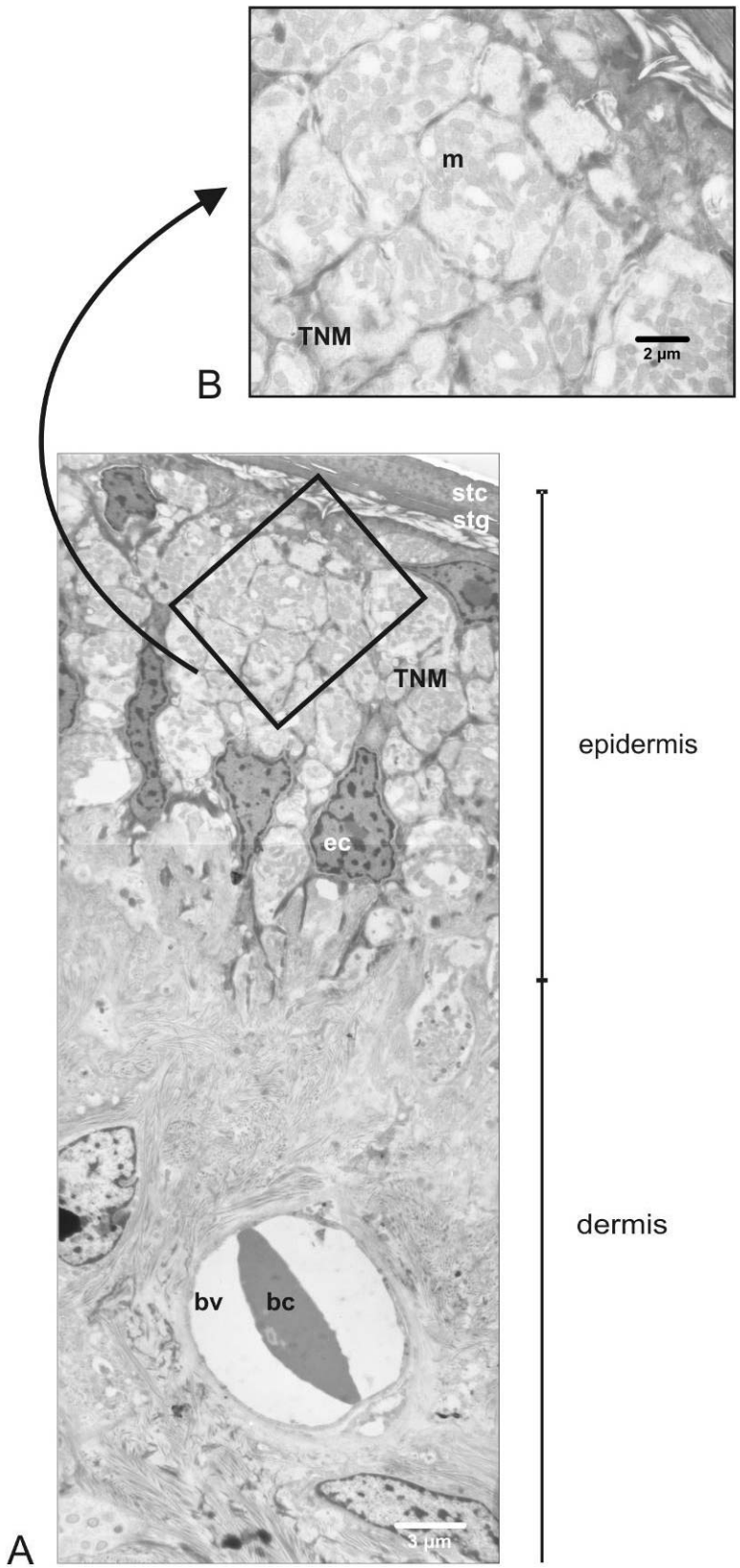

Fig. 25: A) Ultra-thin section showing TNMs. B) The detail shows the densely packed mitochondria (round shaped dark grey areas) in the TNMs. Abbreviations: blood vessel (bv), nucleus of the epithelial cell (ec), terminal nerve mass (TNM), mitochondrion (m), red blood cell (bc), stratum corneum (stc), stratum germinativum (stg)

The TEM investigations also allowed a detailed look at the structure of the layers above the epithelium. As depicted in Fig. 26 the stratum germinativum, the stratum intermedium and the stratum corneum form the outer layers of the epidermis. The investigation of three random samples of the stratum corneum revealed that the stratum corneum above the TNM areas is about one-half up to two-third as thick (Fig. 26 and Tab. 3) as areas bordering the TNM areas.

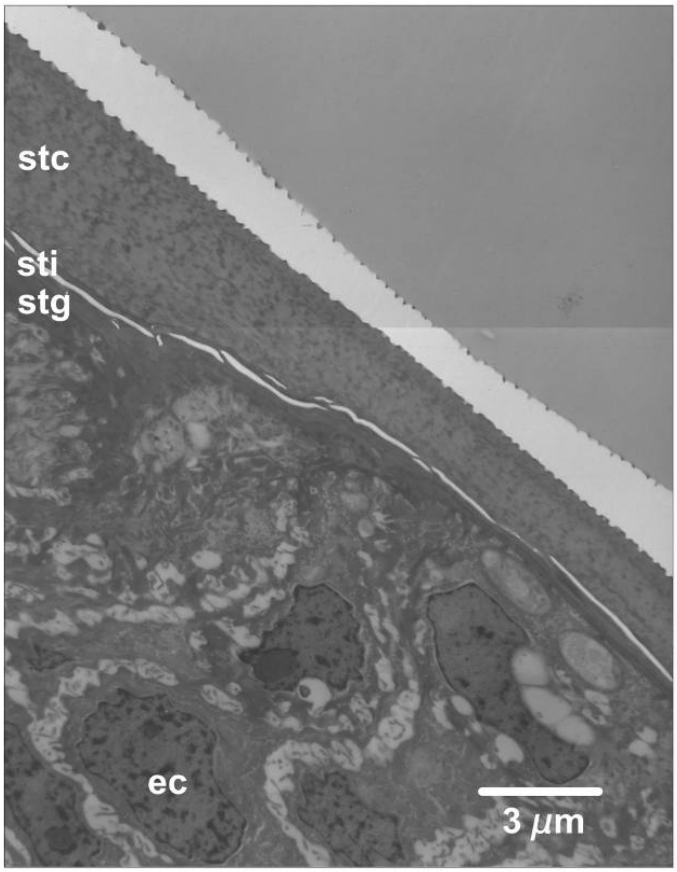

Fig. 26: Ultra-thin section depicting the declining thickness of the stratum corneum from an TNM-void area (left) towards the TNM-rich area (right). Abbreviations: epithelial cell (ec), stratum corneum (stc), stratum germinativum (stg), stratum intermedium (sti)

Tab. 3: Thickness of the stratum corneum investigated at four different labial scale areas (see markings on labial scale row below) on six TEM pictures, n= 32

Labial scale area	**Range of the stratum corneum thickness (µm)**	**Remarks**
1	2.1 – 3.0	above TNMs
2	2.1 – 3.0	
3	1.8 – 3.1	
4	2.3 – 4.6	area bordering TNM area (compare Fig. 26)

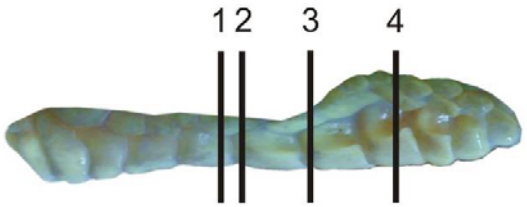

Moreover, microscopic pores covering the scale surface were found (see Fig. 27). Their diameter and depths were investigated exemplarily in three different TNM areas (6 TEM pictures, n=35 pores) of the labial scale (see scale row below Tab. 4). The results are shown in Tab. 4. The diameter of the pores ranged between 0.28 µm and 0.81 µm. The range of the pore depth lay between 0.14 µm and 0.31 µm.

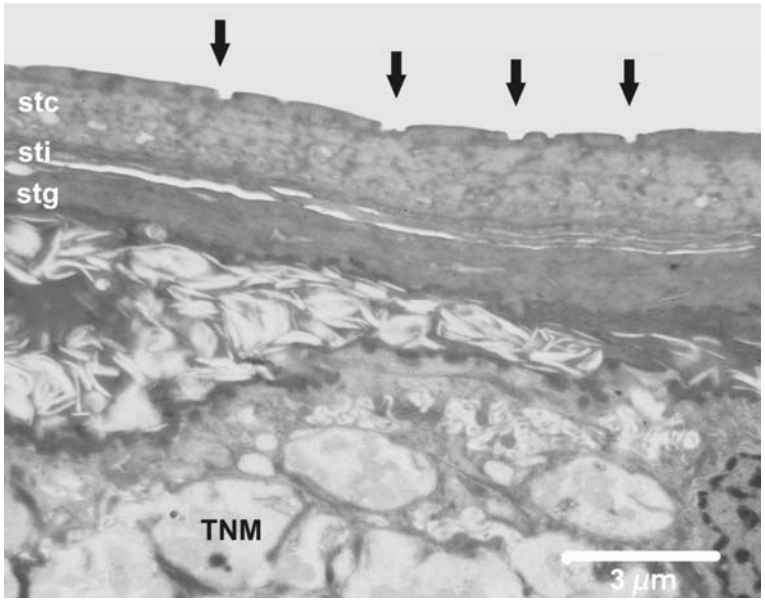

Fig. 27: Ultra-thin section showing the stratum germinativum (stg), stratum intermedium (sti) and stratum corneum (stc) layer above a TNM area. In the stratum corneum layer small indentations, so-called microscopic pores are visible (black arrows).

By comparing the pores of Fig. 26 and Fig. 27 it becomes visible that the distribution of the pores is irregular within one region and also between regions; in Fig. 26 the pores are densely distributed and in Fig. 27 they occur sporadically with larger inter-pore-intervals.

Tab. 4: Ranges of the pore diameters and depths shown for six TEM pictures in three different labial scale row areas above TNMs (see markings on labial scale row below)

Labial scale area	**Range of pore diameters (µm)**	**Range of pore depths (µm)**
1	0.41 – 0.81	0.14 – 0.31
2	0.32 – 0.41	0.16 – 0.23
3	0.28 – 0.79	0.14 – 0.28
Total range	**0.28 – 0.81**	**0.14 – 0.31**

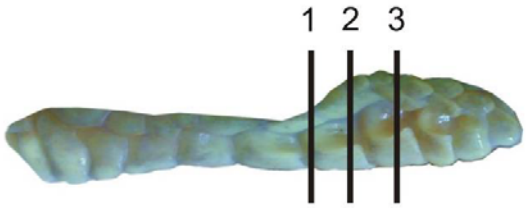

3-D reconstruction of the TNM areas in the 8th-10th supralabial scale depressions

A precise computer-based three-dimensional (3-D) reconstruction of the TNM regions was conducted. The selected area of the three depressions in the 8th, 9th and 10th caudal supralabial scale for the 3-D reconstruction is shown in Fig. 28 A and C (white rectangle).

Two different perspectives of the 3-D reconstruction are depicted for the selected area: the first shows a lateral view (Fig. 28 B), whereas the second shows a semi-frontal view from slightly above (Fig. 28 D). Especially, the lateral view of the labial scales shows that the depressions are arranged in a zigzag formation. Both endings of each scale fall inwards, thus the caudal edge of one scale and the rostral edge of the next scale form the depression (fold). The rostral and the caudal side of one scale together form a ridge. Therefore, each scale has a rising caudal side which reaches up to the ridge and a declining rostral side which drops away from the ridge.

The reconstructions (Fig. 28 B and D) reveal that the TNM areas (coloured in red) are located in the rostrally-forward and caudally-backward-facing scale areas. It is conspicuous, that the forward facing TNM areas (rostral part) extend up to the ridge, however do not reach down into the deep fold between the scales. On the caudal side of the scale ridge the TNM area begins in close proximity to the fold of the depression however does not reach more than

three quarters up the ridge. The exact reconstruction revealed the TNM areas to be quite different in size: the backward-pointing TNM area of the 8th scale (Fig. 28 B, first on the left) had a size of 56 x 10^{-3} µm^2, the forward-pointing TNM area of the 9th scale was almost of the same size (52 x 10^{-3} µm^2), the backward-pointing area of the latter scale turned out to be the biggest with 128 x 10^{-3} µm^2. The forward-pointing TNM area of the 10th scale was 69 x 10^{-3} µm^2 in size; the backward-pointing area of the latter scale was 77 x 10^{-3} µm^2 in size, forming the depression with the forward-pointing area of the 11th scale, which had a TNM area size of 8 x 10^{-3} µm^2.

Each supralabial scale possesses an outgrowth on the bottom edge which curves up and away from the scale emargination and depression. This outgrowth partly shields the scale emargination and depression, just as the bulge of the scale row above the supralabials does (compare lateral view (B) and semi-frontal view (D) of the reconstructions in Fig. 28).

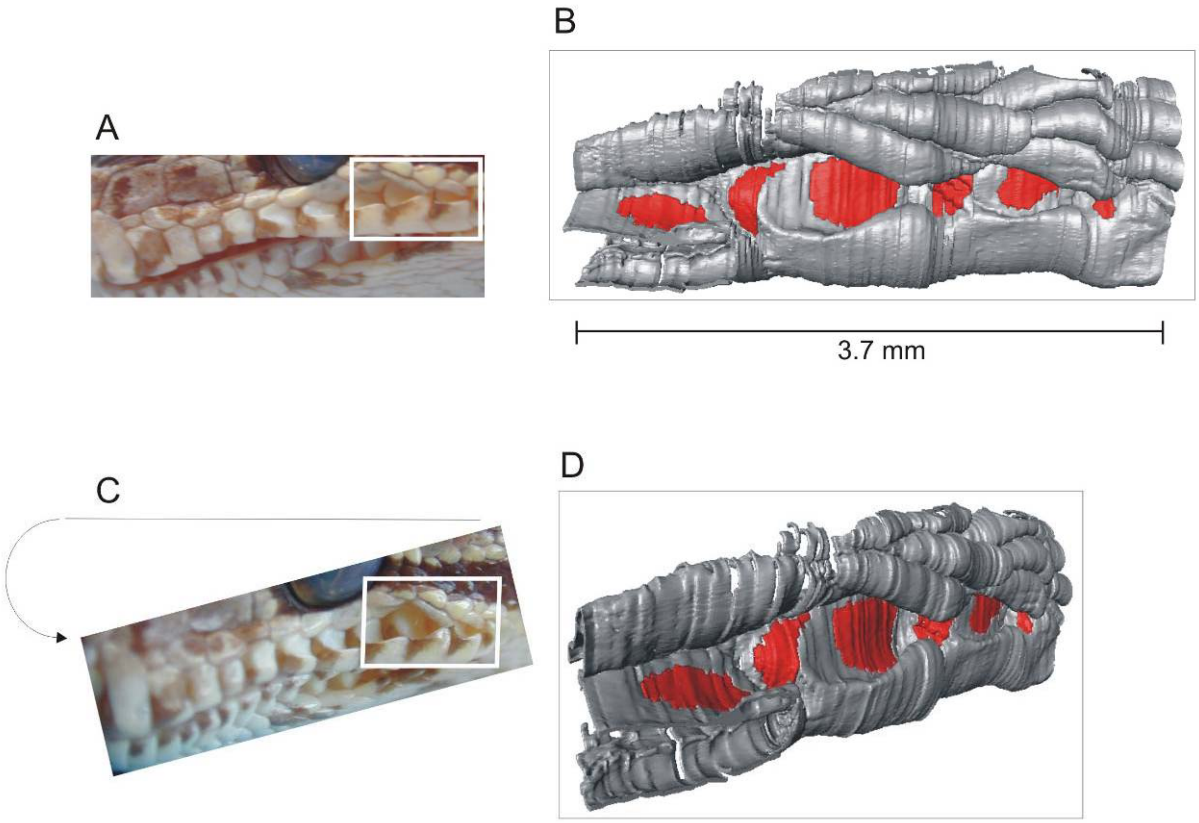

Fig. 28: The white rectangles in the two picture excerpts A and C mark the selected area for the 3-D reconstruction. The details B (lateral view) and D (semi-frontal view) depict the 3-D reconstruction of the TNM areas (marked in red) in the 8th to the 10th supralabial scales.

3.2.3 Scanning electron microscopic examination of the labial scale surface

In order to complement the knowledge of the exact dimensions of the TNM areas in the selected scale area ranging from the 8th to the 10th supralabial scale (see Fig. 29 and compare 3.2.2) and the finding of the pores (and thinning stratum corneum) above these TNM areas an investigation of the scale surface was conducted with the SEM. The aim of this examination was to find out whether there is a correlation between the organisation of the surface structure (i.e. microscopic pores) and the distribution of the TNM areas situated underneath.

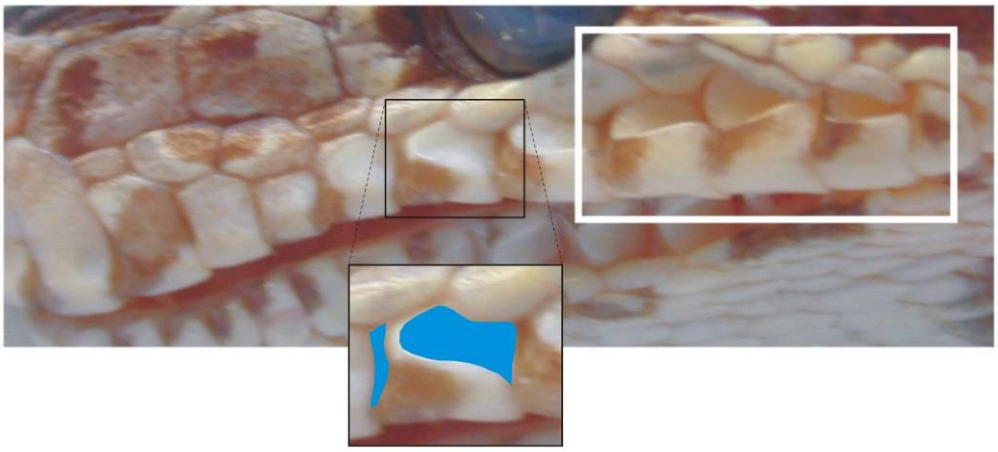

Fig. 29: This picture shows the investigated labial scale area (white rectangle). The blue areas of the black-bordered detail exemplarily depict what is defined as an emargination area of a scale, which is important in the following analysis.

In total 552 SEM pictures of the labial scale surface (above-depicted area of the three last caudal depressions (Fig. 29)) and of control surfaces (e.g. upper head and neck region, dorsal and ventral body scales) were taken. Thereof, a total of 5237 pore areas in 142 SEM pictures of the selected labial scale area and 6 control pictures (with 161 pore areas) were analysed. For the analysis a standardised excerpt of 9 µm^2 of each picture was used.

The size and shape of the pores vary greatly. Fig. 30 shows pictures of the diversity of pores. The pores are not arranged in a regular pattern; however, with a few exceptions they are more or less evenly distributed within the 9 µm^2 excerpts. The smallest pores are of a regular round shape (e.g. Fig. 30 B, E), whereas the shapes of the bigger pores differ from round over oval to elliptical (e.g. Fig. 30 C, D, F). In general, the distance between the pore centres are similar, independent of the pore size, i.e. the larger the pores become, the less interspace is left. In the largest pore sizes this leads to a mesh-like structure (e.g. Fig. 30 A).

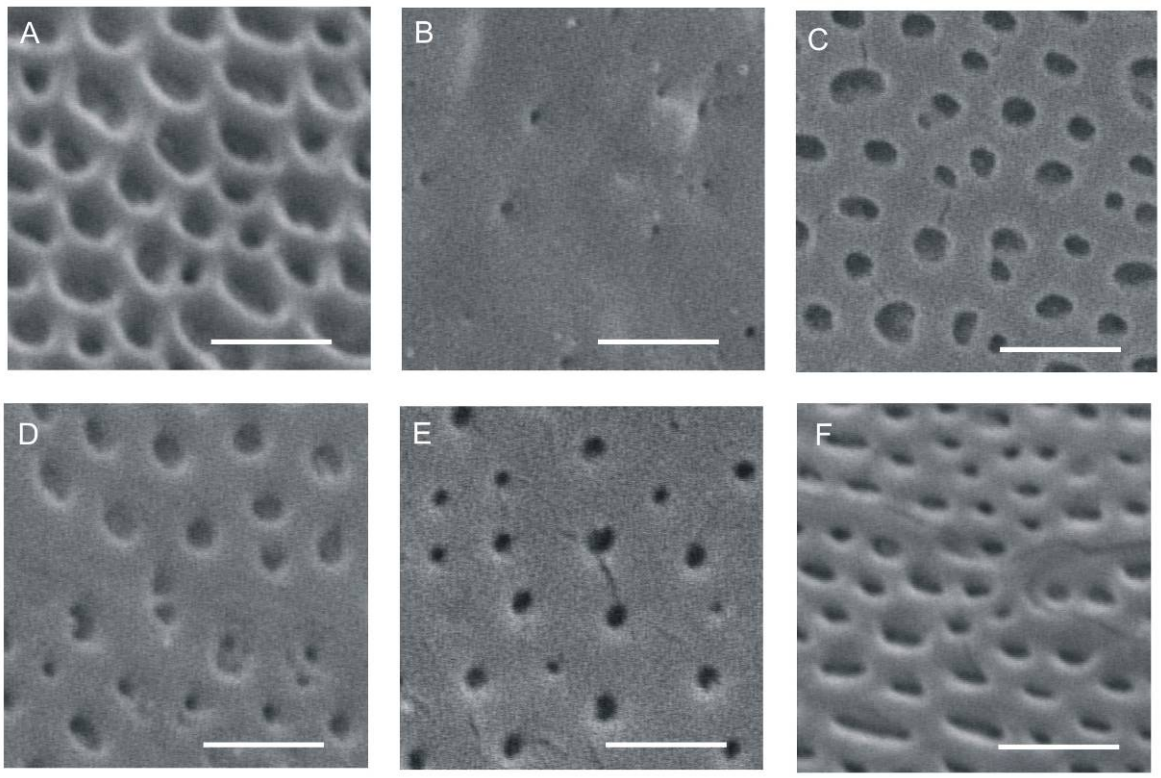

Fig. 30: Each exemplary picture (A-F) shows the distribution and shape of the pores within the defined 9 µm² sections (scale bar is 1 µm).

To analyse the diverse pore pictures, a distinguishing criterion was needed. It was not possible to categorise the pore areas (e.g. into small, middle and large pores) as they represent a continuous set of data without obvious gradations. Therefore, the relative pore area (pore area divided by the total area of the 9 μm^2 sized excerpt) and the number of pores were analysed.

The mean number of pores increases with increasing relative pore areas, but on average the number of pores only increases minimally. The results of the investigated SEM pictures (n=142) are shown in Tab. 5.

Tab. 5: The range of the number of pores and their average is shown for the respective pore area interval.

Relative pore area	**Range of the number of pores**	**Average number of pores**	
%		**per 9 µm²**	**per 1 µm²**
$0 < x \leq 5$	[11, 57]	28	3
$5 < x \leq 10$	[24, 60]	39	4
$10 < x \leq 20$	[25, 55]	40	4
$20 < x \leq 30$	[34, 59]	44	5
$30 < x \leq 40$	[40, 41]	41	5

The average number of pores ranged from 3 to 5 per µm² (28-44 per 9 µm²). The calculation of the mere pore diameter was neither feasible nor expressive due to the greatly variable pore shapes. Moreover, the shape of the pores can already vary greatly within one 9 µm² excerpt (see Fig. 30 C, E). To compare the size of the pores in different areas, the total pore area was measured and divided by the total excerpt area (i.e. 9 µm²)

The relative pore areas were categorised into five intervals (I: $0\ \% < x \leq 5\ \%$, II: $5\ \% < x \leq 10\ \%$, III: $10\ \% < x \leq 20\ \%$, IV: $20\ \% < x \leq 30\ \%$, V: $30\ \% < x \leq 40\ \%$; compare Fig. 31 for examples) and plotted onto the SEM labial scale overview picture (Fig. 32). In the following two pictures (Fig. 31 and Fig. 32) the five categories are referred to in a short version (I: ≤ 5 %, II: ≤ 10 %, III: ≤ 20 %, ect.).

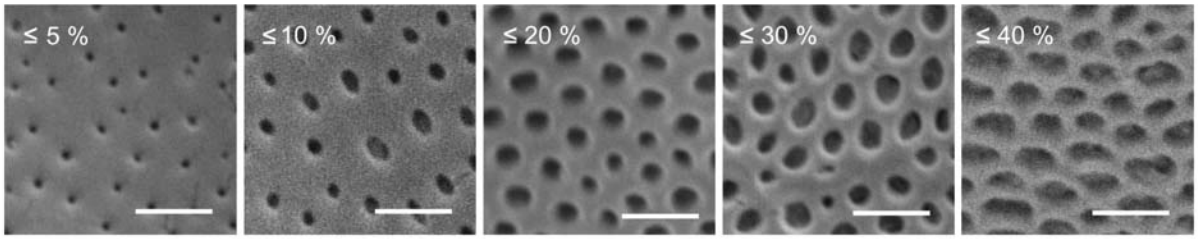

Fig. 31: SEM pictures of the microscopic pores for the five categories of relative pore area sizes. Scale bar is 1 µm.

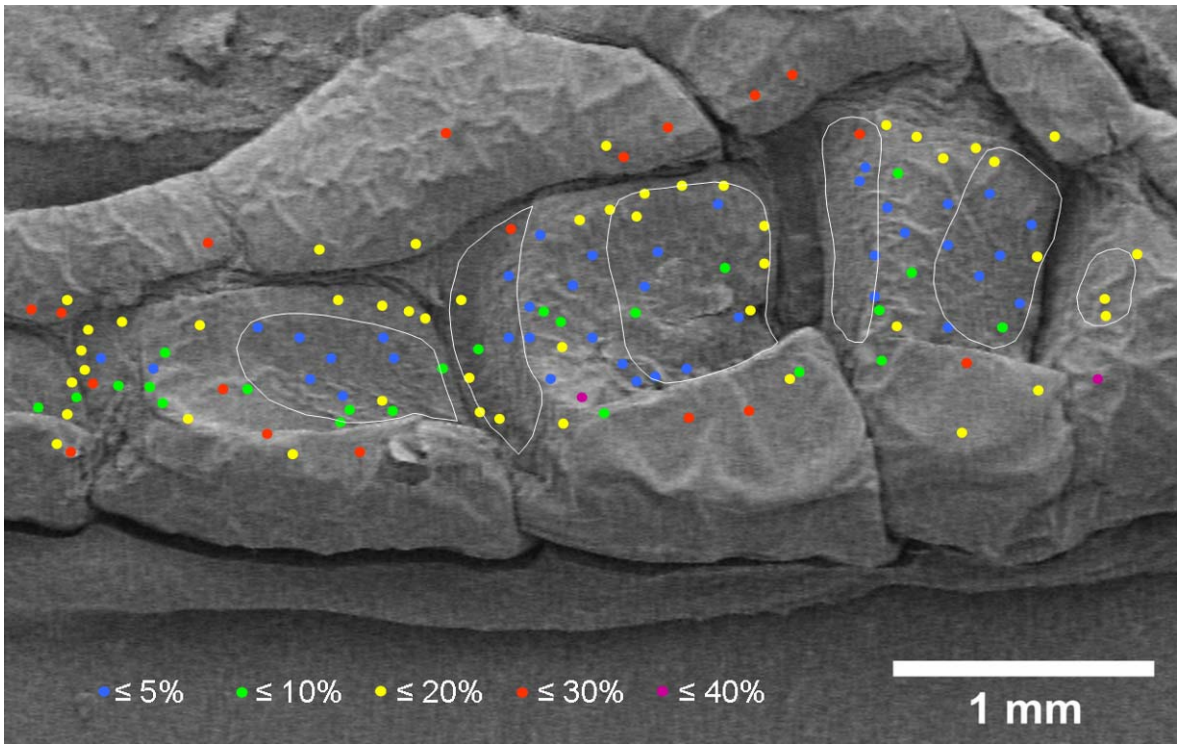

Fig. 32: Overview of the relative pore areas (%) of the SEM pictures randomly taken of the three last caudal supralabial scale depressions. The relative pore areas are depicted in five different colours depending on their percentage value. The TNM areas are encircled in white.

The smaller relative pore areas (≤ 20 %) are mainly distributed over the scale emarginations and also depressions, except on the outgrowths at the lower bottom edges of the scales. The smallest (blue) are centred on the scale. The relative pore areas up to 10 % (green) are similarly distributed as the smallest areas; however, they are shifted more to the scale edges. Except for a few exceptions the relative pore areas ranging between 10 % and 20 % (yellow) lie on the edges and in the depressions of the scales. The larger relative pore areas above 20 % (red and purple) are mainly distributed on the bottom-edge outgrowths of the supralabial scales and on the scales above.

With the knowledge of the exact position and dimension of the TNM areas (gained by the 3-D reconstruction, compare 3.2.2) it was possible to compare whether the distribution of the relative pore areas is linked to the infrared-receptive TNM areas (see white surroundings in Fig. 32). This is under the presumption that the dimension and distribution of the TNM areas of all individuals are similar. The distribution of the specific relative pore areas do not seem to be related to the TNM areas, though in general it seems as if smaller relative pore areas primarily are present in the labial scale emarginations and depressions, whereas the larger pore areas lie outside of these.

To verify this, the amount of relative pore sizes in the respective TNM areas, in the emarginations and outside the emarginations (bottom edge outgrowth of supralabial scales and the scales above the supralabial scales) were examined. The following two tables (Tab. 6 and Tab. 7) show the distribution of the relative pore areas in regard to a) the scale area outside of the emargination and the area within the emargination and b) the area of the TNMs in relation to the emargination area.

Tab. 6: Distribution of the relative pore areas differed from the ones above the emargination areas and the ones outside of the emargination areas.

Relative pore area	**Outside emargination area**	**Emargination area**
%	**%**	**%**
$0 < x \leq 5$	0	100
$5 < x \leq 10$	13	87
$10 < x \leq 20$	17	83
$20 < x \leq 30$	62	38
$30 < x \leq 40$	50*	50*

* account for measurements of only two SEM picture areas

Tab. 7: distribution of the relative pore areas above the TNM areas in relation to the emargination areas.

Relative pore area	**On TNM areas in relation to the emargination areas**
%	**%**
$0 < x \leq 5$	64
$5 < x \leq 10$	40
$10 < x \leq 20$	41
$20 < x \leq 30$	33
$30 < x \leq 40$	0

Within the emarginations most relative pore area sizes do not exceed 20 %; the TNM areas lie within the emargination areas and therefore show similar results. In contrast, the non-emargination areas do not contain relative pore areas smaller than 6 %. The subdivision of the

first 10 % into two categories (≤ 5 % and ≤ 10 %) was sensible, since over ¾ of the relative pore areas above the TNMs are smaller than or equal to 5 %. All relative pore areas with sizes of ≤ 5 % lie entirely within the emargination areas and thereof 64 % lie on the TNM areas.

3.2.3.1 Examination of the surface structure of control scale areas

The surfaces of the control areas revealed more or less meshlike structured pores (see Fig. 33 for examples) with relative pore areas ranging from just below 30 % up to more than twice as much (Tab. 8). The number of pores per μm^2 varies between 2 and 7 for the SEM pictures of the control areas shown in Fig. 33.

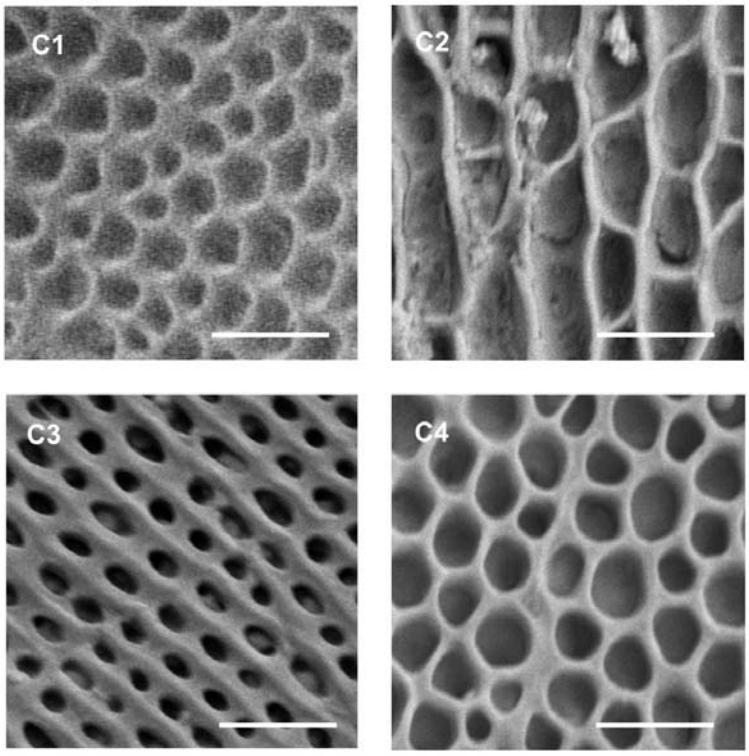

Fig. 33: Examples for SEM pictures of the surfaces of control scale areas. C1: scale of the upper neck region, C2, C4: dorsal body scale, C3: ventral body scale; scale bar is 1 µm.

Tab. 8: The relative pore areas and the number of pores depicted for the respective control scale areas shown in Fig. 33.

Scale area	**Relative pore area (%)**	**Number of pores (per 9 µm^2)**	**Number of pores (per 1 µm^2)**
C1	41	36	4
C2	65	18	2
C3	28	65	7
C4	60	42	5

The shape of the pores differ, however, they all are more or less meshlike in structure. The pores of the upper neck region (Fig. 33 C1) are similar to the pores of the non-emargination areas and to the scales above the labial scale row, whereas the pores of the dorsal and ventral body scales (Fig. 33 C2, C3, C4) differ completely in their shape, even within one similar region (compare Fig. 33 C2 & C4, both are dorsal body scales).

3.2.4 Tracer experiments

The scale morphology of the boas clearly possess forward- and backward-pointing labial scale areas (zigzag), which leads to the hypothesis that the forward- and backward-pointing TNM areas are processed in different parts of the IR processing brain area (LTTD), i.e. the (IR) information of one direction is processed in a different LTTD region than the information from the other direction.

In total 7 tracing experiments were conducted. For the investigation, the brain stem was cross-sectioned from the caudal end of the mesencephalon to the caudal end of the medulla oblongata (see Fig. 34). The first tracing experiment (BDA on the left 2nd caudal supralabial depression, scale area pointing backward) revealed staining in the ipsilateral LTTD region (Fig. 35). Approximately half of the lower LTTD region contained stained fibres (see Fig. 35, detail on the left). The exact location of the cross-section (A) depicted in Fig. 35 is shown in Fig. 34.

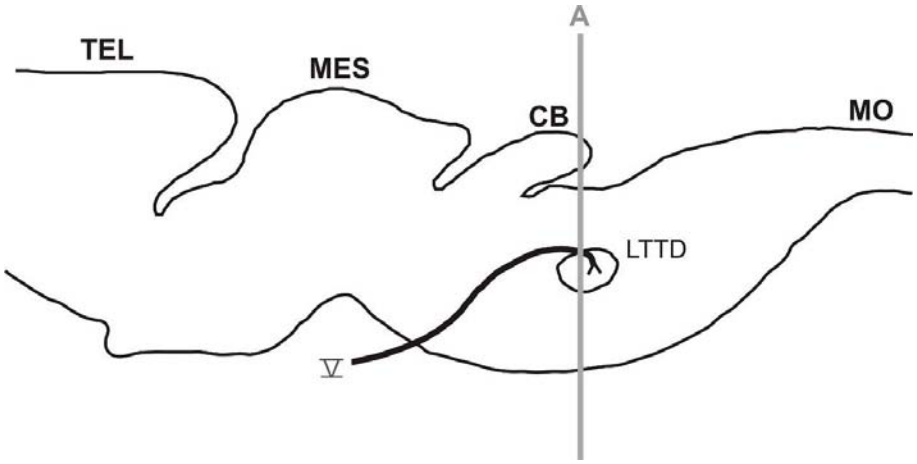

Fig. 34: Schematic sagittal section of a boid brain altered after Molenaar & Fizaan-Oostveen (1980) depicting the position of the cross-section (A) shown in Fig. 35. Abbreviations: CB: Cerebellum, LTTD: Nucleus descendens lateralis nervi trigemini, MES: Mesencephalon, MO: Medulla oblongata, TEL: Telencephalon, V: Nervus trigeminus

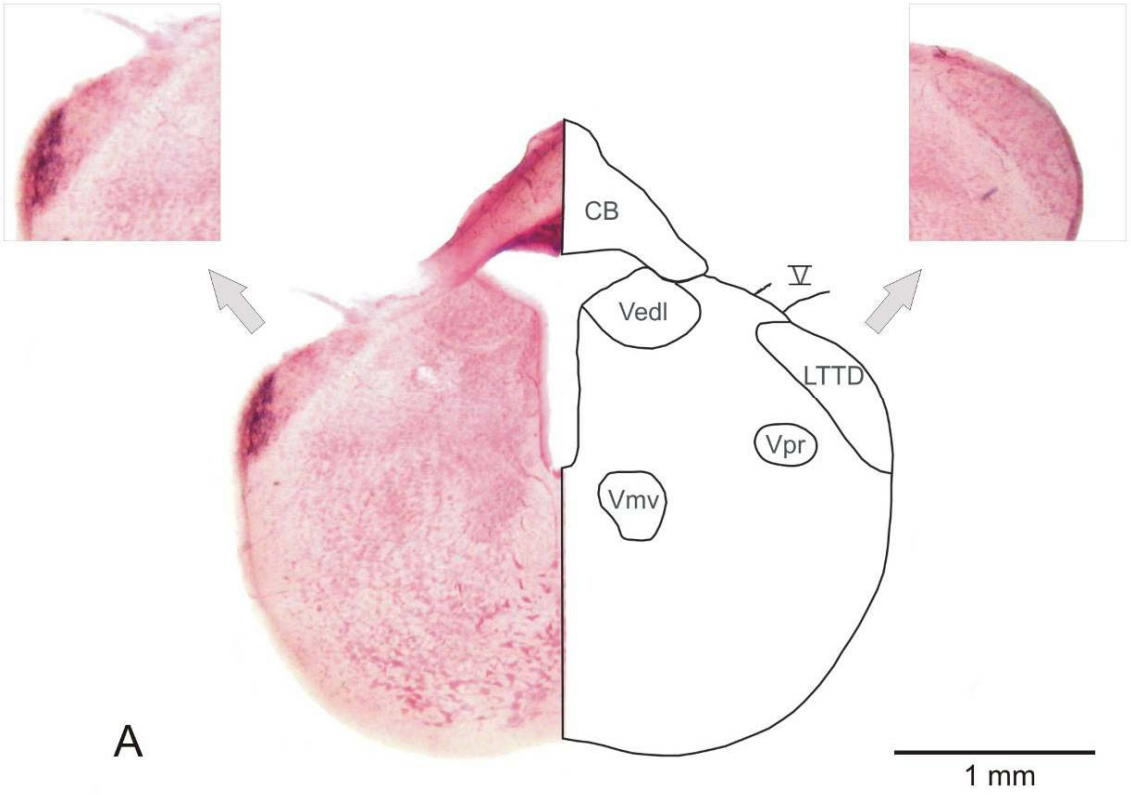

Fig. 35: Cross-section (100 µm) of the brain stem. The LTTD on the left side of the picture is partly stained (see detail on the left) in contrast to the LTTD region on the right side (see detail). Abbreviations: CB: Cerebellum, LTTD: Nucleus descendens lateralis nervi trigemini, Vedl: Nucleus vestibularis dorsolateralis, Vmv: Nucleus motorius nervi trigemini, Vpr: Nucleus sensorius principalis nervi trigemini, V: Nervus trigeminus

The successful staining in just approximately the lateral half of the LTTD region encouraged the working hypothesis that the zigzag-morphology (forward- and backward-pointing TNM areas) of the labial scales might be directionally represented in the infrared processing LTTD region.

Although the first tracing experiment was successful, none of the six following experiments revealed any staining, despite systematically altered parameters of the procedure protocol to check for methodical errors (compare 2.3.4 and appendix 8.2). Thus, the hypothesis of a directional representation of the special labial scale morphology in the LTTD could neither be verified nor disproved.

3.2.5 Investigation of the IR visual field

The extraordinary zigzag-shape of the labial scale areas containing the IR receptors led to the investigation of the field of view for IR radiation. A head cast made out of plaster was built as a functional model. The positions of the TNM areas were marked onto the forward- and backward-pointing labial scales on the basis of the SDH staining results (see 3.2.1). To examine the 3-D IR field of view of the boa, the head cast was investigated in a horizontal as well as in a 45° upward- and downward-pointing position. The summed TNM areas of the respectively forward- and backward-pointing supra- and infralabials, which were visible at the respective angles (-40° to 150°) were put in relation to each other. These resulting percentage values were the basis for the calculation of the entire 3-D IR visual field.

Pictures of the head cast are shown exemplarily at different angles in the three different head positions (+45°, 0°, -45°) in Fig. 36 (A-C).

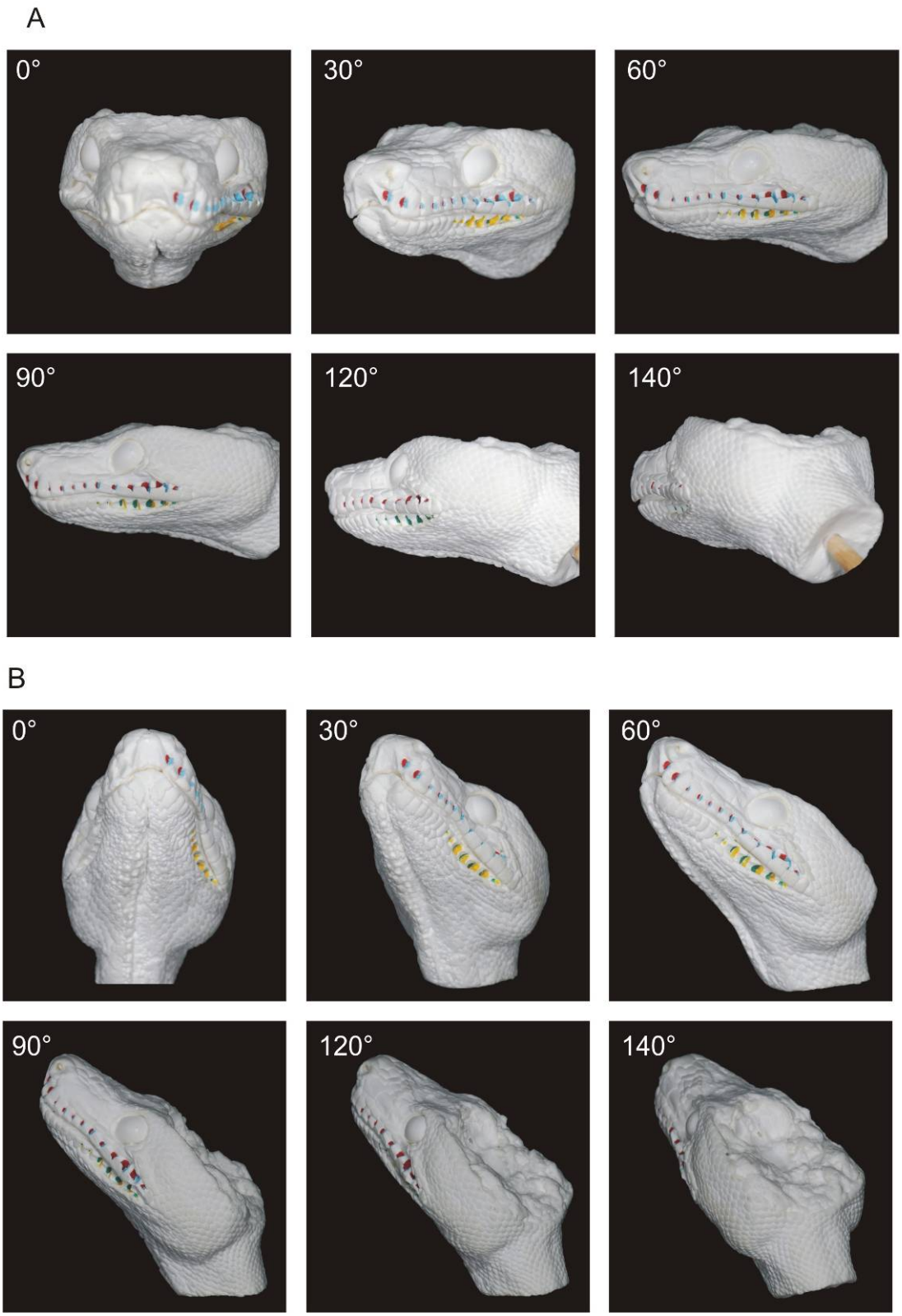
A
0°
30°
60°
90°
120°
140°
B
0°
30°
60°
90°
120°
140°

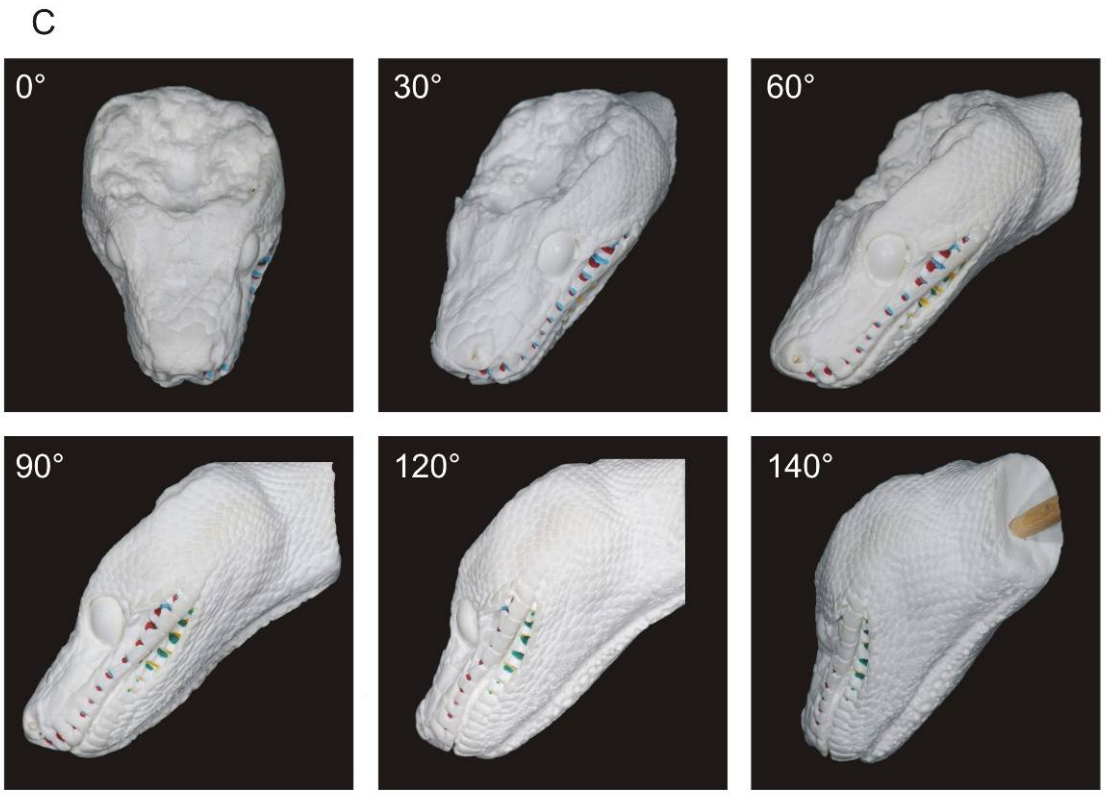

Fig. 36: Exemplary pictures of the boa head cast photographed in A) the horizontal head position (0°), B) the head pointing upwards position (+45°), C) the head pointing downwards position (-45°) at different angles.

The picture series shows that the proportions of the visible coloured areas shifted in accordance to the different angles. On the basis of this series the total TNM area sizes pointing forward and backward for the supra- and infralabial scales were calculated and plotted against the respective angles (Fig. 37 and Fig. 38). The measurements were not restricted from 0° to 150°, because frontal IR radiation does not only impinge on one side of the head (see 0° angle in Fig. 36A), therefore, the range of -40° to 0° was included. Furthermore, the receptive areas span the entire supralabial scale row, whereas the receptive areas in the infralabial scale row are confined to approximately the posterior half (see 2.3.5, Fig. 13) of the scale row. Accordingly, the supralabial TNM areas (coloured blue and red) are larger in total than the infralabial TNM areas (coloured yellow and green) (see Fig. 37 and Fig. 38). Yet, the exact sizes of the TNM areas are not paramount. The main focus lies on the proportions of the backward- and forward-pointing areas of the supra- and infralabial TNM areas to one another at different angles in the respective head positions. Errors resulting from the plotting of the SDH results onto the head cast are uniformly distributed and are therefore negligible.

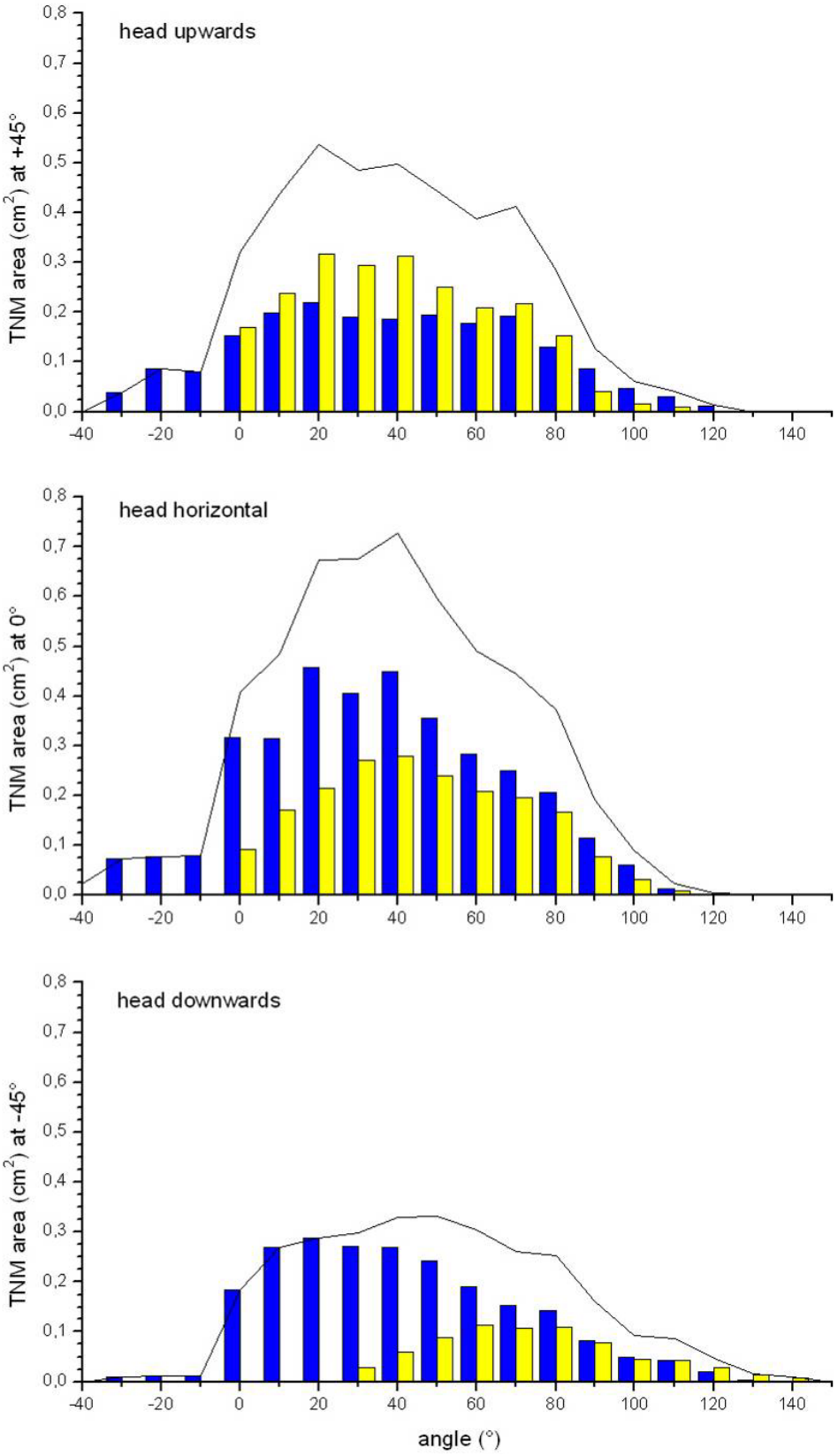

Fig. 37: Sizes of the TNM areas of the supra- (blue) and infralabial (yellow) scales pointing forward in the three different head positions (+45°, 0°, -45°) at different angles (from -40° up to 150°). The black line depicts the envelope for the total area of the forward-pointing TNMs in the respective head position.

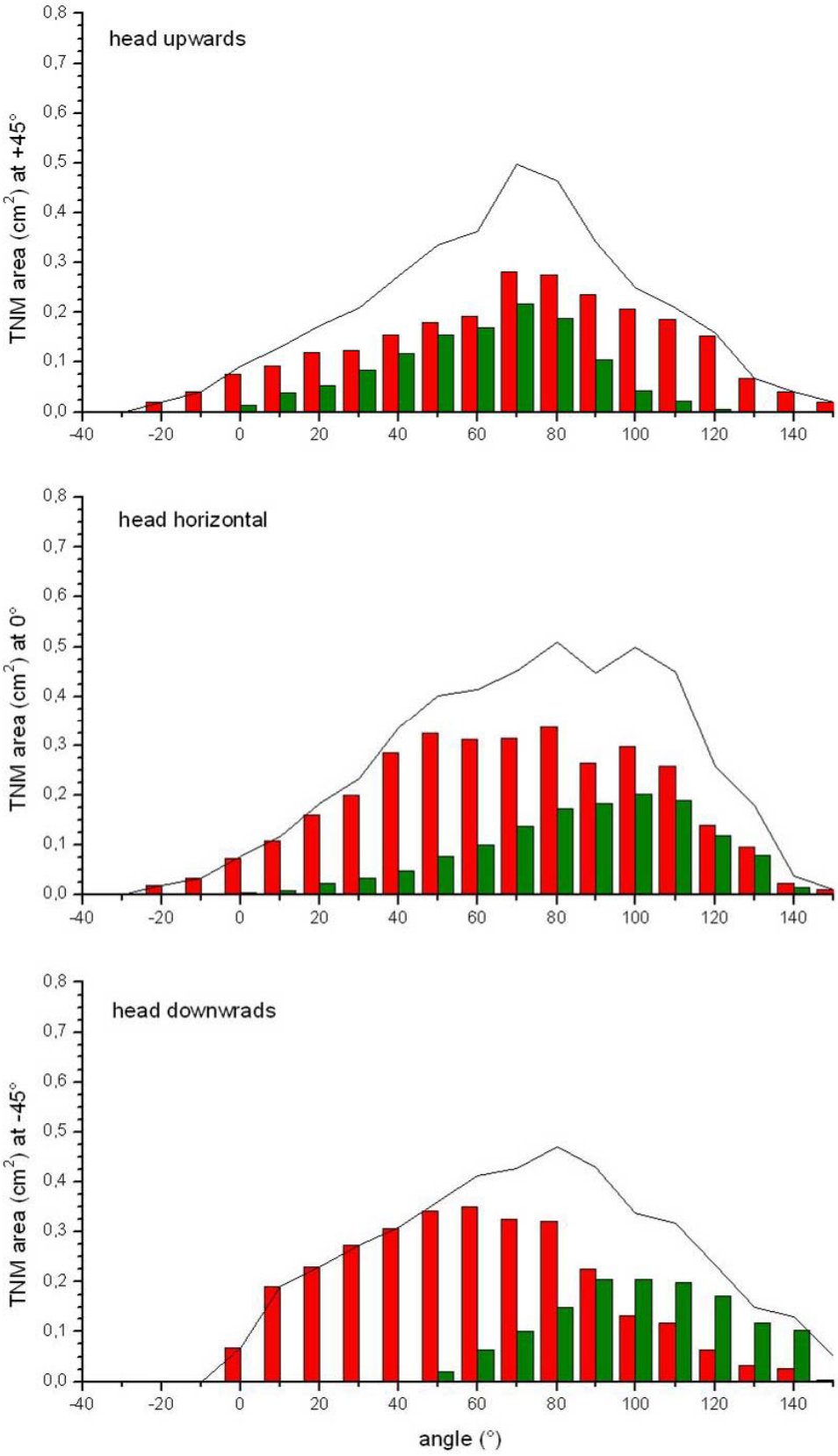

Fig. 38: Sizes of the TNM areas of the supra- (red) and infralabial (green) scales pointing backward in the three different head positions (+45°, 0°, -45°) at different angles (from -40° up to 150°). The black line depicts the envelope for the total area of the backward-pointing TNMs in the respective head position.

The values of the graphs in Fig. 37 and Fig. 38 show the different measured visible forward- and backward-pointing TNM areas in cm^2 of the supra- and infralabial scale row of one head side. As the total areas of the forward- and backward-pointing supra- and infralabial TNMs are different, all forward pointing areas were added up to one total graph (see Fig. 37, black line: envelope), likewise all backward pointing areas were added up to one total enveloping curve (see Fig. 38, black line). In all three head positions the sum of all forward-pointing TNM areas show a peak (see enveloping curve) in the horizontal angle range of 20° to 50°. In contrast, the sum of all backward-pointing visible TNM areas peak in the angle range from 70° to 100° in the three head positions, i.e. they mainly cover the lateral and caudal part of the IR visual field.

At certain angles (0° to 30°/40°) not only one side of the head receives IR radiation, the frontal part of the other side of the head does, too. Thus, the values of the TNM areas of the other head side need to be added, i.e. the values for the -10° angle have to be added to the values of the +10° angle, the values for the -20° angle have to be added to the values of the +20° angle, and so on. In the horizontal head position this was necessary for angles up to 40°, whereas for upward- and downward-pointing head positions it was necessary up to an angle of 30°. Furthermore, in the frontal head position (horizontal plane: 0°) the respective TNM areas receive full input from both head sides, i.e. double input.

Fig. 39 (A-C) depicts the IR field of view for all four coloured TNM areas. To reveal the relations of the respective areas to one another, the proportions are expressed in percent. The maximal TNM area size value (i.e. in the 0° angle of the horizontal head position the forward-pointing areas of the supralabial scales (blue)) was set as 100%. All other values were put into relation to this maximal TNM area value.

A

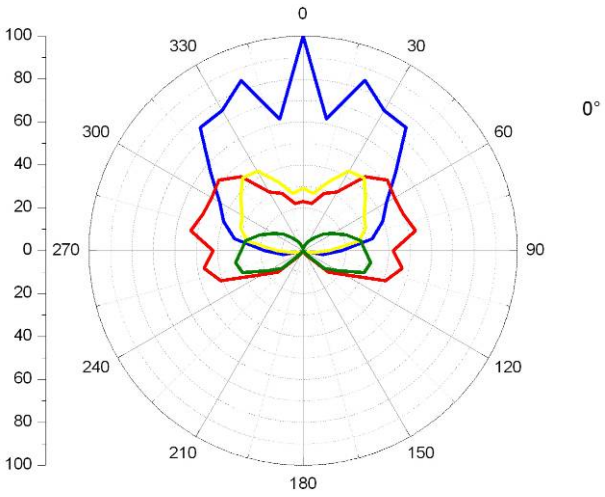

B

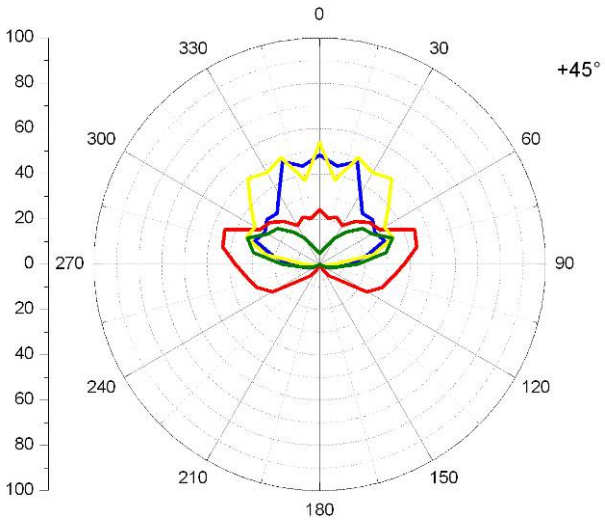

C

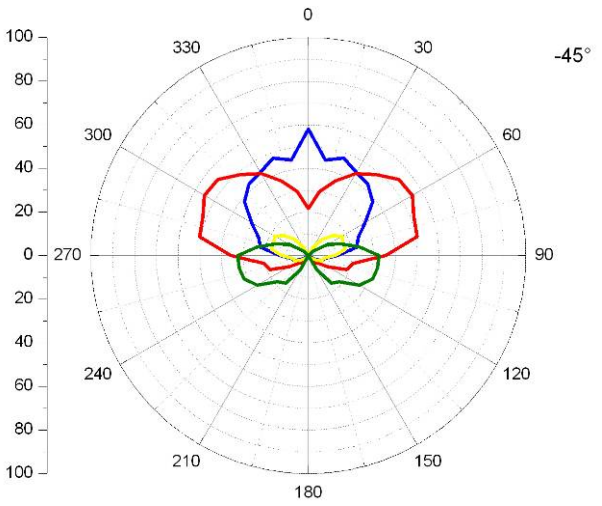

Fig. 39: IR vision field of *C. hortulanus* in the three different head positions: A: horizontal (0°), B: upward (+45°), C: downward (-45°). The y-axis depicts the percentage of the receptive TNM area.

In the horizontal and downward-pointing head positions the forward-facing supralabial TNM areas (blue) receive most of the frontal IR input (about –30° to +30° angles in the horizontal plane). However, in the upward-pointing head position the forward-facing infralabial areas (yellow) are slightly larger than the forward-facing supralabial areas (blue). Conspicuously, the size of the forward-facing infralabial area (yellow) alters greatly between the upward-pointing (large area) and the downward-pointing head position (small area).

In all three head positions the backward-facing supralabial areas (red) are mainly involved in the lateral IR reception (approx. 50° to 90° on each side), however they additionally cover the caudal IR reception in the horizontal (up to 120°) and upward-pointing (up to 150°) head positions. Their sizes and proportions hardly differ within the different head positions. The backward-facing infralabial areas (green) are of similar size in all three head positions. They also cover a similar angle range in the horizontal (50° to 130°) and downward- (70° to 150°) pointing head positions, i.e. the lateral to caudal range. In contrast, in the upward-pointing head position the backward-facing infralabial areas (green) only play a role for angles from 30° to 90°. Furthermore, in all three head positions it is conspicuous that the IR visual field shows a peak at 0° due to the double input (see above) and a drop in input at the -10° and +10° angles.

In the horizontal head position the supralabial TNM areas both the forward- (blue) and backward- (red) pointing areas cover the receptive field of view (see Fig. 39 A). In the range of -40° to +40° the forward-pointing supralabials (blue) make up most of the visual field. In the upward-pointing head position (see Fig. 39 B) the frontal field of view is about half the size of the forward-pointing supralabial area (blue) in the horizontal head position. The frontal field is mostly covered by the forward-orientated infralabials (yellow) and the rear field of view by the backward-orientated supralabial scales (red). In the downward-pointing head position (see Fig. 39 C) the field of view has about the same dimensions as the upward-pointing head position. It is frontally formed by the forward- (blue) and partially by the backward-facing (red) supralabial TNMs, whereas the rear field of view is covered by the backward-pointing infralabial areas (green).

To reconstruct the complete 3-D IR visual field of the boa, the sum of the forward- and backward-orientated TNM areas of the supra- and infralabial scales per head position were added. Again, the highest cm^2 value was classified as 100 % and all other values set into relation thereof. The complete IR fields of view in the three investigated head positions are shown in Fig. 40.

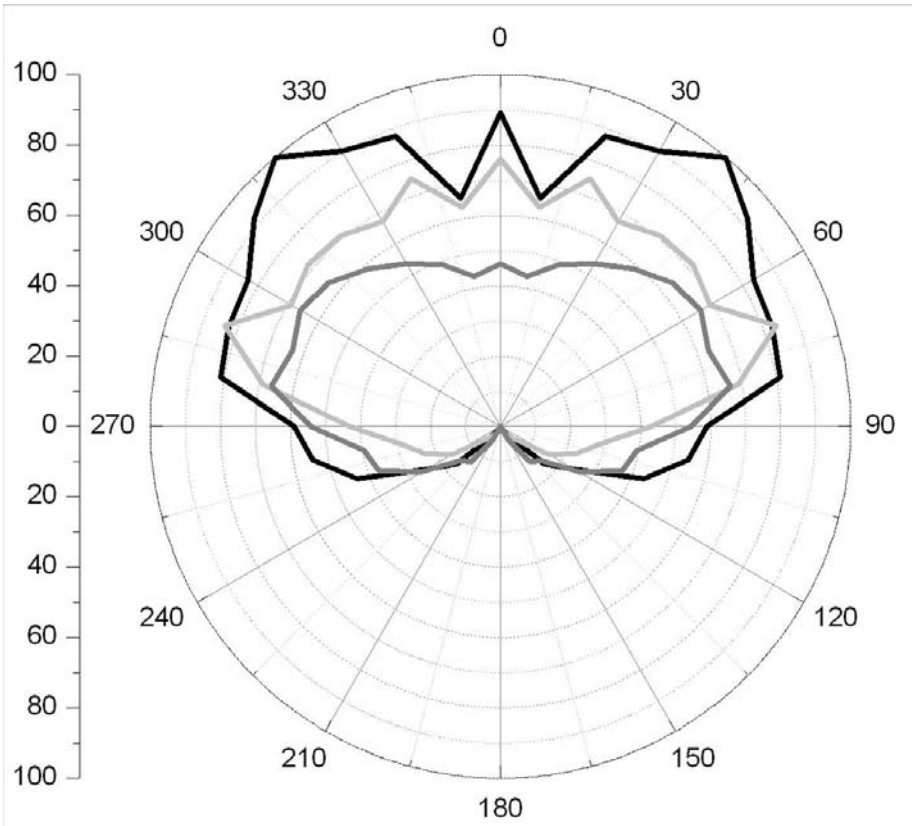

Fig. 40: IR vision fields at the three investigated head positions (horizontal (0°): black, upward-pointing (+45°): light grey, downward-pointing (-45°): dark grey).

The IR visual field reaches to about 120° on both head sides in the horizontal and upward-pointing head position, and even up to 150° on both head sides in the downward-pointing head position. The largest IR visual field is in the horizontal plane (black), especially in the 20° to 80° on both head sides with an obvious peak at the 0° angle and a drop in the -10° to +10° angle area. A similar 'frontal pattern' can be revealed in the upward-pointing head position (light grey). It is almost as large as in the horizontal head position, although it does not cover the areas between 20° and 70° as extensively as in the horizontal head position. In comparison, the downward-pointing head position (dark grey) has the smallest field of view and its emphasis lies more on the lateral angles than on the frontal angles.

4 Discussion

4.1 Behavioural experiments

The aim of the behavioural investigations was to determine and compare the behavioural detection thresholds of the western diamondback rattlesnake (*C. atrox*) and the ball python (*P. regius*) by quantifying the distance at which the snakes behaviourally responded to a moving IR source resembling a mouse in temperature and size. The outstanding advantage of this behavioural approach was not only that the snake's entire neural processing of the stimulus perception was taken into account; but that additional information on the relevance to the snake of the perceived information was revealed, too.

4.1.1 Detection distance of the IR stimulus and behavioural responses

The results reveal a detection distance of 100 cm for *C. atrox* and of 30 cm for *P. regius*. At these source distances the incidence of positive responses is still significantly above baseline value for these behaviours, but beyond 100 cm for the rattlesnakes and beyond 30 cm for the pythons the responses to the IR stimulus could not be distinguished from baseline (rattlesnakes: 29 %, pythons: 9 %). The baseline reveals the rate of spontaneously occurring behaviour (i.e. arbitrary and not stimulus-elicited behavioural changes). The statistical testing of the evaluated responses in respect to the baseline reveals that the evaluated responses of the snakes were responses to the presented IR stimulus.

The rattlesnakes' continuing responses do not only reflect a greater sensitivity (than the pythons), but also reflect the relevance of the stimulus at farther distances. *C. atrox* responded most frequently with 'tongue flicking', 'head jerks' and 'fixing'. These behaviours were displayed solitarily or in combination with each other. 'Tongue flicking' occurred independently of the IR source distance and is interpreted as an attempt to perceive a possible odour from the direction of the stimulus. Smelling is a long-distance sense (accounts for all vipers; Greene, 1992; Schwenk, 1995) and is employed to gather further information about unknown stimuli. Furthermore, 'head jerks', especially in combination with 'fixing' (which occurred more often in distances below 100 cm) are interpreted as an assessment-behaviour to evaluate a stimulus and its distance. The last mentioned interpretation also accounts for the 'freezing and fixing' behaviour of *P. regius*, which was the most frequent behavioural response within the 30 cm distances, together with the 'S-form' and the combination of both. The 'S-form' is an essential posture for a precise strike application, which is only possible within a given fraction of the python's body length. A response to a stimulus is assumed to be

a combination of detection ability and the relevance of the IR stimulus to the python. Assuming that the striking distance of juvenile and adult pythons differs, it is possible that the distances at which they respond to the IR stimulus also differ. Yet, the response rates of juvenile and adult pythons were not significantly different from each other in each distance interval.

4.1.1.1 IR detection threshold of *C. atrox*

For the rattlesnakes the irradiance contrast of the presented IR stimulus was calculated for the distance range of 10 cm to 160 cm using a modified Stefan Bolzmann formula (see 2.2.8 or de Cock Buning, 1983b). The temperature difference between the IR source and the shutter (T_2 - T_1) as well as the radiating area (A) of the IR source determine the irradiance contrast at the critical distance (D) to the snake. The temperature of the IR stimulus and the temperature of the shutter revealed a difference of 10.9 °C ± 1.0 °C. Taking the IR source size of 16 cm^2 and this temperature difference into account at distances from 10 cm to 160 cm, the calculated irradiance contrasts range from (0.3463 ± 0.0335) mW/cm^2 to (0.0014 ± 0.0002) mW/cm^2 respectively. Viewing the curve of the irradiance contrast it is conspicuous that the decline of the rattlesnakes' positive responses is not aligned to it. The sharp drop of responses at a distance of about 100 cm has no relation to the decline of the irradiance contrast. As this is a typical characteristic progression for sensory response curves (Bleckmann, 1980), the percentage of positive responses is rather related to motivation than sensitivity of the rattlesnakes to the stimulus.

C. atrox detected the IR stimuli up to a distance of 100 cm. In the theoretical model of Jones et al. (2001) the size and surface temperature of a mouse and the absorption of the atmosphere of IR radiation was taken into account to calculate the respective detection distance. According to their model the temperature of the membrane surface increases at the threshold of 0.003 °C at a distance of 5 cm (shown by Bullock and Diecke, 1956). The detection distance in the rattlesnake study exceeds this value about 20 times. Furthermore, it also exceeds the calculated detection range of 66.6 cm proposed by de Cock Buning (1983a). The responses of tectal neurons of the pitviper *Calloselasma rhodostoma* were examined at different IR source distances. Applying the modified Stefan Bolzmann formula in the current study, the irradiance contrast of the behavioural IR threshold of *C. atrox* is 3.35×10^{-3} mW/cm^2 at a distance of 100 cm. Thus, this study presents the lowest threshold value reported for any IR sensitive snake and any IR sensory system known in animals so far (compare Campbell et al., 2002). For *Calloselasma* de Cock Buning (1983a) calculated a

value of 10.76 x 10^{-3} mW/cm^2, i.e. a value that is 3.2 times larger. This difference might be due to the different species used in the study but more likely reflects differences in the methodology (behavioural versus electrophysiological investigation). In addition, the stimulus in the present study was moving and presented for 10 s, whereas in de Cock Bunings study a stationary stimulus was presented for 3.6 s. Neither the duration of the IR stimulus presentation nor the velocity of movement within the receptive field influences the irradiance contrast of the IR stimulus. In the current studies, the motion of the IR stimulus was necessary to evoke a behavioural response. In contrast, a moving stimulus is not necessary to evoke an electrophysiological response recorded from the peripheral receptor, the afferent nerve or the primary sensory area (midbrain tectum) within the central nervous system (e.g. Bullock and Diecke, 1956; de Cock Buning, 1983b).

4.1.1.2 IR detection threshold of *P. regius*

To calculate the detection threshold for the pythons, again the Stefan-Boltzmann was applied to a radiating area of 16 cm^2, a temperature difference of 11°C ±1°C between stimulus and background and a distance range from 10 cm to 100 cm, resulting in an irradiance contrast range from (0.3496 ± 0.0335) mW/cm^2 to (0.0035 ± 0.0003) mW/cm^2 respectively. As the IR stimulus was detected up to a distance of 30 cm by *P. regius*, the corresponding irradiance contrast for the applied IR stimulus is 38.83 x 10^{-6} W/cm^2. This was determined as the behavioural IR detection threshold for *P. regius*, which is about one third lower (revealing a 1.5-times higher sensitivity) than de Cock Bunings (1983b) electrophysiological results for *P. reticulatus* (59.79 x 10^{-6} W/cm^2). Although the threshold level of *P. regius* is one third more sensitive than the value reported by de Cock Buning, the calculated distance of IR stimulus detection seems to be similar in both studies (28.3 cm de Cock Buning versus 30 cm current study). However, in the calculation of de Cock Buning a much larger surface area of the stimulus was used (25 cm^2 versus 16 cm^2 current study). If we take the same surface area (16 cm^2) and background temperature (difference 11°C) into account and calculate the critical distance for de Cock Bunings value (about 60 x 10^{-6} W/cm^2) we gain a value of 24 cm as the critical distance for detecting the IR stimulus.

The link between the different methods is the calculation of a detection threshold using the modified Stefan Bolzmann formula, which necessitates a critical distance, the size of a stimulus, as well as the temperatures of a stimulus and its background. The method of determining these factors differs, considering whether single neurons and neural pathways in anesthetized snakes were investigated (electrophysiologically) or whether an intact sensory

system of an alert snake was tested (behaviourally). Behavioural thresholds are usually lower than physiological thresholds (e.g. Bleckmann, 1994), which is confirmed by the results of the two studies. They indicate that the IR detection thresholds of the rattlesnakes and pythons are lower and the detection range for a mouse-like stimulus farther than assumed so far. The design of these experiments suggests that some IR perception did not lead to a behavioural response, so these studies probably under-report the IR sensitivity and detection threshold in both snake species.

4.1.2 Possible influences on the results

A distinct behavioural change had to be displayed during the 10 s period of stimulus presentation to be counted as a positive response to the IR stimulus. Independent blind scoring of the videos confirmed the accuracy of the evaluation of the responses and showed that the behavioural results were rather under- than over-estimated.

Nonetheless the willingness to behaviourally respond to stimuli was a crucial factor in the present studies, because conclusions can only be drawn from positive reactions. The pythons, though alert, were overall less responsive than the rattlesnakes. They responded to only about a third of the stimuli within their detection distance (i.e. up to 30 cm), whereas the rattlesnakes responded to over half of the stimuli within their detection distance (up to 100 cm). In contrast to *P. regius*, *C. atrox* is a very alert and irritable species (e.g. Tennant and Bartlett 2000), which will display distinct behavioural responses to IR stimuli even while in their accustomed housing boxes. However, even if the snakes sensed a stimulus, they might not display a distinct behavioural response. Therefore, it cannot be ruled out that some IR stimuli were perceived, but did not evoke a behavioural response. So it might be possible that the actual detection thresholds of *C. atrox* and *P. regius* are lower than determined by these studies. It is also possible that *P. regius* has detected the stimulus at greater distances, but there is normally no obvious behavioural response in this species. In contrast, the more agile *C. atrox* could show responses even at greater distances. So the differences in detection range here may be due to species-specific behavioural differences.

The differences in behaviour and nature between the two species are reflected in the baseline. The large difference between the baseline values of *C. atrox* and *P. regius* probably results from the difference between the previously determined evaluation criteria for the behavioural responses of each snake species. For example, tongue flicking is a frequently observed behaviour in vipers generally (Schwenk, 1995) and mainly caused the relatively high percentage values of arbitrary responses in the control experiments of the rattlesnakes

(3.1.1.1). In contrast, pythons hardly show distinct arbitrary behaviours, therefore most behaviours were clearly stimulus-evoked, keeping the baseline low.

The influence of habituation on the experimental results was tested. The pythons habituated to the stimulus presented at the near distance of 15 cm, with increasing number over the course of a session. However, the pythons did not show a habituation effect over the course of all experimental sessions with varying distances. Though there were large inter-individual differences, habituation seems to have only played a minor role in the investigation of pythons. In contrast, all rattlesnakes habituated to IR stimuli, with habituation increasing over the course of a session with increasing number of stimuli. The rattlesnakes might have learned quicker than the pythons that IR stimuli were neither harmful nor an indication of prey. Furthermore, in contrast to the pythons, each rattlesnake underwent more than four experimental sessions during the study. This could have enhanced the habituation effect. It should be noted that there were also large inter-individual differences. While some rattlesnakes habituated rapidly, others continued to respond to the IR stimuli. The inter-individual differences shown by *P. regius* and *C. atrox* confirm that response readiness is not only a function of the IR stimulus applied, but also a function of the general response readiness of the snake. In general, habituation increased with increasing source distance. This also indicates that the drop of responsiveness with source distance is more an issue of motivation than of IR perception sensitivity. In terms of the present studies it is important to note that habituation would produce false negative, not false positive results, and thus would lead to an underestimation of the snakes' IR sensitivity range.

Generally, *P. regius* is a rather defensive species that is not inclined to immediately interact with altered surroundings. Thus, it has to be expected that the level of general response is lower than in a more offensive species like *C. atrox*. This is confirmed by the investigation with *C. atrox*, in which the rattlesnakes initially responded with 67 %. Considering that both snake species feed on a similar diet the artificial stimulus should be regarded with the same relevance, hence motivation. Furthermore, the snakes which were used in the current studies were always hungry regardless whether they had been recently fed or not. A single mouse (or in case of the adult pythons one rat) was not sufficient for them to be fully fed, thus it seems unlikely that time spans longer than two days between feeding and experiments would have altered the motivation of the snakes. Nonetheless, the snakes were kept hungry by way of precaution; however, it is unlikely that the snakes regard the stimulus as potential prey considering the artifice of the IR stimulus, including its constant speed (unmoved IR stimuli failed to evoke a response) and constant amplitude as well as the square-

typed form and the almost homogenous thermal profile of the IR emitter. The area of the temperature regulatory sensor covered about 1 % of the upper edge of the IR emitter and, although only 0.2 mm thick, might have thermally insulated this area marginally affecting the homogenous profile. In contrast, a mouse shows a heterogeneous (2.2.6) and, when in motion, constantly changing thermal profile based on numerous minute thermal gradients. A biological IR stimulus presented in a natural environment may be more likely to evoke a behavioural response. Nevertheless, the stimulus needed to fulfil the requirements of defined experimental conditions, to ensure the exclusion of other hidden sensory cues. However, temperature and size were chosen to reflect natural conditions of stimulus intensity and the initial response rate of 55 % of the pythons in the first distance interval (10-20 cm) is a hint that there is no general motivational problem concerning the artifice of the stimulus. Even more, if the artifice of the IR stimulus decreased the responsiveness, this would again support the hypothesis that the detection threshold is actually lower than determined here.

4.1.3 Considerations on the results

The behavioural approach, applied for the first time in this context, allowed an examination of the entire process of IR perception (i.e. the reception of the IR stimulus, the processing of the stimulus and the response to the stimulus) and thus provides an ecologically-relevant perspective on the sensory abilities of both investigated snake species as discussed below (4.1.4). However, the employed IR stimulus, which resembled a mouse in temperature and size, stands for just one typical prey item. Changes in the surface temperature and size of prey items could alter the findings (compare Fig. 41).

Interestingly, laboratory mice seem to be less insulated (i.e. have a higher surface temperature) than small mammals in the wild. The surface temperature of the latter is just a few degrees above ambient (Bakken and Krochmal, 2007, Krochmal pers. comm.). Therefore, it has to be assumed that the employed IR stimulus was more intense than a natural target of the same size. It is in the nature of IR stimuli that objects of higher temperature or larger surface emit more energy. Thus, applying the Stefan Boltzmann equation (see 2.2.8), a larger or warmer stimulus would result in a farther detection distance considering a constant detection threshold of the snake. This would implicate that a rat can be detected from a farther distance than a mouse. The correlation of the detection distance with stimuli of different sizes but same temperature and stimuli of different temperatures but the same size is illustrated in Fig. 41.

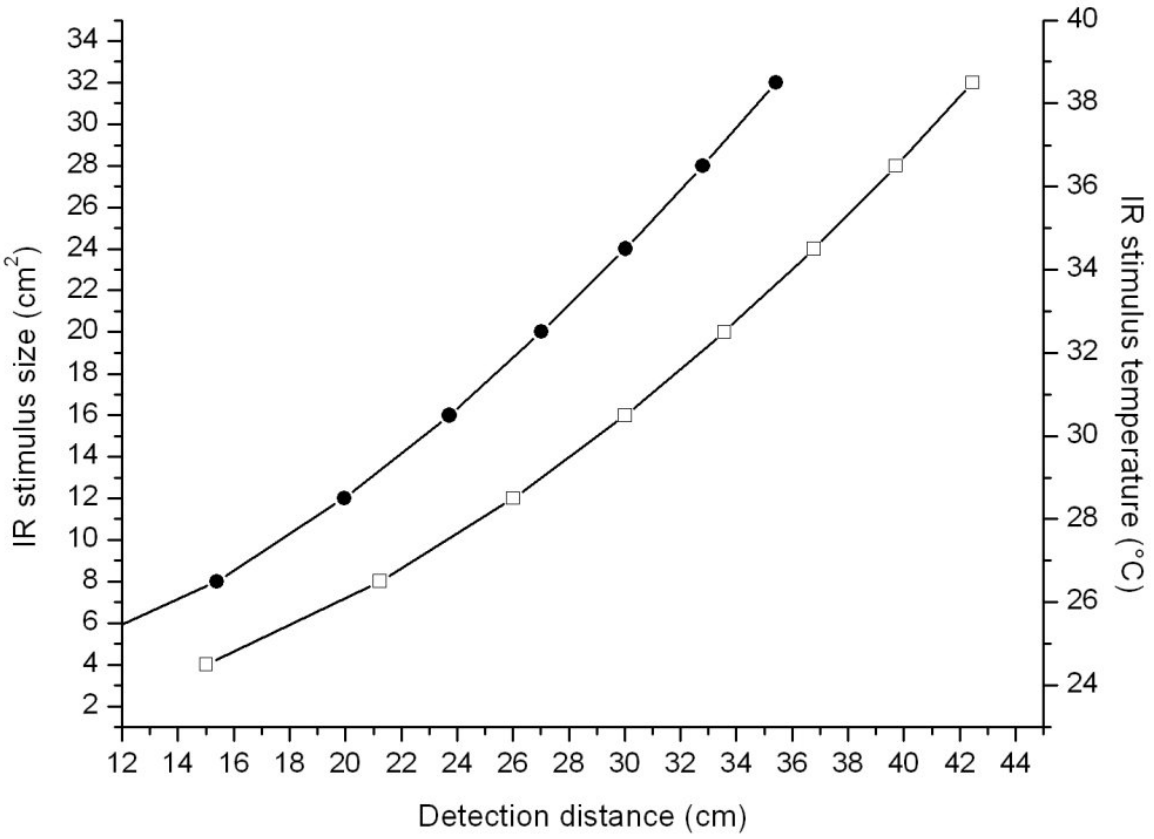

Fig. 41: Correlation of either varying IR stimulus size (white squares) but same temperature (34.5 °C) or varying stimulus temperature (black dots) but same size (16 cm^2) plotted against the calculated critical distance using the threshold level of the irradiance contrast according to the Stefan Boltzmann formula.

Furthermore, Fig. 41 shows that variances of the stimulus size have a much lower impact on the detection distance than changes in temperature (quadratic increase, see Stefan Bolzmann equation). Consequently, marginal changes in temperature can be perceived more easily than size differences. Small deviations in surface temperatures of the snakes' environment seem to play an important role in IR perception.

4.1.4 Pythons' versus rattlesnakes' IR sensitivity and its implications

The pythons prove to be less sensitive than pitvipers, both in electrophysiological studies (de Cock Buning, 1983b) as well as in the presented behavioural investigations. The value in behavioural threshold sensitivity is 3.88 x 10^{-5} W/cm^2 in *P. regius* and 3.35 x 10^{-6} W/cm^2 in *C. atrox*. The different detection thresholds of the two species to the IR stimulus, determined using similar methods, derive from the morphological differences of their pit organs (see Molenaar, 1992). Pit organs of pitvipers are more sensitive as their IR receptors are situated in a thermally insulated membrane located between the outer and the inner cavity of the loreal

pits. In boids with labial pits, the receptors are located in the fundus of the labial pits which lack an insulating underlying cavity. Thus, the incoming energy flux from IR radiation is lost by heat conduction into the underlying tissue. Hence, the IR threshold of neural response is lower in pitvipers.

The relative importance of infrared perception in the behaviour of these snakes is reflected in the threshold sensitivity of their pit organs (Molenaar, 1992). Both snake species are terrestrial, exhibiting lurking behaviour and sedentary hunting tactics. Ball pythons usually do not forage in open sites, preferring to feed in underground cavities, e.g. rodent burrows, or under rock crevices with a 'sit-and-wait' hunting strategy (Merthens, 1987). Their IR sense would primarily be applied within narrow and branching tunnel systems, i.e. it needs to function in close distances (within 30 cm). Rattlesnakes are described as active ambush hunters, i.e. they are actively searching for an optimal hunting spot and often approaching visible moving prey (Greene, 1992). This is in accordance with the findings of the presented study. The IR sense of *C. atrox* is a longer-distance sense with at least 100 cm of coverage, which is suitable for ambush hunting while surveying the surrounding area. Furthermore, the use of the IR sense for purposes other than hunting has been shown for pitvipers (Krochmal and Bakken, 2000, 2003; Krochmal et al., 2004). Using a behavioural approach, Krochmal and Bakken (2003) tested *C. atrox´* ability to direct successful thermoregulatory movements and decisions on thermal radiation cues with intact or disabled pits. The results indicated the pits to be part of a more generalised sense, used to survey the environment aiding behavioural thermoregulation, i.e. escaping stressful temperatures of their natural habitats in addition to prey acquisition. Furthermore, the IR sense is hypothesised to be involved in predator detection or den site selection (e.g. Greene, 1992; Sexton et al., 1992); however, experimental data still awaits conduction. There is no reason to assume that the IR sense is confined to hunting behaviour in boid snakes either. Although experimental data for pythons (and boas) is lacking, the IR sense may be involved in thermoregulatory behaviour as well. The presented data suggest that the IR sense of *P. regius* rather functions as a close distance sense. Regardless of the use of their IR sense for hunting in burrows, the low distance may either be an adaptation to the secluded way of life (thermoregulation in burrows is not a priority) or a general attribute of pythons. In contrast to *C. atrox*, *P. regius* inhabits a natural habitat with relatively constant temperatures.

4.2 Anatomical investigations

The anatomical investigation of *C. hortulanus´* IR sense is discussed in four sections. The first deals with the experiments investigating the processing pathway from the IR receptors via the Nervus trigeminus to the first relay station (LTTD) in the brain and the possible role of the exceptional labial scale morphology. The main topic of the second section is the examination of the IR receptor areas themselves. In the third section investigations of the outer labial scale surface are discussed in context to the receptor areas. The fourth section covers the examination of the IR visual field of *C. hortulanus* and takes its environment into consideration.

4.2.1 Examination of a possible directional representation with tracing experiments

The distribution of the neuronal marker in all tracing experiments is based on the axonal transport system within nerve cells. Limiting factors of the active tracer transport are the tracer molecule size, the axon diameter, and the metabolic activity of the experimental animal or nerve cell, all of which determine the optimal tracer running time. Histological processing, i.e. fixation of the tracer in the tissue, allows an examination of the connection between brain areas or the projections of peripheral nerves.

The aim of this part of the study was to find out whether IR receptors facing backward project to different areas within the LTTD than IR receptors facing forward. The application of BDA to a small injury in the TNM area of a backward-pointing labial scale led to stained neural terminals in the ipsilateral LTTD (3.2.4, Fig. 35). This shows that the fibres of the TNMs took up the tracer and transported it via the trigeminal nerve and ganglion to the LTTD. This is further evidence that the TNMs in the labial scales are indeed specialized IR receptors since the LTTD is a derived structure, only present in IR sensitive snakes and solely involved in IR reception (e.g. Kishida et al., 1982; Molenaar, 1974; Schroeder and Loop, 1976).

After tracer application to a backward-facing IR receptor area, labelled fibres were present in the ventral half of the LTTD only. This clearly shows that this receptor projects to only a restricted portion of the LTTD. Tracer was also applied to other IR receptors on the upper or lower lip in scales facing backward or forward, but none of these experiments were successful. What was expected is that the projection area within the LTTD depends more on the direction the IR receptor is facing than on its topographic position. Due to the zigzag-pattern of scale morphology, neighbouring IR receptors face alternating directions. If the direction of a given receptor would determine the projection area within the LTTD,

neighbouring receptors would terminate in different areas since they face alternating directions.

Unfortunately, only one tracer experiment was successful. But this experiment proposes that a certain IR receptor only innervates a certain part of the LTTD. The critical question is whether there is a topographic representation of the receptor position within the labial scales or a representation of the field of view. The zigzag-pattern of the labial scales of *C. hortulanus* offers a unique way to distinguish between these possibilities because of the alternating directional sensitivity (see below).

It remains unclear, why the tracer experiments were only successful in one case. Presumably, the tracer application was faulty. The injuries had to be deep enough to reach the TNMs (which are situated only 20 µm below the scale surface on average), but not too deep to cause heavy bleeding (as this would wash out the tracer and prevent it from reaching the TNMs).

In principal, BDA tracer seems to be a suitable tracer as it led to a successful result in the first experiment and was frequently used with success in other tracing experiments (e.g. Fritsch and Wilm, 1990). As an alternative tracer biocytin was applied. Biocytin has the advantage of a much smaller molecule size than BDA and therewith underlies a much faster active transport.

Furthermore, different batches of tracer were used, which avoided the use of a malfunctioning tracer. As proven by the background staining, the AB-complex reaction procedure was successful in all cases. All involved boas were healthy and survived the tracer application procedure without any complications.

Because of the low number of animals available, further tracer experiments were not possible. However, more experiments are needed to find out whether there is a map in the LTTD that represents the location of objects in space as opposed to the location of the receptor in the labial scales.

4.2.2 Structure and location of the IR receptors

To understand the functional morphology it is essential to determine the location and structure of the IR-receptive TNMs. Despite differences in methodology in the SDH staining of the frozen sections (i.e. no whole body perfusion, staining was applied directly onto the sections; compare Amemiya et al., 1995, 1996a; Goris et al., 1989), the enzyme reaction was successful in this current investigation.

A sequence of semi-thin sections functioned as the basis for a 3-D reconstruction of the TNM areas of the conspicuously formed three last caudal supralabial scale depressions. The 3-D reconstruction had the advantage of allowing a more detailed and precise examination of TNM distribution. For example, the SDH- reconstruction did not indicate that what appears to be one TNM area of a depression actually consists of two separate TNM areas. The 3-D reconstruction revealed one TNM area on the caudal edge of the preceding scale and one on the rostral edge of the following scale. Furthermore, these two areas do not lie adjacent to each other; the folds of the depressions do not contain TNMs. The TNM area width of the SDH stained sections and of the semi-thin sections differ greatly despite being measured in similar supralabial regions. This difference (80 µm SDH opposed to 320 µm semi-thin sections) derives from the different methodical approaches, i.e. different thicknesses of the sections (20 µm versus 0.5 µm) and the fact that losses of sections in between lead to a larger gap in the SDH staining. Another reason for this difference lies in the form-unstable sections, which only allow a linear approximation of the SDH stained areas. Possible differences of the cutting planes might also have influenced the precision of measurements. Moreover, different individuals, though of similar size and age, have been employed. In her study of the pitless *B. constrictor,* von Duering (1974) found the position of the TNM areas of equally sized individuals to be relatively constant. Von Duering (1974) reconstructed the TNM areas of a selected supralabial scale area of a juvenile *B. constrictor* (from a series of semi-thin sections). She revealed two TNM areas in the supralabial scales, one upper rostral and one lower caudal TNM area. Furthermore, *B. constrictor* possesses TNM areas in the scale rows above the labial scale row, although these areas are smaller and positioned on the midfrontal part of each scale. In comparison to *B. constrictor* the TNM areas of *C. hortulanus* were much larger and restricted to the labial scale rows and the depressions. These differences can be ascribed to the fact that these are two different boa species with differently structured (and sized) labial scales. The correlation between scale morphology, TNM distribution and IR detection sensitivity in other boid species has to be investigated until a structure-function correlation can be established.

Cross-sections revealed the macroanatomy of the labial depressions of *C. hortulanus* to be slightly different in comparison to pythons (e.g. *P. regius*, Amemiya et al., 1995). *P. regius* pits appear as U-shaped invaginations, in which the fundus contains an array of IR receptors. In *C. hortulanus,* only in the labial scale areas with the deep depressions was the U-shape present. However, the TNMs are also only restricted to the epithelium of the fundus.

The irregularity of the labial scale structure around the TNMs varies somewhat even from depression to depression. Thus, the impinging IR radiation of an IR source moves across the TNM areas when moving past the depressions, i.e. the impinging IR radiation on the TNM arrays will vary in shape and length in relation to the angle and position. The structure of the labial scales of *C. hortulanus* does not act as a pinhole camera as there is no pit as such in pitvipers or 'pit-like' structures as in some other boid species (e.g. *P. regius*).

In general, the microstructure of the labial scales of *C. hortulanus* is similar to the labial scale structures of other IR sensitive boids (e.g. Amemiya et al., 1995, 1996a; von Duering, 1974). Both, the surface depth of the TNMs and the TNM epithelium width of *C. hortulanus* are concordant with the structures of *B. constrictor* and *P. regius*. The TNMs are located 2 µm to 6 µm just below the surface of the scales, i.e. beneath the three cornified strata and span over the entire epithelium. This is consistent with findings of *B. constrictor* (von Duering, 1974) and of *P. regius* (Amemiya et al., 1996a), in which the intraepithelial TNMs were situated about 5-8 µm beneath the scale surface. Furthermore, von Duering (1974) described the epithelium containing the TNMs to attain a width of 15 µm, which is consistent with the findings of Amemiya et al. (1996a) who presented a width range of 15-20 µm, and is also consistent with the width of *C. hortulanus´* (11-30 µm, median: 18 µm). The epidermal area containing TNMs was usually thicker than the regular epithelial layer.

The TNMs were embedded between epithelial cells and were densely packed with mitochondria, as has been described for other boids (e.g. Amemiya et al., 1996a; de Robertis and Bleichmar, 1962; Hirosawa, 1980; Terashima et al., 1970; von Duering, 1974). The confirmation of the densely packed mitochondria in the TNM areas fortifies that the SDH staining is confined to the TNM areas, as the mitochondria contain SDH, whose activity can be demonstrated with NBT (Nachlas et al. 1957; Ogawa and Barrnett, 1964, Rosa and Tsou, 1965).

The TNM areas are associated with nerve bundles deriving from the Nervus trigeminus, which branch off, sending their dendrites to the receptors. According to von Duering (1974) and Amemiya et al. (1996a, b) IR sensitive areas are always associated with capillary beds beneath the epidermal layer. This was also the case for *C. hortulanus.* Amemiya et al. (1996a, b; 1999) postulated the capillaries to be essential for a quick energy and oxygen supply for the mitochondria in the TNMs. Even more importantly, the capillaries are considered to carry off excess heat and thereby stabilise the temperature of the receptors (Goris et al., 2007; Nakano et al., 2000). Nakano et al. (2000) found special octopus-like pericytes on the TNM associated

capillaries. These pericytes seem to control (i.e. by increasing) the amount and velocity of blood flow when the TNMs are stimulated. An increase of both causes a cooling effect on the TNMs. Moreover, Goris et al. (2007) showed the TNMs to directly and locally control the pericytes of the blood vessels in response to stimulation.

All in all it was possible to show that the ultra-structure of the TNMs is similar to other boid species.

4.2.3 Surface structure of the receptor-bearing labial scales

The investigation of the labial scale surface of *C. hortulanus* revealed an array of microscopic pores that are different from the ones found on other scale areas of the body (e.g. dorsal or ventral body scales). The microscopic pores situated on the labial scales however, look similar to the pores described by Amemiya et al. (1995), which they also found on the labial scale area of *B. constrictor*. Amemiya et al. (1995) described the pores to be a characteristic of the surface structure of snake IR receptor organs, which is different from any other surface structure in squamate reptiles. According to Amemiya et al. (1995) the array of pores can only be found in IR sensitive snakes and amongst them, only in immediate association with the IR receptors themselves. The pores have been hypothesized to function as spectral filters or anti-reflective coatings with respect to incident electromagnetic radiation by reflecting away longer wavelengths of the visual spectrum (as these might have enough energy to raise the temperature of the receptors), and thus facilitate IR perception by sharpening the IR image (Amemiya et al., 1995, 1996a; Campbell et al., 1999). Thereby, the longer IR wavelengths are supposed to have unimpeded passage through the three strata to the TNMs. However, physical background to support this hypothesis is lacking.

With the knowledge of the exact location of the TNM areas it was able to investigate a possible correlation between the labial scale surface structure (i.e. pores) and receptor distribution. The examination revealed that the surface of the labial scales exhibit a variety of different and considerably smaller pores than those of other scale areas of the snake body (which are also diversely shaped, but larger in comparison). As these smaller pores are restricted to the TNM bearing labial scale depressions (emargination area), it can be assumed that their presence is not coincidental and fulfils a function. On the labial scales, the area sizes of the pores were arbitrarily distributed. It was conspicuous that most pores within the labial scale depressions had relative pore area sizes of up to 20 %, whereas the pores with relative area sizes above 20 % were mainly distributed on the bottom edge outgrowths of the

supralabial scales and on the scales above the labial scales. The surface of the body scales displayed even larger relative pore area sizes of about or above 30 %. So, two-thirds of the smallest pore area sizes (≥ 5 %) were found above the TNM areas, and although they were not restricted to the TNM areas, they were nonetheless confined to the emargination areas of the labial scales. This means that the distribution of the smallest pores loosely correlates with the distribution of the receptive areas. Nevertheless, the correlation is not a sufficient condition for causation. Various explanations can be considered for the association of the small pores and the TNM areas without necessarily implying a connection to IR reception.

Chaisson and Lowe (1989) hypothesized the pores to act as fasteners which secure the outer keratinized epidermal layer to the inner layer until the skin is removed during shedding. Furthermore, it has been suggested that the pores allow the transport of a lipid containing exudate to the surface of the scales (Chaisson and Lowe, 1989). However, the speculated function of lipid secretion and shedding facilitation has not been proven yet. Ultra-thin sections of *C. hortulanus* labial scales revealed no evidence for this hypothesis as the microscopic pores only occur in the uppermost layer of the stratum corneum with no channels leading from a lipid-secreting organ or other organ (neither in the epidermis nor in the dermis) to the pores.

It could also be possible that the small pores occurring in the labial depressions are caused by (massive) restructuring of the labial scales during the development of the pit organs. Each scale would originally have a 'model pattern' of a certain amount of pores per scale. When the pit organs evolved, this model pattern was consistently forced to change with the morphological reconstruction of the labial scales. Since these small pores occur on the surface of loreal as well as on labial pits, it would mean that the pores developed (likewise the IR sense) independently from each other repeatedly. Since the shapes of the labial pits are quite diverse even within closely related IR sensitive snake species but the microscopic pores are merely of the same size (in all IR sensitive snake species) and even occur on the labial scales of the pitless *B. constrictor*, this hypothesis seems unlikely.

Furthermore, it could be possible that the pore area size is simply subject to mechanical strains. During the feeding process the labial scales are much demanded by tractive forces. The smallest pores (≤ 5 % relative pore area) were restricted to the emargination areas of the labial scales, which are also the least demanded areas while opening the mouth widely. The more mesh-shaped pores likely have a greater structural flexibility, and accordingly were mainly distributed on the edges and in the folds of the depressions of the scales.

All the above mentioned possibilities imply that the pores do not necessarily stand in a functional context to the snakes´ IR sense. However, certain findings support the assumption of the surface structure to facilitate IR reception in some way. It is conspicuous that in contrast to surrounding skin structures the pit membranes of crotaline loreal pits as well as the depressions of the boids labial pits are shiny and light in colour (see 2.1.2, Fig. 2 for an example). According to my own observations, but also to Amemiya at al. (1995), the pit surfaces are extremely reflective of visual light. In vivo, the pit organ epidermis is significantly more reflective of visible light than the non-pit organ epidermis (Grace unpublished results in Campbell et al., 1999). Grace at al. (1999) found that the in vivo pit organ was highly absorptive of IR radiation in the ranges of 3 μm to 5 μm and 8 μm to 12 μm, while non-pit organ epidermis reflects incident IR radiation. Furthermore, video camera analysis revealed that the pit organ scales appear to scatter visible light more readily than the other investigated scale types (Campbell at al., 1999). However, this is difficult to comprehend from a physical point of view. If the scale surface should support scattering visible light then one would expect an even grating structure of the pores.

Moreover, all structures of less than 1 μm in size are too small to have an effect on the longer wavelengths, even of the visual spectrum (Bergmann and Schäfer, 1987). Amemiya et al. (1995) took pore measurements (diameter, depths, distribution, density per μm^2) of representatives of crotaline (*Agkistrodon blomhoffii*) and boid species (*Python molurus*, *P. regius*, *B. constrictor*). Although the results differ a certain amount according to species, all (including my results of *C. hortulanus*) fall below 1 μm in size. Therefore, there is no plausible explanation for the assumption of the array of pores to effect IR radiation by reflecting away the longer wavelengths.

Amemiya et al. (1995) hypothesised, the pore sizes were suitable to influence wavelengths of the visual spectrum. There are some arguments against this assumption. The first argument is that the boas (as most IR sensitive snakes) are primarily nocturnal, usually hunting between dusk and dawn. Therefore the wavelengths of the visual spectrum can be considered to play a minor role in situations where the IR sense is employed (e.g. hunting). Another argument against an advantageous influence of the microscopic pores on the wavelengths of the visual spectrum is the irregular distribution pattern of the pores. If serving as a spectral filter one would expect the pore pattern to be regular. Furthermore, the pore diameters of *C. hortulanus* (0.3-0.8 μm) but also of other investigated snake species (e.g. *B. constrictor*: 0.3-0.5 μm, *P. regius*: 0.1-0.15 μm, *Agkistrodon blomhoffii*: 0.25-0.5 μm; compare Amemiya et al., 1995)

correspond loosely with the wavelengths of the visual spectrum (about 400-750 nm). This could mean that the pores are not suitable for reflection but rather for dispersion.

It can be assumed that small pores were developed to achieve an utmost thin and homogenous surface structure. This would imply that the normal surface structure of snake scales is not so suitable for optimal IR reception. However, the finding of the thinner Stratum corneum above the TNM areas leads further to the assumption that the thickness possibly influences the absorption ability for the IR wavelengths (by impeding transmission). The stratum corneum above the TNM areas is only about one-half up to two-third as thick as areas bordering the TNM areas. This finding indicates that the structures directly above the TNMs are different in comparison to the common scale surface and therefore encourages the assumption that the IR reception and the surface structure (i.e. the pore size) are causally associated. But from a physical point of view, the small pore size is not advantageous for reflecting visible light. It is more likely that the small pores serve to homogenise the surface structure and thus the surface temperature.

In conclusion, it can be assumed that the small pores of the labial scale surface and the thinning stratum corneum above the TNM areas, thus the entire structure above the TNMs, support the reception of IR radiation, i.e. functionality of the TNMs.

4.2.4 Considerations to the IR visual field and environmental relevance

The extent of the IR receptive field of the sensory labial scales of *C. hortulanus* was measured by using a head cast onto which the SDH reconstructed TNM areas were painted on. This method was used to gain information about the dimension and directionality of the boas IR receptive field. Therefore, the focus lay on the proportions of the backward- and forward-pointing areas of the supra- and infralabial TNM areas to one another at various receptive field angles in three different head positions and not on exact TNM area sizes. Thus, the inaccuracy of the method (e.g. copying the SDH based TNM reconstructions onto the cast) is of no account. Quite the reverse, this methodical approach has the great advantage of being relatively simple and is here used for the first time to size an IR receptive field. This method was especially suitable for the reconstruction of the IR receptive field of the complex-structure of the labial scale morphology of *C. hortulanus*.

However, in order to determine the IR receptive field a few preconditions had to be assumed: 1. the supra- and infralabial scale rows of both head halves are symmetrical (so that the measurement values of one head side can be mirrored); 2. IR sensitive receptors are functionally identical and have the same distribution density in different pits; 3. the

receptivity of the TNM area correlates with the size of the TNM area, i.e. the larger the receptive area, the higher the sensory IR input. 4. the placement of the TNM areas of individuals is alike (proven by von Duering, 1974).

C. hortulanus is primarily an arboreal snake. Thus, a 3-D perception for precise location and targeting can be considered as essential. This examination reveals that *C. hortulanus´* extraordinary labial scale morphology (zigzag-formation, forward- and backward-pointing TNM areas are not equally sized, and areas forming the depressions exhibit varying inclination angles) in combination with its head form (broadens from rostral to caudal) strongly supports the snakes' ability to precisely detect the direction of an IR source. In the horizontal head position both the supra- and infralabial depressions receive input from an IR stimulus in the horizontal plane. In this plane the forward- and backward-pointing areas of the supra- and infralabials are necessary to locate the position of the IR stimulus. If the head is elevated or lowered the relative portions with which the supra- and infralabial areas receive IR stimulation differ, i.e. they are not equally exposed. In the vertical plane the assessment of the direction of the IR stimulus presumably does not only occur with the aid of the forward- and backward-pointing areas, but rather more by means of computation between the stimulated supra- and infralabial TNM areas. As described previously, the supralabial caudal scales (from the 7^{th} to the 11^{th} scale) have an outgrowth on the lower edge which probably enables the directional perception in the vertical plane by shielding off the radiation from the TNM areas relative to the position of the IR source. It is striking that the location of the infralabial TNM areas are restricted to the area beneath the supralabial scales with the outgrowth. This enhances the difference between the supra- and infralabial input (hypothesis of contrast enhancement), because the outgrowths shield the caudal supralabial depressions from IR input coming from beneath the head as well as shielding off the infralabial depressions from IR input coming from above the head. Furthermore, this special scale morphology most likely causes a contrast enhancement, especially in the horizontal head position (blue: maximum). If the snake raises its head then the forward-pointing infralabial TNMs (yellow) take over the IR reception from the forward-pointing supralabial TNMs (blue). If the boa lowers its head then the forward-pointing supralabial TNMs (blue) play the leading role in IR reception as it is the case in the horizontal head position.

In the horizontal plane the forward- and backward-directed areas are presumably responsible for the directional (front/back) perception. In the vertical plane the supralabial and infralabial depressions in association with the supralabial outgrowth probably allows the

directional (above/below) perception. The combination of these two planes results in a 3-D directional perception.

The IR receptive field encompasses in total 240° for the horizontal and upward-pointing head positions, and even about 300° in the downward-pointing head position. The large size of the IR field, especially in the downward-pointing head position, along with the well covered side regions, supports the assumption, that the IR sense is primarily applied in prey acquisition. The premise is that the boas primarily prey on flying animals, or at least on animals that live at about 'eye-level' of the boa. A few studies and random field observations of *C. hortulanus´* diet supports the precise capture of such prey items, e.g. birds and bats, but also rodents and frogs (e.g. Cundall et al., 2007; Pendlebury, 1974). Hardly anything is known about the capacity of the visual sense (of snakes in general). It can be assumed that *C. hortulanus* mainly relies on its IR sense, at least when capturing prey such as bats. Precise prey capturing under visually deprived conditions (dawn/dusk) or even under exclusion of the visual sense (night time) in a 3-D environment is an outstanding achievement which necessitates a high-performance directional IR sense. The underlying mechanism (predetermined by the scale morphology) has been elucidated in this study.

In comparing the importance of the specific proportions of the boas' IR visual field as deduced from the head cast, the front region is optimized in comparison to the lateral regions, and the lateral regions are optimized in comparison to the hind region of the snakes' head. The upward-facing IR field of view is optimized in comparison to the downward-facing one.

When viewing the single receptive IR fields the focus clearly lies in the frontal head region with the horizontal plane, as expected for a predator. The IR input of the forward-pointing TNM areas along the supralabial scale row in the horizontal head position seems to be most important, as deduced from the TNM area sizes. A special enhancement occurs when the angle of the boas head reaches 0° frontal to the IR source (see 3.2.5). Here the boa receives double IR input, because the TNMs areas of both sides of the head are fully exposed to the IR source.

A small deviation of an IR source from the frontal (0°) position leads to a lower IR input through a smaller receptive area. (This principle is given in all three head positions.) Thus, when in movement (either the boa itself or potential prey) the boa receives a sudden drop in IR stimulation (at about 10°) immediately before facing the IR source (e.g. prey) frontally and receiving double input. This immediate drop of IR radiation input most probably serves as the neural trigger for precise targeting when striking (speed and accuracy is required). If there

were a continuous linear increase of IR sensory input until it reached a maximum, it would be too late to accurately behaviourally respond to the stimulus (as a flying bird would have already passed the optimal (frontal) striking position). However, the neural response will be triggered while the potential prey still moves through the boas IR receptive visual field towards its maximum sensory IR input. As a result the given narrow time frame (of perception and response) is herewith used optimally. All the combined information (increase, sudden drop, double IR radiation input) enables the boa to a precise and fast striking performance. And in fact, this horizontal head position is the position in which the boa actually conducts a strike.

The boa inhabits an environment offering places of deprived view, e.g. dense trees and woodland bushes, suggesting that the IR sense is of advantage even during daytime. Information of the TNMs as well as of the eyes converges in the brain (tectum opticum), where it is processed together. The IR and visual sensory systems can cooperate, but also substitute each other under the deprivation of one sense, as Grace and Matsushita (2007) have shown for *P. regius*.

This anatomical examination suggests that the IR sense in *C. hortulanus* has surpassed the visual sense with respect to functional importance (i.e. to utilize its 3-D environment best possible). This is in accordance with Grace and Matsushita (2007), who suggested a possible dominance of the IR sensory system over the visual system in boids. However, the size of the field of view does not solely determine its importance, as the principles of the visual and IR system differ. Although the focus probably lies on the IR system, the visual system has several advantages in resolution due to structures such as a lens, and functions like accommodation and motility (Grace and Matsushita, 2007).

C. hortulanus´ IR sense covers the lateral to near caudal angles very well (up to 300°), therefore it is probable that the IR field of view is larger than the visual field of view. Large IR and or visual fields of view are usually typical for arboreal snakes, as a good 3-D overview improves both prey detection and predator avoidance. Indeed, (homeothermic) vertebrates are not only important sources of prey, but are also potential predators of boids. Therefore, one could speculate that the IR sense is also employed in defence behaviour, e.g. for detecting and identifying predators such as birds of prey or monkeys. One incidental field observation documented a *C. hortulanus* being attacked by a group of saddleback tamarins (*Saguinus fuscicollis*) (Bartecki and Heymann, 1987). Greene (1992, 1997) suggested predator-

avoidance to possibly be an important selective factor in the evolution of the IR imaging system.

Apart from the IR sense functioning as a prey/predator detection and targeting mechanism other uses of the IR sense are also possible. Associated with prey detection is the ambush perch site selection. As proposed for the pitviper *Gloydius shedaoensis* (Shine et al., 2002) it is possible that the arboreal perch site selection for *C. hortulanus* also serves to provide a high thermal contrast between flying prey (e.g. bird) and the cool background of the sky. This is in accordance with Bakken and Krochmal (2007) who also assume a high thermal background contrast of importance for snakes and furthermore even suggest thermoregulation as the driving force for the evolution of the IR sense. As observed for the above mentioned arboreal pitviper *G. shedaoensis* (Shine et al., 2002), it is likely that *C. hortulanus* also uses its IR sense for thermoregulation.

Whatever the exact function and selective pressure for evolving such a complicated IR receptor morphology, *C. hortulanus* shows a unique and so far unknown mechanism of IR reception to enhance spatial resolution. In all investigated IR sensitive snakes, the main principle to increase spatial resolution is to lower the receptors into a cavity and to decrease the size of the aperture in order to form a kind of pinhole camera. In rattlesnakes, only one pair of pits is present, whereas pythons have a series of pits along the lips. *C. hortulanus*, in contrast, evolved a zigzag-pattern in the labial scales that divides each scale into a forward-facing and a backward-facing part. Together with the curvature of the head and labial scale rows, this enhances spatial resolution while maintaining sensitivity. The biggest problem in a pinhole camera is that spatial resolution is increased by decreasing the aperture. This at the same time decreases sensitivity, because less radiation can enter the pit. In the visual system, this problem was solved by evolving a lens. *C. hortulanus* may have solved this problem by evolving a zigzag-pattern that increases spatial resolution without sacrificing sensitivity. Future studies should focus on this mechanism by either computer modelling of such a 'perception-type' or actually constructing a model with (photo)-receptors in a zigzag-formation to see how spatial resolution could be increased while maintaining sensitivity.

In this study, a new 'perception-type' may have been discovered that is different from all other IR systems and perception mechanisms.

5 Summary

The ability to detect infrared (IR) radiation is a characteristic of boids and pitvipers. These snakes possess highly sensitive IR receptors, often embedded in pit organs, which enable them to locate IR sources independently of visual cues. It was aimed to behaviourally determine IR detection thresholds of two separately evolved IR sensory systems.

Electrophysiological studies have been conducted to determine IR detection thresholds in boids and pitvipers. This is the first behavioural study which focuses on the detection thresholds of a pitviper and a boid snake to IR stimuli. Blindfolded Western diamondback rattlesnakes (*Crotalus atrox*) and Ball pythons (*Python regius*) were exposed to a moving IR stimulus of constant size and temperature at various distances (*C. atrox*: 10-160 cm, *P. regius*: 10-100 cm). The threshold for eliciting distinct behavioural changes during stimulus presentation was used to assess their IR detection thresholds. *C. atrox* can detect a moving IR stimulus resembling a mouse in temperature and size up to a distance of 100 cm, which corresponds to an irradiance contrast of 3.35×10^{-6} W/cm^2. *P. regius* detected the IR stimulus up to a distance of 30 cm, which corresponds to an irradiance contrast of 3.83×10^{-5} W/cm^2. These irradiance contrast detection thresholds reveal a sensitivity 3.2-times higher (*C. atrox*) or 1.5-times higher (*P. regius*) than sensitivities found in previous electrophysiological investigations, confirming that behavioural approaches determine sensory sensitivities far more accurately. The differing IR sensitivities of *C. atrox* and *P. regius* presumably result from their different habitats, i.e. *C. atrox* prefers open spaces, whereas *P. regius* primarily inhabits narrow burrows and rocky areas. Naturally, their IR detection thresholds should be adapted to the distance ranges at which they can be employed usefully.

The pit morphology of pitvipers, pythons and boas varies greatly. Pitvipers possess loreal pits, and most pythons have labial pits, whereas most boas lack labial pits or depressions. Pitvipers and pythons are quite well investigated; however, the pit morphology of pit-bearing boas has hardly been examined. The IR sensitive Amazon tree boa (*Corallus hortulanus*) possesses extraordinarily shaped deep labial scale depressions, which are arranged in a zigzag-formation resulting in backward- and forward-facing scale areas. This unique directional morphology is assumed to be the basis for the IR perception mechanism of *C. hortulanus*. To build a model for assessing the function of this pit arrangement for IR reception, it was necessary to determine the occurrence, structure and distribution of the IR receptors, i.e. terminal nerve masses (TNMs), within the labial scales. Their structure was investigated by light microscopy and transmission electron-microscopy, whereas the location and size of the TNM areas was

determined by succinate dehydrogenase staining. Furthermore, tracing experiments with neurobiotin should have exhibited the central neural projection of the TNMs, however only one trial successfully revealed projections up to the IR processing LTTD.

Certain small pores have previously been hypothesised to aid IR reception therefore the surface of the labial scales was inspected with scanning electron microscopy (SEM). These SEM results were combined with a precise 3-D reconstruction of the labial scales, revealing a loose correlation between TNM areas and specific small pores. However, these pores do not seem suitable for reflecting away non-IR wavelengths as hypothesised. Indeed it seems more probable that these pores aid IR reception by homogenising the surface structure, and thereby the surface temperature.

To investigate the functional morphology, the SDH staining results were necessary to reconstruct the TNM areas of the supra- and infralabial scales and transfer these onto a plaster head cast of *C. hortulanus*. This model was used to decode the directional reception characteristics of the 3-D IR field of view, which covers an angular range of up to 300°. It was possible to show that the radiation of an IR source impinges on different proportions of forward- and/or backward-facing TNM areas when coming from different angles, thus giving exact directional information. Additionally, the spatial resolution is enhanced by the sophisticated shape of some labial scales. Moreover, a novel enhancement mechanism was discovered: when a boa turns its head to frontally face an IR source, it receives a sudden drop in IR stimulation at the 10° angle, before receiving doubled IR radiation input when facing the IR source frontally (0° angle). Only then does the IR radiation impinge fully on both sides of the boas head and labial scales. The swift drop at 10° most probably serves as a neural trigger for precise targeting when striking. With *C. hortulanus* a new IR sensing system has been discovered and the results help to understand how morphology can function to increase the spatial resolution power of sensory systems.

6 References

Amemiya F, Goris RC, Atobe Y, Ishii N, Kusunoki T. 1996 a. The ultrastructure of infrared receptors in a boid snake, *Python regius:* evidence for periodic regeneration of the terminals. Anim. Eye Res. 15:13-25.

Amemiya F, Goris RC, Masuda Y, Kishida R, Atobe Y, Ishii N, Kusunoki T. 1995. The surface architecture of snake infrared receptor organs. Biomedical Research 16(6):411-421.

Amemiya F, Nakano M, Goris RC, Kadota T, Atobe Y, Funakoshi K, Hibiya K, Kishida R. 1999. Microvasulature of crotaline snake pit organs: possible function as a heat exchange mechanism. The Anatomical Record 254:107-115.

Amemiya F, Ushiki T, Goris RC, Atobe Y, Kusunoki T. 1996 b. Ultrastructure of the crotaline snake infrared pit receptors: SEM confirmation of TEM findings. The Anatomical Record 246:135-146.

Bakken GS, Krochmal AR. 2007. The imaging properties and sensitivity of the facial pits of pitvipers as determined by optical and heat-transfer analysis. J. Exp. Biol. 210:2801-2810.

Barrett R, Maderson PFA, Meszler RM. 1970. The pit organs of snakes. In: C. G, Parsons TS, editors. Biology of the Reptilia. London, New York: Academic Press. p 277-300 (Chapter 4).

Bartecki U, Heymann EW. 1987. Field oservations of snake-mobbing in a group of saddle-back tamarins, *Saguinus fuscicollis nigrifrons*. Folia Primatol. 48(3-4):199-202.

Bergmann L, Schaefer C. 1987. Lehrbuch der Experimentalphysik - Optik. Berlin, New York: Walter de Gruyter.

Berson DM, Hartline PH. 1988. A tecto-rotundo-telencephalic pathway in the rattlesnake: evidence for a forebrain representation of the infrared sense. J. Neurosci. 8:1074-1088.

Beynon, PH, Cooper, JE (Hrsg.): Kompendium der Heimtiere, Schlütersche, 1. Auflage, S. 262-263, 1997

Bleckmann H. 1980. Reaction time and stimulus frequency in prey localization in the surface-feeding fish *Aplocheilus lineatus*. J. Comp. Physiol. A 140:163-172.

Bleckmann H. 1994. Reception of hydrodynamic stimuli in aquatic and semiaquatic animals. Stuttgart, Jena, New York: Gustav Fischer Verlag. 112 p.

Bleichmar H, de Robertis E. 1962. Submicroscopic morphology of the infrared receptor of pit vipers. Z. Zellforsch. mikrosk. Anat. 56:748-761.

Bullock TH, Barrett R. 1968. Radiant heat reception in snakes. Communications in Behavioral Biology 1:19-29.

Bullock TH, Cowles RB. 1952. Physiology of an infrared receptor: the facial pit of pit vipers. Science 115(5):541-543.

Bullock TH, Diecke FPJ. 1956. Properties of an infrared receptor. J. Physiol. 134:47-87.

Bullock TH, Fox, W. 1957. The anatomy of the infra-red sense organ in the facial pit of pit vipers. Quarterly Journal of Microscopial Science 98 , part 2:219-234.

Butler JA, Reid J. 1986. Habitat preference of snakes in southern cross river state Nigeria. In: Rocek Z, editor. Studies in herpetology. Prag. p 483-488.

Campbell AL, Bunning TJ, Stone MO, Church D, Grace MS. 1999. Surface ultrastructure of pit organ, spectacle, and non pit organ epidermis of infrared imaging boid snakes: a scanning probe and scanning electron microscopy study. Journal of Structural Biology 126:105-120.

Campbell AL, Naik RR, Sowards L, Stone MO. 2002. Biological infrared imaging and sensing. Micron 33:211-225.

Chiasson RB, Lowe CH. 1989. Ultrastructural scale patterns in Nerodia and Thamnophis. J. Herpetol. 23:109-118.

Chiszar D, Castro CA, Smith HM, Guyon C. 1986. A behavioral method for assessing utilization of thermal cues by snakes during feeding episodes, with a comparison of crotaline and viperine species. The Annals of Zoology 24:123-131.

Cundall D, Deufel A, Irish F. 2007. Feeding in boas and pythons: motor recruitment patterns during striking. In: Henderson RW, Powell R, editors. Biology of boas and pythons: Eagle Mountain Publishing.

de Cock Buning T. 1984. A theoretical approach to the heat sensitive pit organs of snakes. J. theor. Biol. 111:509-529.

de Cock Buning T. 1985. Qualitative and quantitative explanation of the forms of heat sensitive organs in snakes. Acta Biotheoretica 34:193-206.

de Cock Buning T, Terashima S, Goris RC. 1981 a. Crotaline pit organs analyszed as warm receptors. Cellular and Molrcular Neurobiology 1(1):69-85.

de Cock Buning T, Terashima S, Goris RC. 1981 b. Python pit organs analysed as warm receptors. Cellular and Molrcular Neurobiology 1(3):271-278.

de Cock Buning TJ. 1983 a. Thermal sensitivity as a specialization for prey capture and feeding in snakes. Amer. Zool. 23:363-375.

de Cock Buning TJ. 1983 b. Thresholds of Infrared Sensitive Tectal Neurons in *Python reticulatus*, *Boa constrictor* and *Agkistrodon rhodostoma*. J Comp Physiol A 151:461-467.

de Cock Buning TJ, Goris RC, Terashima S. 1981. The role of thermosensitivity in the feeding behavior of the pit viper, *Agkistrodon blomhoffi brevicaudus*. Jap. J. Herpetol. 9:7-27.

de Robertis E, Bleichmar H. 1962. Mitochondriogenesis in nerve fibers of the infrared receptor membrane of pit vipers. Z. Zellforsch. 52:572-582.

Dullemeijer P. 1959. A comparative functional-anatomical study of the heads of some Viperidae. Morph. Jb. 99(4):881-985.

Ebert J, Mueller S, Westhoff G. 2007. Behavioural examination of the infrared sensitivity of ball pythons (*Python regius*). Journal of Zoology 272(3):340-347.

Ebert J, Westhoff G. 2006. Behavioural examination of the infrared sensitivity of rattlesnakes (*Crotalus atrox*). Journal of Comparative Physiology A 192:941-947.

Evans WG. 1964. Infrared receptors in *Melanophila acumniata* de Geer. Nature 202:211.

Evans WG. 1966. Preception of infrared radiation from forest fires by *Melanophila acuminata* (Buprestidae, Coleoptera). Ecology 47:1061-1065.

Evans WG, Kuster JE. 1980. The infrared receptive fileds of *Melanophila acuminata* (Coleoptera: Burprestidae). Can. Ent. 112:211-216.

Fritsch B, Wilm C. 1990. Dextran amines in neuronal tracing. Trends Neurosci 13:14-24.

Gamow RI, Harris JF. 1973. Infrared receptors of snakes. Sci. Amer. 228:94-100.

Gopalakrishnakone P. 1984. Light and scanning electron microscopic study of the pit organ of the reticulate python, *python reticulatus*. The snake 16(1):33-42.

Goris RC, Nakano M, Atobe Y, Funakoshi K. 2007. The infrared sight of boas and pythons. In: Henderson RW, Powell R, editors. Biology of the boas and pythons: Eagle Mountain Publishing, LC.

Goris RC, Kadota T, Kishida R. 1989. Innervation of snake pit organ membranes mapped by receptor terminal succinate dehydrogenase activity. Current Herpetology in East Asia:8-16.

Goris RC, Nomoto M. 1967. Infrared reception in oriental crotaline snakes. Comp. Biochem. Physiol. 23:879-892.

Grace MS, Church D, Kelly CT, Lynn WF, Cooper TM. 1999. The python pit organ: imaging and immunocytochemical analysis of an extremely sensitive natural infrared detector. Biosensors & Bioelectronics 14:53-59.

Grace MS, Matsushita A. 2007. Neural correlates of complex behavior: vision and infrared imaging in boas and pythons. In: Henderson RW, Powell R, editors. Biology of the boas and pythons: Eagle Mountain Publishing, LC.

Grace MS, Woodward OM. 2001. Altered visual experience and acute visual deprivation affect predatory targeting by infrared-imaging boid snakes. Behavioural Brain Research 919:250-258.

Grace MS, Woodward OM, Church DR, Calisch G. 2001. Prey targeting by the infrared-imaging snake Python: effects of experimental and congenital visual deprivation. Behavioural Brain Research 119:23-31.

Greene HW. 1992. The ecological and behavioral context for pitviper evolution. In: Campbell AJ, Brodie, E. D., editor. Biology of the pitvipers. Tyler: Selva. p 107-118.

Greene HW. 1997. Snakes: The evolution of mystery in nature. Berkeley: University of California Press.

Greer GC. 1994. Nest sites of royal pythons in West Africa. Reptile & Amphibian Magazine 1994:44-55.

Hartline PH. 1974. Thermoreception in snakes. In: Fessord A, editor. Handbook of Sensory Physiology. p 297-312/313?

Haverly JE, Kardong KV. 1996. Sensory deprivation effects on the predatory behavior of the rattlesnake, Crotalus viridis oreganus. Copeia(2):419-428.

Henderson RW. 1993. Foraging and diet in West Indian *Corallus enydris* (Serpentes: Boidae). Journal of Herpetology 27(1):24-28.

Henderson RW, Winstel RA. 1995. Aspects of habitat selection by an arboreal boa (*Corallus enydris*) in an area of mixed agriculture on Grenada. Journal of Herpetology 29(2):272-275.

Hirosawa K. 1980. Electron microscopic observations on the pit organ of a crotaline snake *Trimeresurus flavoviridis*. Arch. Histol. Jap. 43:65-77.

Hisajima T, Kishida R, Atobe Y, Nakano M, Goris RC, Funakoshi K. 2002. Distribution of myelinated and unmyelinated nerve fibers and their possible role in blood flow control in crotaline snake infrared receptor organs. The Journal of Comparative Neurology 449:319-329.

Jones BS, Lynn WF, Stone MO. 2001. Thermal modeling of snake infrared reception: Evidence for limited detection range. Journal of Theoretical Biology 209(2):201-211.

Kardong KV. 1993. The predatory behavior of the Northern Pacific Rattlesnake (*Crotalus viridis oreganus*) - laboratory versus wild mice as prey. Herpetologica 49(4):457-463.

Kardong KV. 1996. Sensory deprivation effects on the predatory behaviour of the rattlesnake *Crotalus viridis*. Copeia 2:419-428.

Kardong KV, Mackessy SP. 1991. The strike behavior of a congenitally blind rattlesnake. J Herpetol 25:208-211.

Kass L, Loop MS, Hartline PH. 1978. Anatomical and physiological localization of visual and infrared cell layers in tectum of pit vipers. J. Comp. Neur. 182:811-820.

Kesel AB, Junge MM, Nachtigall W. 1999. Einführung in die angewandte Statistik für Biowissenschaftler. Basel, Boston, Berlin: Birkhaeuser Verlag.

Kirschner A, Seufer H. 2003. The ball python - care, breeding and natural history. Keltern-Weiler, Germany: Kirschner & Seufer Verlag. 1-94 p.

Kishida R, Amemiya F, Kusunoki T, Terashima S-I. 1980. A new tectal afferent nucleus of the infrared sensory system in the medulla oblongata of crotaline snakes. Brain Research 195:271-279.

Kishida R, Goris RC, Terashima S-I, Dubbeldam JL. 1984. A suspected infrared-recipient nucleus in the brain stem of the vampire bat, *Desmodus rotundus*. Brain Research 322:351-355.

Kishida R, Terashima S, Goris RC, Kusunoki T. 1982. Infrared sensory neurons in the trigeminal ganglia of crotaline snakes: transganglionic HPR transport. Brain Res. 241(1):3-10.

Klauber LM. 1982. Rattlesnakes - their habits, life histories, and influences on mankind. Berkeley, Los Angeles: University of California Press, Ltd. 1-350 p.

Kluge AG. 1991. Boine snake phylogeny and research cycles. Misc. Publ. Mus. Zool., Univ. Michigan 178:1-58.

Kreiss EJ, Schmitz A, Schmitz H. 2005. Morphology of the prothoracic discs and associated sensilla of Acanthocnemus nigricans (Coleoptera, Acanthocnemidae). Arthropod Structure and Development 34(4):419-428.

Krochmal AR, Bakken GS. 2000. Evidence for the use of facial pits for behavioral thermoregulation in the western diamondback rattlesnakes (*Crotalus atrox*). American-Zoologist 40(6):1092-1093.

Krochmal AR, Bakken GS. 2003. Thermoregulation is the pits: use of thermal radiation for retreat site selection by rattlesnakes. J Exp Biol 206:2539-2545.

Krochmal AR, Bakken GS, LaDuc TJ. 2004. Heat in evolution's kitchen: evolutionary perspectives on the functions and origin of the facial pit of pitvipers (Viperidae: Crotalinae). J Exp Biol 207:4231-4238.

Kuerten L, Schmidt U. 1982. Thermoeception in the common vampire bat (*Desmodus rotundus*). Journal of Comparative Physiology A 146:223-228.

Luiselli L, Akani GC, Capizzi D. 1998. Food resource partitioning of a community of snakes in a swamp rainforest of south-eastern Nigeria. J. Zool. 246:125-133.

Luiselli L, Angelici FM. 1998. Sexual size dimorphism and natural history traits are correlated with intersexual dietary divergence in royal pythons (*Python regius*) from the rainforests of southeastern Nigeria. Ital. J. Zool. 65:183-185.

Lynn WG. 1931. The structure and function of the facial pit of the pit vipers. Amer. J. Anat. 49:97-139.

Maderson PFA. 1970. The distribution of specialized labial scales in the Boidae. In: Gans C, Parsons TS, editors. Biology of the reptilia. London, New York: Academic Press. p 301-304.

Mainz T, Schmitz A, Schmitz H. 2004. Variation in number and differentiation of the abdominal infrared receptors in the Australian "fire-beetle" Merimna atrata (Coleoptera, Buprestidae). Arthropod Structure and Development 33(4):419-430.

Mattison C. 1995. The encyclopedia of snakes. New York: Facts on File, Inc.

Mattison C. 1996. Rattler! A natural history of rattlesnakes. London: Blandford.

Mehrtens JM. 1987. Living snakes of the world in color. New York: Sterling Publishing Co., Inc.

Mehrtens JM. 1993. Schlangen der Welt - Lebensraum, Biologie, Haltung. Stuttgart: Franckh-Kosmos Verlags-GmbH & Co.

Meschede D. 2002. Gerthsen Physik. Berlin, Heidelberg, New York: Springer-Verlag.

Meszler RM. 1970. Correlation of ultrastructure and function. In: Gans C, Parsons TS, editors. Biology of the reptilia. London, New York: Academic Press. p 305-314.

Meszler RM, Webster DB. 1968. Histochemistry of the rattlesnake facial pit. Copeia 1968:722-728.

Moiseenkova V, Bell B, Motamedi M, Wozniak E, Christensen B. 2003. Wide-band spectral tuning of heat receptors in the pit organ of the copperhead snake (Crotalinae). Am J Physiol Regul Integr Comp Physiol 284:R598-R606.

Molenaar GJ. 1974. An additional trigeminal system in certain snakes possessing infrared receptors. Brain Research 78:340-344.

Molenaar GJ. 1978. The sensory trigeminal system of a snake in possession of infrared receptors. 1. The sensory trigemnial nuclei. J Comp Neurol 179:123-136.

Molenaar GJ. 1992. Anatomy and physiology of infrared sensitivity of snakes. In: Gans C, editor. Biology of the Reptilia: University of Chicago Press. p 368-453.

Molenaar GJ, Fizaan-Oostveen JL. 1980. Ascending projections from the lateral decending and common sensory trigeminal nuclei in python. J Comp Neurol 1989 (3):555-572.

Molenaar GJ, Fizaan-Oostveen JLFP, Van der Zalm JM. 1979. Infrared and tactile units in the sensory trigeminal system of Python reticulatus. Brain Res. 170:372-376.

Mueller S. 2005. Verhaltensstudie zur Infrarot-Perzeption bei Königspythons (*P. regius*) [Diploma Thesis]. Bonn: Rheinische Friedrich-Wilhelms Universitaet Bonn.

Nachlas MM, Tsou K-C, De Souza E, Chang CS, Seligman AM. 1957. Cytochemical demonstration of succinic dehydrogenase by the use of a new P-nitrophenyl substituted ditetrazol. J. Histochem. Cytochem. 5:420-436.

Nakano M, Atobe Y, Goris RC, Yazama F, Ono M, Sawada H, Kadota T, Funakoshi K, Kishida R. 2000. Ultrastructure of the capillary pericytes and the expression of smooth muscle alpha-actin and desmin in the snake infrared sensory organs. Anat. Rec. 260:299-307.

Nation JL. 1983. A new method using hexamethyldisilatane for preparation of soft inscet tissue for scanning electron microscopy. Stain technology 58(6):347-351.

Newman EA, Gruberg ER, Hartline PH. 1980. The infrared trigeminotectal pathway in the rattlesnake (*Crotalus viridis*) and in the python (*Python reticulatus*). J. Comp. Neurol. 191:465-477.

Newman EA, Hartline PH. 1982. The infrared 'vision' of snakes. Science 20:116-127.

Noble GK, Schmidt A. 1937. The structure and function of the facial and labial pits of snakes. Proceedings of the american philosophical society 77(3):263-288.

Ogawa K, Barrnett RJ. 1964. Electron histochemical examination of oxidative enzymes and mitochondria. Nature 203:724-726.

Pendlebury GB. 1974. Stomach and intestine contents of *Corallus enydris*; a comparison of island and mainland specimens. Journal of Herpetology 8(3):241-244.

Ros M. 1935. Die Lippengruben der Pythonen als Temperaturorgane. Jena Zeitschrift für Medizin und Naturwissenschaft 70:1-32.

Rosa CG, Tsou K-C. 1965. Histochemistry. Demonstration of Sjöstrand membrane particles by an electron cytochemical method. Nature 206:103-105.

Rubio M. 1998. Rattlesnake - portrait of a predator. Washington, London: Smithsonian Insitution Press. 1-240 p.

Schmitz H, Bleckmann H. 1998. The photomechanic infrared receptor for the detection of forest fires in the beetle *Melanophila acuminata* (Colepoptera: Buprestidae). J Comp Physiol A 182:647-657.

Schmitz H, Schmitz A, Trenner S, Bleckmann H. 2002. A new type of insect infrared organ of low thermal mass. Naturwissenschaften 89(5):226-229.

Schmitz H, Trenner S, Hofmann MH, Bleckmann H. 2000. The ability of Rhodnius prolixus (Hemiptera: Reduviidae) to orient towards a thermal source solely by its infrared radiation. Journal of Insect Physiology 46(5):745-451.

Schroeder DM, Loop MS. 1976. Trigeminal projections in snakes possessing infrared sensitivity. J Comp Neurol 169:1-14.

Schwenk K. 1995. Of tongues and noses: chemoreception in lizards and snakes. Tree 10(1):7-12.

Seigel RA, Collins JT, editors. 1993. Snakes - ecology and behaviour. New York, London, Singapore, Sydney: McGraw Hill, Inc.

Sexton OJ, Jacobson P, Bramble JE. 1992. Geographic variation in some activities associated with hibernation in nearctic pitvipers. In: Campbell AJ, Brodie, E. D., editor. Biology of the pitvipers. Tyler: Selva. p 337-345.

Shine R, Sun L-X, Kearney M, Fitzgerald M. 2002. Thermal correlates of foraging-site selection by Chinese pitvipers (*Gloydius shedaoensis*, Viperidae). J. Thermal Biol. 27:405-412.

Stafford P. 2000. Snakes. Washington D.C., London: Smithsonian Institution Press in association with the Natural History Museum London.

Stanford LR, Schroeder DM, Hartline PH. 1981. The ascending projection of the nucleus of the lateral descending trigeminal tract: a nucleus in the infrared system of the rattle snake (*Crotalus viridis*). J Comp Neurol 201:161-174.

Sternstein M. 1996. Statistics. New York: Barron´s Eduactional Series, Inc.

Tennant A, Bartlett RD. 2000. Snakes of North America: Eastern and Central Regions: Houston: Gulf Publishing.

Terashima S-I, Goris RC, Katsuki Y. 1970. Structure of warm fiber terminals in the pit membrane of vipers. J. Ultrastruct. Res. 31:494-506.

Terashima S-I, Goris RC. 1975. Tectal organization of pit viper infrared reception. Brain Research 83:490-494.

Terashima S-I, Goris RC, Katsuki Y. 1968. Generator potential of crotaline snake infrared receptor. J. Neurophysiol. 31:682-688.

Terashima S-I, Goris, R. C. 1976. Receptive area of an infrared tectal unit. Brain Research 101:155-159.

Theodoratus DH, Chiszar D, Smith HM. 1997. Rattlesnake orientation to prey as a function of thermal backgrounds and edges. Physiol Record 47:461-472.

Trutnau L. 2002. Ungiftige Schlangen. Stuttgart: Eugen Ulmer GmbH & Co.

von Duering M. 1974. The radiant heat receptor and other tissue receptors in the scales of the upper jaw of *Boa constrictor*. Z. Anat. Entwickl.-Gesch. 145:299-319.

von Duering M, Miller MR. 1979. Sensory nerve endings of the skin and deeper structures. Biology of the Reptilia. London: Academic Press. p 407-439.

Walls JG. 1998. The living pythons - a complete guide to the pythons of the world: T.F.H. Publications, Inc., USA. 1-256 p.

Warren JW, Proske U. 1968. Infra red receptors in the facial pits of Australian python *Morelia spilotes*. Science 159:439-444.

Welker E, Hoogland PV, al e. 1983. Tectal connections in *Python reticulatus*. J Comp Neurol 220:347-354.

Young BA, Aguiar A. 2002. Response of western diamondback rattlesnakes *Crotalus atrox* to airborne sounds. J. Exp. Biol. 205:3087-3092.

Zoefel P. 1992. Statistik in der Praxis. Paris, Stuttgart, Jena: Gustav Fischer Verlag.

7 Abbreviations

Aqua dest.	distilled water
BDA	biotinylated dextran-amine
DAB	diaminobenzidin
HMDS	hexamethyldisilazane
Hz	Hertz
IR	infrared
M	molar
MW	molecular weight
NBT	nitro blue tetrazolium
PE	Peltier element
pH	potentia hydrogenii
SDH	succinate dehydrogenase
SEM	scanning electron microscopy
TEM	transmission electron microscopy
TNM	terminal nerve mass

8 Appendix

8.1 Recipes

8.1.1 SDH staining

Unfixed, fresh tissue was frozen and cut on a cryostat at 20 µm. Sections were collected directly onto slides and allowed to dry for a few hours. A solution of 10 ml 0.1M phosphate buffer (pH=7.4) with 0.5 g succinate and 10 mg NBT (approx. 98%, Sigma-Aldrich, Germany) sufficient for about 5 slides was mixed and the slides were incubated for 3-4 hours at room temperature. Then, the slides were fixed in 4% paraformaldehyde (1 l 0.1M phosphate buffer solution mixed with 40 g paraformaldehyde) over night. Dehydration was conducted by an increasing ethanol series (70%, 80%, 90%, 96%, 100%, isopropanol (I-II), xylol (I–III)) with 10 min incubation time in each. The slides were covered with Roti Histokit-II (Roth, Germany) and allowed to dry thoroughly.

Phosphate buffer: 2l Aqua dest. + 28.4 g Na_2HPO_4 + 5.4 g KH_2PO_4

8.1.2 Light microscopy and transmission electron-microscopy

8.1.2.1 Epon embedding procedure

The material fixation was conducted by incubation in a solution of 2.5% glutardialdehyde in 0.1M phosphate buffer overnight. Then, the samples were washed with phosphate buffer (3x) and thereafter cacodylate buffer (3x), both at 2°C. An incubation of the samples in 1.5 % osmium tetroxide solution on ice for 2 h followed. The samples needed to be washed in cacodylate buffer (3x, 2°C), before they underwent dehydration with an increasing ethanol series (70% at 2°C, 80%, 90%, 98%, 100%, isopropanol) for 10 min in each, except in the 70% ethanol, which was for 60 min to warm to room temperature. Then, the samples were transferred in intermedia, for 10 min in each: 1. 50% propylen oxide (1,2-Epoxypropan) in isopropanol, 2. 75% propylene oxide in isopropanol, 3. 3x 100% propylene oxide. Thereafter, the samples were transferred into a propylene oxide- epon –suspension in a ratio of 9:1 for 12 h. Then, the propylen oxide was left to evaporate. The samples were transferred into 100% Epon for 24 h and embedded in silicon-rubber-troughs filled with Luft's Epon. Polymersation occurred in an incubator at 60°C for about 48 h.

Sörensens phosphate buffer

Solution A: 27.6 g 0.2M $NaH_2PO_4 \cdot H_2O$ (Natriumdihydrogenphosphate-monohydrate) dissolved in 1l Aqua dest.

Solution B: 28.4 g 0.2M Na_2HPO_4 (Di-natriumhydrogenphosphate) dissolved in 1l Aqua dest.

The pH of the buffer was adjusted to 7.2 by mixing 280 ml of solution A and 720 ml of solution B. This buffer solution had an osmolarity of approximately 226 mOsm and was 0.1M. For reptile tissues, an adjustment to 300-340 mOsm with NaCl was needed.

0.05M **Cacodylate buffer**: 1.06 g cacodylate (approx. 98%), 9.2 g sucrose, 0.4 ml HCl (1 n) dissolved in 100 ml Aqua dest., (pH=7.1)

2.5% **Glutardialdehyde fixative**: 25 ml glutardialdehyde (25%) in 125 ml phophate buffer

1.5% **Osmium tetroxide solution**: 1 ml osmium tetroxide (4%) in 1.7 ml 0.1M cacodylate buffer

Epon 812 after Luft:

Mixture A: 15.5 g Epon 812 (Glycidether 100) + 25 g DBA (dodecenyl- succinic acid-anhydride)

Mixture B: 10 g Epon 812 + 8.9 g MNA (methylen- domethylenphtal acid- anhydride)

Mixture A and mixture B were mixed in a ratio of 7:3 (40.5 g mixture A and 17.38 g mixture B) and 0.86 g accelerator (DMP-30,2,4,6-tri(dimethylaminomethyl)phenol was added.

8.1.2.2 0.05% **Toluidine blue-borax-solution**

2.5 g Toluidine blue (0.5%) and 2.5 g borax (0.5%) was mixed with 1 l distilled water. The solution was diluted in a ratio of 1:5 and filtered before use.

8.1.2.3 Uranyl acetate and lead citrate staining

The ultra-thin sections were applied onto grids (slit 2x1 mm, Plano), which were coated with a pioloform layer.

Pioloform solution: 1.5 g pioloform (Polyvinylformaldehyde) diluted in 100 ml chloroform

For the TEM investigation the ultra-thin sections needed to be contrasted. To do so, each section was transferred onto one drop of uranyl acetate and incubated for 30 min in darkness. Uran(yl acetate) contrasts the nucleine acids and proteins.

Uranyl acetate solution: 2 g uranyl acetate and 100 ml distilled water

The sections were washed in boiled Aqua dest. and dried. Then, each section was transferred onto a drop of lead citrate and incubated for 15 min under the removal of CO_2 with NaOH pellets. Lead (citrate) contrasts lipoprotein-membranes, glycogen and proteins.

Lead citrate solution after Reynolds:
Solution A (1.33 g lead nitrate + 15 ml Aqua dest.)
Solution B (1.76 g sodium citrate + 15 ml Aqua dest.)

Solution A and B was mixed and 8 ml 1n NaOH added, then diluted with 50 ml Aqua dest..
Again, the sections were washed and dried as described above.

8.1.3 Tracer injections

8.1.3.1 ABC-Elite-Kit

ABC –solution preparation: 1 drop of solution A and 1 drop of solution B of the ABC-Elite-Kit dissolved with 10 ml phosphate buffer with 50 µm 0.1% TritonX100
Brain sections were washed in phosphate buffer (I-III) for 5 min in each, followed by 10 min incubation in 1% H_2O_2. Then, the sections were washed again in phosphate buffer (I-III) for 5-10 min in each, before they were incubated in the ABC- solution for at least 2 h. Again, the sections were washed in phosphate buffer (I-III) for 5-10 min in each.

8.1.3.2 DAB solution

10 ml phosphate buffer mixed with 50 µl DAB, 50 µl CoCl (1%) were added and then 50 µl $NiSO_4$ (1%) as well as 50 µl H_2O_2 (0.3%). The sections were incubated for some minutes until staining was visible and were then washed in phosphate buffer (I-III), mounted on slides and allowed to dry.

8.1.3.3 Neutral red staining procedure

After the DAB reaction some sections were counterstained with neutral red. Slides were incubated in a decreasing ethanol series (xylol (I-III), isopropanol (I-II), 96%, 90%, 80%, 70%) for 5 min in each. Then, the sections were kept in neutral red/ kresylviolett for about 1 min followed by phosphate buffer (pH=7) for 30 s. Then, the sections underwent dehydration in an increasing ethanol series (70%, 80%, 90%, 96%), isopropanol (I-II) and xylol (I-III) for 5 min in each. Thereafter, the sections on the slices were coversliped with Roti Histokit-II.

8.1.4 Head cast

The fixative consisted of phosphate buffer mixed with 2% paraformaldehyde and 2% glutaraldehyde.

8.2 Additional data

Tracer investigation

Tab. 9: The variations of the experimental procedures in chronological progression of the involved boas (j=juvenile, a=adult) are shown. The running time of the tracer equals the survival time of the boa, except in one case (see boa 7).

boa 1 (j)	left side, 2nd caudal supralabial pit, scale area pointing backward: biotinylated dextran-amine (BDA), (MW 3000, Lot: 65A11, Molecular Probes, Eugene, USA)	right side, 2nd rostral infralabial pit, scale area pointing backward: BDA (MW 3000, Lot: 65A11, Molecular Probes, Eugene, USA)	tracer running time: 7 days
boa 2 (j)	left side, 2nd caudal supralabial pit, scale area pointing backward: BDA (MW 3000, Lot: 65A11, Molecular Probes, Eugene, USA)	right side, 2nd rostral infralabial pit, scale area pointing backward: BDA (MW 3000, Lot: 65A11, Molecular Probes, Eugene, USA)	tracer running time: 7 days
boa 3 (j)	left side, 2nd caudal supralabial pit, scale area pointing backward: BDA – fluorescein (MW 3000, Lot:R0720, Molecular Probes, USA) left side, 2nd caudal infralabial pit, scale area pointing forward: DBA – texas red (MW 3000, Lot: Q0507, Molecular Probes, USA)	right side, 2nd caudal supralabial pit, scale area pointing forward: dextran, tetramethylrhodamine (MW 3000, Lot: 65A11, Molecular Probes, USA) right side, 2nd caudal infralabial pit, scale area pointing backward: dextran – fluorescein (MW 3000, Lot: 65011, Molecular Probes, USA)	tracer running time: 10 days
boa 4 (a)	left side, 2nd caudal infralabial pit, scale area pointing forward: BDA – fluorescein (MW 3000, Lot:R0720, Molecular Probes, USA)	right side, 2nd caudal supralabial pit, scale area pointing forward: BDA – fluorescein (MW 3000, Lot:R0720, Molecular Probes, USA)	tracer running time: 6 days

	scale area pointing backward: dextran, tetramethylrhodamine (MW 3000, Lot: 65A11, Molecular Probes, USA)	scale area pointing backward: dextran, tetramethylrhodamine (MW 3000, Lot: 65A11, Molecular Probes, USA)	
boa 5 (j)	left side, 2nd caudal infralabial pit, scale area pointing forward: BDA – fluorescein (MW 3000, Lot:R0720, Molecular Probes, USA) scale area pointing backward: dextran, tetramethylrhodamine (MW 3000, Lot: 65A11, Molecular Probes, USA)	right side, 2nd caudal supralabial pit, scale area pointing forward: BDA – fluorescein (MW 3000, Lot:R0720, Molecular Probes, USA) scale area pointing backward: dextran, tetramethylrhodamine (MW 3000, Lot: 65A11, Molecular Probes, USA)	tracer running time: 4 days
boa 6 (j)	left side, 2nd caudal supralabial pit, scale area pointing forward: BDA – fluorescein (MW 3000, Lot:R0720, Molecular Probes, USA) right side, 2nd caudal infralabial pit, scale area pointing backward: dextran, tetramethylrhodamine (MW 3000, Lot: 65A11, Molecular Probes, USA)	right side, 3nd caudal supralabial pit, scale area pointing backward: BDA – fluorescein (MW 3000, Lot:R0720, Molecular Probes, USA) right side, 3nd caudal infralabial pit, scale area pointing forward: dextran, tetramethylrhodamine (MW 3000, Lot: 65A11, Molecular Probes, USA)	tracer running time: 5 days
boa 7 (a)	left side, 2nd and 3rd caudal supralabial pits, scale area pointing forward: BDA (MW 3000, Lot: 65A11, Molecular Probes, USA) tracer running time: 6 days	right side, 2nd and 3rd caudal supralabial pits, scale area pointing forward: biocytin (FW: 372.5, Lot: 117H9190, Sigma-Aldrich, Germany) tracer running time: 2 days	tracer running time: 6 days -> biocytin tracer running time differs from survival time!

9 Acknowledgements

I wish to thank Prof. Dr. Horst Bleckmann and Dr. Guido Westhoff for giving me the opportunity to work on this interesting topic at the Institute of Zoology, Department of Comparative Neurophysiology. Furthermore, I thank Guido for introducing me to the wonderful world of snakes. Thanks to him, I learned lots about dos and dont's in keeping and handling these fascinating creatures.

I also very gratefully acknowledge and thank PD Dr. Michael Hofmann for his inspiring discussions and invaluable support concerning my work, especially with the anatomical investigations. Special thanks to PD Dr. Anke Schmitz for all her help and excellent guidance throughout the histological examinations, especially for her help with the scanning and transmission electron microscopes as well as preparations of ultra-thin sections, and most of all for being always approachable. Special thanks, also, to PD Dr. Helmut Schmitz for his help with the IR camera and scanning electron pictures and his prompt advice on my work whenever needed.

Also, my appreciation goes to Wjatscheslav Braun for his helpfulness and reliability, and for excellent support with animal care.

My sincere gratitude to all people who contributed their advice, help and encouragement throughout my work. In this sense I especially wish to thank Tom Wegner, Gunnar Meyer, Martin Müller and Björn Scholze for their professional support with hard- and software problems that I encountered over the years. I am grateful to Eva Kreiβ for her support with the 'Amira' software. I thank Sabine Büttner for her help with cutting semi-thin sections. Special thanks go also to Dr. Michael Gebhard for his valuable discussions and comments. Special thanks for sharing hours of lab work to Ines Nauroth, Boris Chagnaud, Arne Rüter, Anja Preschbilla, Stephanie de Pury, and Silke Fest.

I am most grateful to Sarah Müller for carrying out the behavioural experiments on the infrared sensitivity of ballpythons with great enthusiasm and always cheering up the atmosphere during the time of her diploma thesis. Very special thanks to Maike Braemer for her excellent support, numerous critical comments and all the laughter we shared. I am also very thankful to Dr. Julia Vettin and Kerri Bigler for critically proof-reading my thesis.

Without the support and constant encouragement of my mother Ute Ebert and my brother Sven Ebert this work would not have been possible. From the bottom of my heart I thank my love Sven Haupt for his understanding and invaluable support with all his heart.

Rheinische Friedrich-Wilhelms-Universität Bonn
Institut für Zoologie
Poppelsdorfer Schloss
53115 Bonn

Bonn, 19. September 2007

Eidesstattliche Erklärung

Hiermit erklare ich an Eides statt, dass ich für meine Promotion mit dem Titel „Infrared sense in snakes – behavioural and anatomical examinations (*Crotalus atrox, Python regius, Corallus hortulanus*) keine anderen als die angegebenen Hilfsmittel benutzt habe, und dass die inhaltlich und wörtlich aus anderen Werken entnommenen Stellen und Zitate als solche gekennzeichnet sind.

(Jill Ebert)